# JOURNAL OF APPLIED PHYSICS

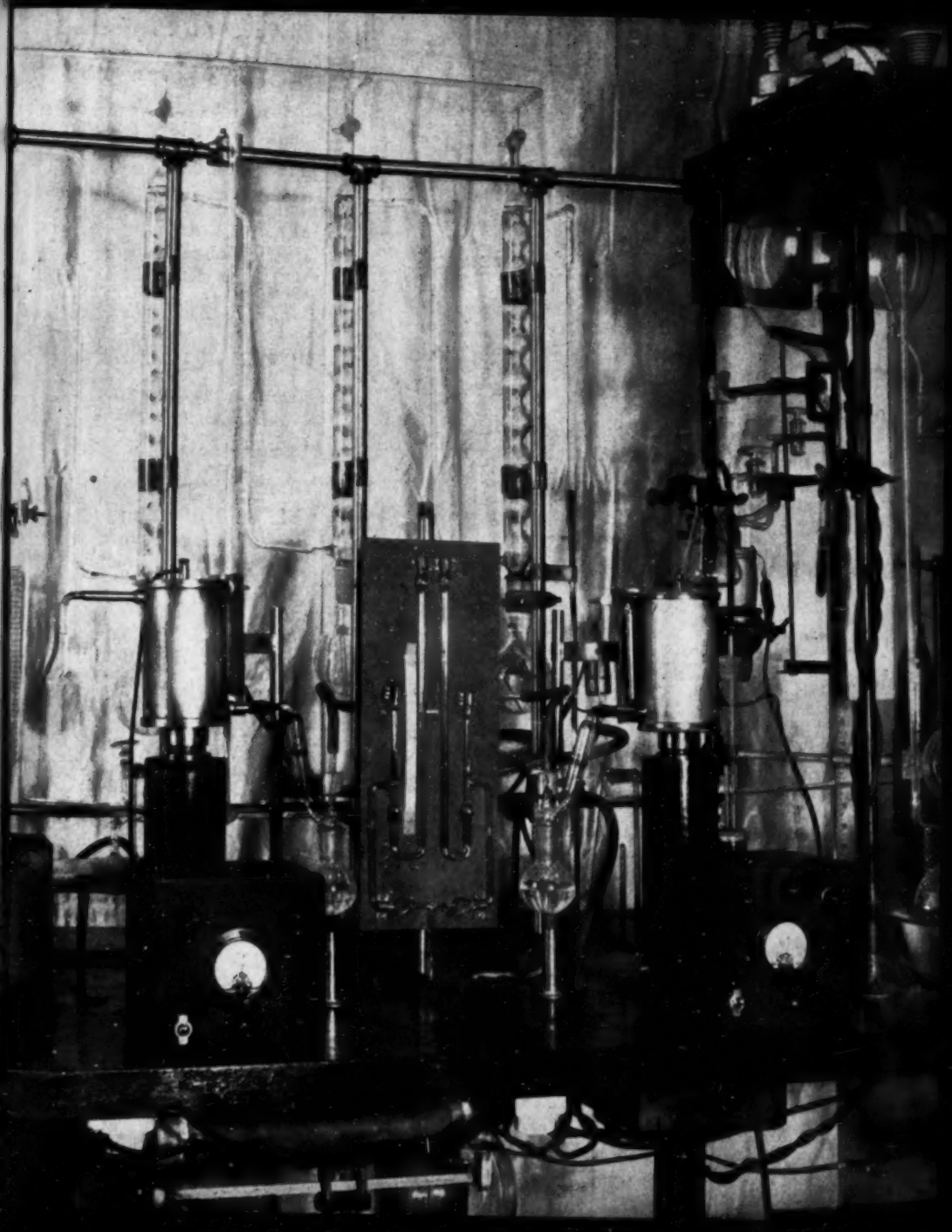

# JOURNAL OF APPLIED PHYSICS

MAY, 1942 Vol. 13, No. 5


## *In This Issue*


| | | *Page* |
|---|---|---|
| **Finishing the Job** | L. A. HAWKINS | 275 |
| **Geological Applications of Nuclear Physics** | CLARK GOODMAN | 276 |
| **Frictional Phenomena. IX** | ANDREW GEMANT | 290 |
| **Bactericidal Radiation** | A. PAULUS | 300 |
| **Résumés of Recent Research** | | 304 |

*Contributed Original Research*

| | | |
|---|---|---|
| **On the State of Stress in Thick Bars** | M. M. FROCHT AND M. M. LEVEN | 308 |
| **Measurement of the Initial Inner Permeability of Iron over a Wide Radiofrequency Range** | ROBERT W. WOODS | 314 |
| **Demagnetizing Factors of Rods** | R. M. BOZORTH AND D. M. CHAPIN | 320 |
| **The Electrical Oscillations of a Perfectly Conducting Prolate Spheroid** | ROBERT M. RYDER | 327 |

*Letter to the Editor*

| | | |
|---|---|---|
| **Effect of Machining and Aging on the Damping Capacity of Steel** | LESTER TARNOPOL AND JAMES R. MORGAN | 343 |

*In Every Issue*

| | |
|---|---|
| **New Books** | 306 |
| **Here and There** | 307 |
| **Calendar of Meetings** | 307 |
| **Index to Advertisers** | x |



**BOARD OF EDITORS**

ELMER HUTCHISSON, *Editor*

*Associate Editors*

FRANCIS BITTER
W. F. BUSSE
S. H. CALDWELL
ROBLEY D. EVANS
MORRIS MUSKAT
FREDERICK SEITZ
B. E. WARREN
J. B. WHITEHEAD

**Publication of the American Institute of Physics**

**ADMINISTRATIVE STAFF**

HENRY A. BARTON, *Director*

MADELINE M. MITCHELL, *Publications Manager*

JOHN T. TATE, *Adviser on Publications*

**GOVERNING BOARD**

PAUL E. KLOPSTEG, *Chairman*
GEORGE B. PEGRAM, *Secretary*
R. B. DOW
L. A. DUBRIDGE
FLOYD A. FIRESTONE
HARVEY FLETCHER
R. C. GIBBS
K. S. GIBSON
ARTHUR C. HARDY
GEORGE R. HARRISON
HERMANN MARK
A. G. WORTHING
JOHN T. TATE
N. W. TAYLOR
WALLACE WATERFALL



The JOURNAL OF APPLIED PHYSICS, published monthly at Prince and Lemon Sts., Lancaster, Pa., is devoted to physics in its role as the science basic to other natural sciences and to the arts and industries. Previous to 1937 this publication was known as PHYSICS. It aims to be of service not only in physical laboratories, but also in the laboratories of industrial, chemical, geological, geophysical, meteorological, radio, and similar concerns. The JOURNAL OF APPLIED PHYSICS publishes editorials, news of physicists and reviews, as well as technical papers of applied physics.

**Manuscripts** should be submitted to Elmer Hutchisson, Editor, American Institute of Physics, 175 Fifth Avenue, New York, New York.

**Subscriptions** and orders for back numbers should be addressed to Prince and Lemon Streets, Lancaster, Pa. or to the American Institute of Physics, 175 Fifth Avenue, New York, N. Y.

SUBSCRIPTION PRICE

| | U. S. AND CANADA | ELSEWHERE |
|---|---|---|
| To members of scientific societies | $5.00 | $5.70 |
| To all others | 7.00 | 7.70 |

**Single copies** are $.70 each.

**Changes of address** and proofs should be addressed to the Publications Manager.

**Advertising rates** supplied on request. Orders, advertising copy and cuts should be sent to the American Institute of Physics.

Entered as second class matter at the Post Office at Lancaster, Pennsylvania, under the Act of March 3, 1897. Accepted for mailing at the special rate of postage provided for in the Act of February 28, 1925, authorized May 2, 1932.



Copyright 1942, by the American Institute of Physics.

Journal
of
Applied Physics

Volume 13 May, 1942 Number 5

# Finishing the Job

By L. A. Hawkins
*General Electric Company, Schenectady, New York*

COMMON to all loyal citizens today must be the resolution to contribute, each to the limit of his ability, to the winning of this war which imperils our most cherished institutions. The greater the ability to contribute, the greater must be the inner compulsion to all-out effort, and since, as Dr. Conant has said, this is a physicist's war, especial obligation rests on them to devote to the war problems their continuous intensive effort of brain and hand, laying aside for the duration all vocational and intellectual interests, however alluring, which would detract from the effectiveness or quantity of their war work.

But such concentration should not bar a thoughtful response to such a presentation of vital post-war problems as is given in Dr. Bridgman's "Challenge to Physicists" in the April issue of this journal. Bitter experience has taught us that we may win a war but lose the peace. When this war is won, the work will be only half done. However intensive our present war effort, surely we should give thought to the consolidation and lasting protection of the temporary security that victory will bring.

If we must look forward to a mere respite of barely two decades, such as the victory of 1918 brought us, to be followed in endless cycle by new wars more terrible still, we might well despair of the future. But the physicist knows that past evils need not be forever endured, and that new conceptions, adequately acted upon, may completely change the course of events.

If a serious defect develops in the operation of a complicated apparatus, and if a repair is made and the apparatus continues to function for a time, only to develop similar but more serious trouble, it requires no special brilliance for a physicist to deduce that the repair was inadequate, that it did not reach the seat of the trouble, or that it was insufficient in its execution.

So, too, the physicist, looking back to 1918, and the decisive victory then attained at the cost of so much blood and treasure, and reflecting on how short a time after that victory the world remained "safe for democracy," is forced to conclude that winning the war was not enough, that it was only an emergency repair job which did not reach the real cause of the trouble. He must conclude that we left the job only half done, when, after the armistice, we yielded to war weariness, discarded all international responsibilities and commitments, and shut our eyes to the sores which were left festering in Europe and which invited all sorts of malignant growths, while we reveled in a post-war business boom.

He sees that victory alone will not safeguard and perpetuate peace and security. He will agree with Dr. Bridgman that new conceptions and a new morale are needed, and that it is his duty to try to make others see the need.

# Geological Applications of Nuclear Physics

BY CLARK GOODMAN

*Massachusetts Institute of Technology, Cambridge, Massachusetts*

## INTRODUCTION

FULLY a decade before nuclear phenomena were recognized as such, radioactivity was improving our knowledge of the earth's heat. Since this beginning, nuclear physics has aided to some extent in understanding each of the three major branches of geological study, i.e., the history, the structure, and the composition of the earth. In the discussion which follows, these applications are briefly reviewed and possible future developments are outlined. It should be emphasized at the outset, however, that the benefits have not been unidirectional. Nuclear physicists have acquired new knowledge of their own field through collaborative researches with geologists.

## RADIOACTIVITY OF TERRESTRIAL MATERIALS

### Distribution

Most geological applications of nuclear physics depend either directly or indirectly on the radioactive properties of certain naturally occurring atomic species. The physical properties, estimated abundance and modes of occurrence of the geologically more important of these elements are given in Table I. The only commercially important ones in this group are potassium, radium, thorium, and to a lesser extent, uranium. Except for potassium, each of these elements averages less than 0.001 percent in the crust of the earth. However, because of the energetic radiations which they emit, the radioactive elements can be studied with considerably greater accuracy than many of the more abundant elements.

The primordial source of all rocks appears to be a substratum of basaltic* material lying a few tens of kilometers below the surface of the earth. The radioactive elements presumably are distributed fairly uniformly throughout this layer but at concentrations substantially lower than are found in acidic surface rocks. This decrease of radioactive content with depth and increasing basicity is the result of differentiation from the source material. Upon cooling of any molten mass, crystallization begins and chemical separation takes place in accordance with the existing pressure, temperature, and composition conditions.[2] Certain mineral species, such as allanite, zircon, and sphene, seem to have crystal structures admitting a greater number of the large uranium and thorium atoms.[3] Accordingly, if conditions are favorable to the formation of these minerals, which are usually only minor constituents in igneous rocks, the resulting rock may show localized concentrations of the radioactive elements. On the other hand, the more common rock-forming minerals, such as quartz, feldspar, pyroxene, amphibole, micas, and magnetite, are less tolerant of foreign radioactive atoms. During crystallization only relatively few uranium or thorium atoms are admitted, and these are found randomly distributed throughout the structures of the crystals.†

The rejected radioactive atoms, together with other incompatible, stable atoms, thus become concentrated in the uncrystallized portion of magmatic solutions. In some instances a relatively small residuum may contain the bulk of the uranium and thorium originally distributed throughout a volume several orders of magnitude larger. These concentrated solutions may cause replacement of other minerals or may crystallize directly into minerals such as uraninite, thorite, thorianite, and monazite. Such minerals contain the parent elements as primary constituents ($\geqslant 0.1$ percent) and are generally classified as "radioactive minerals." Because of these genetic relationships, radioactive minerals are often found in coarsely crystalline intrusive rock bodies known as pegmatites.

* The schematic classification of igneous rocks given in Fig. 1 is included for the benefit of non-geologists.

† Piggot (reference 4) observed a localized concentration of radium on the surface of micas. However, too few measurements of this effect have been made to draw any conclusions as to its generality.

## Properties

Regardless of their chemical combination or physical environment in the earth, the radioactive elements spontaneously disintegrate at known, systematic rates. All experimental attempts to alter this disintegration by changes of pressure and temperature have failed. On the basis of present concepts of the nature of atomic nuclei, no effect is to be expected. However, geological phenomena furnish the most convincing evidence of the constancy of radioactive decay during the lifetime of the earth. The Geiger-Nuttall law relates the range of $\alpha$-rays with the disintegration constant $\lambda$ of the emitting nucleus. Alpha-rays produce a pleochroic discoloration in certain minerals, micas and fluorite in particular. This effect results in a microscopically visible sphere, or halo in the central section, surrounding minute inclusions of $\alpha$-active material, usually a tiny crystal of zircon or allanite. In numerous direct photometric measurements of pleochroic haloes,[5] many of which have required geological periods of time for their formation, no variation in range, and hence no variation in $\lambda$, have been observed for any radioactive element.

After an $\alpha$-ray has lost its energy by absorption, it settles down as a normal, well-behaved

TABLE I. Physical properties, abundance and occurrence of the geologically important radioactive elements.

| Element | Active isotope | Radiations | Energy in Mev | Decay constant $\lambda$ in sec.$^{-1}$ | Half-period $T$ | ‡Mean abundance of active isotope g/g rock | Occurrence |
|---|---|---|---|---|---|---|---|
| Potassium | $K^{40}$ | $\beta$ | 1.2 | $1.4\pm0.3\times10^{-17}$ | $1.6\pm0.3\times10^{9}y$ | $2.2\pm0.4\times10^{-6}$ | Rocks, evaporites, and sea-water. |
| | $K^{40}$ | $\gamma$ | 2.0 | $4\times10^{-19}$ | $5\times10^{10}y$ | | |
| Rubidium | $Rb^{87}$ | $\beta$ | 0.13 | $3.5\pm1\times10^{-19}$ | $6.3\pm2\times10^{10}y$ | ca $6\times10^{-6}$ | Lepidolite and other Li-bearing minerals. |
| Samarium | $Sm^{148}$ | $\alpha$ | 2.55 | $2.5\times10^{-19}$ | $0.9\times10^{11}y$ | ca $10^{-6}$ | Samarskite, cerite and monazite. |
| Radon | Rn | $\alpha$ | 5.49 | $2.10\times10^{-6}$ | $3.82d$ | ca $3\times10^{-18}$ | Genetically associated with uranium, thorium, and actino-uranium, respectively, in rocks, radioactive minerals, atmosphere, mineral waters, and sea water. |
| | Tn | $\alpha$ | 6.28 | $1.27\times10^{-2}$ | $54.5s$ | ca $7\times10^{-22}$ | |
| | An | $\alpha$ | 6.82 | 0.177 | $3.92s$ | ca $2\times10^{-24}$ | |
| Radium | Ra | $\alpha$ | 4.87 | $1.4\times10^{-11}$ | $1600y$ | $0.5\pm0.1\times10^{-12}$ | Genetically associated with uranium and thorium, respectively, also found separately in certain mineral springs. |
| | ThX | $\alpha$ | 5.78 | $2.20\times10^{-6}$ | $3.64d$ | ca $4\times10^{-18}$ | |
| Thorium | Th | $\alpha$ | 4.31 | $1.58\times10^{-18}$ | $1.40\times10^{10}y$ | $5.6\pm1\times10^{-6}$ | Rocks, monazite, thorite, and thorianite. Ionium genetically associated with uranium. |
| | RdTh | $\alpha$ | 5.47 | $1.16\times10^{-8}$ | $1.9y$ | ca $8\times10^{-16}$ | |
| | Io | $\alpha$ | 4.66 | $3\times10^{-13}$ | $8\times10^{4}y$ | ca $3\times10^{-11}$ | |
| Protactinium | Pa | $\alpha$ | 5.1 | $7.0\times10^{-13}$ | $3.1\times10^{4}y$ | ca $4\times10^{-13}$ | Genetically associated with actino-uranium ($U^{235}$). |
| Uranium | $U^{238}$ | $\alpha$ | 4.13 | $4.87\times10^{-18}$ | $4.52\times10^{9}y$ | $1.4\pm0.3\times10^{-6}$ | Rocks, uraninite pitchblende and carnotite. |
| | $U^{235}$ | $\alpha$ | 4.4 | $3.1\pm0.1\times10^{-17}$ | $7.1\pm0.3\times10^{8}y$ | $1.0\times10^{-6}$ | |

‡ Abundances obtained as follows: $K^{40}$ from average chemical analyses of intermediate igneous rocks, see Daly (reference 1) and Grout (reference 12), and isotopic abundance by Nier (reference 13), $Rb^{87}$ and $Sm^{148}$ from Hevesy (reference 14) with isotopic abundances by Nier (reference 13) and Dempster (reference 15), respectively; Th and Ra from Evans and Goodman's (reference 7) averages; others calculated from known genetic relations using indicated decay constants.

helium atom, presumably lodged by self-enforced admittance in the structure of the mineral. The heat produced by absorption of the $\alpha$-rays constitutes the major source of terrestrial radioactive heat.* After the entire series of transformations has taken place, the residual products of the three main radioactive families are the stable isotopes of lead $Pb^{206}$, $Pb^{207}$, and $Pb^{208}$. The genetic relations for the series are shown diagrammatically in Fig. 2.

Even though the parent elements are distributed as individual atoms in a rock or mineral, the number within only one milligram is more than sufficient to allow application of statistical averages. It requires about one million years to establish radioactive equilibrium in the UI series, and a much shorter time suffices for the AcU and Th series. Once this condition obtains, the rate of production of heat, helium, and radiogenic lead by the entire series is known from a determination of the concentration of any one member or from direct $\alpha$-count measurements. In practice the chemically inert, gaseous emanations, Rn, An, and Tn, are usually the most convenient individual members to separate and measure.

Because the electrical effects produced by the minute contents of radioactive elements in terrestrial materials are so small, a number of analytical precautions must be taken to insure reliable results. While satisfactory techniques now appear to be established,[7,8] these have evolved only after four decades of research by numerous investigators. During this time hundreds of measurements were made, most of which are now of qualitative value only. Because of these inaccuracies, a number of the earlier interpretations have undergone rather complete revision.[8–10] The National Research Council's Committee on Standards of Radioactivity in collaboration with the National Bureau of Standards recently has made available[11] dilute radium standards and standard rock samples which should aid materially in avoiding errors in future terrestrial radioactivity measurements.

* The $\beta$-rays and the $\lambda$-rays, which have much greater ranges of penetration than $\alpha$-rays and which cause much less distortion of the crystal structure, contribute about 11 percent of the heat (reference 7).

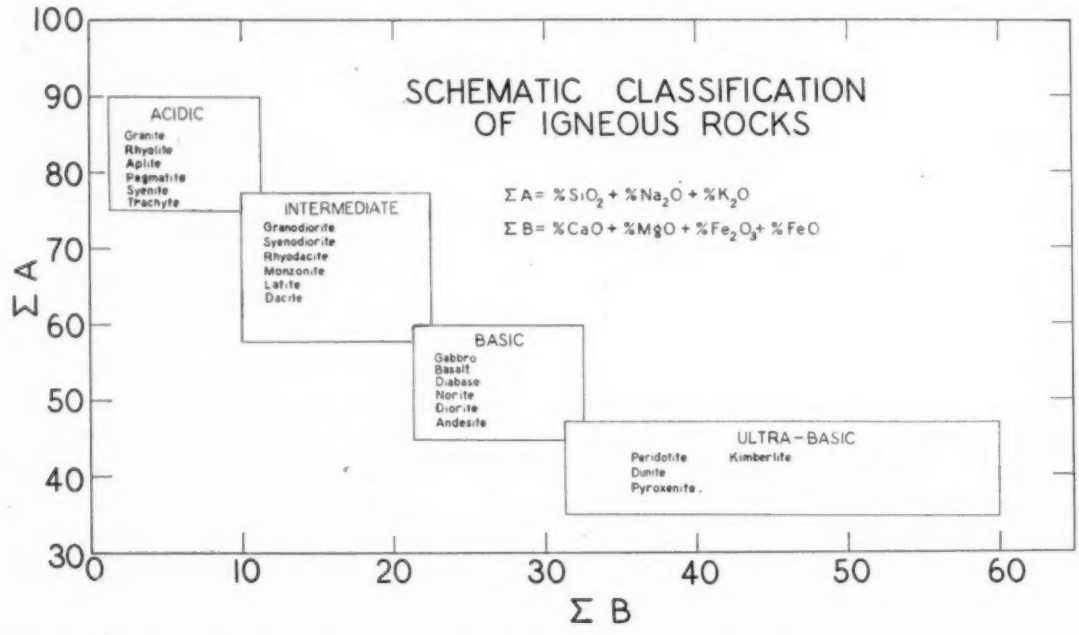


FIG. 1. *Classification of igneous rocks.* Igneous rocks are classified on the basis of chemical composition into four major groups. The proportions of acidic and basic constituents (geologically speaking) are designated by $\Sigma A$ and $\Sigma B$, respectively. The center of each rectangular area coincides with the world-wide averages (reference 1) for the rock types included. The horizontal and vertical spread has been chosen to include at least 90 percent of the rocks of each group with some overlapping to indicate the lack of a sharp boundary. The basaltic substratum in the earth is considered to have an average composition corresponding to about the center of the basic group.

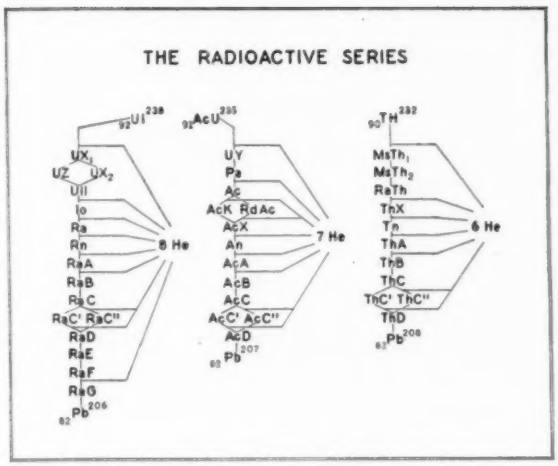


FIG. 2. *The radioactive series.* Both UI and AcU are isotopes of uranium and thus occur in a definite proportion in all uranium-bearing minerals. Because AcU decays more rapidly than UI, the AcU/UI ratio has decreased systematically during geological time. The diagram includes the recently discovered (reference 6) branch product AcK.

## GEOCHRONOLOGY

### General Principles

Radioactivity provides the only quantitative method of measuring geological time. This application aids the geologist in correlating igneous rocks, in measuring the span of paleontological and diastrophic changes, and in determining the rate of erosion and deposition. In some instances such knowledge is of considerable economic value.

If the *age* of a rock or mineral is defined as the time $t$ that has elapsed since final solidification or crystallization, it can be expressed as the ratio:

$$Age = \frac{\text{Amount of disintegration product}}{\text{Rate of production of product}} \quad (1)$$

in which the numerator represents the amount of radiogenic lead, Pb*, or helium, He, formed and the denominator measures the rate at which the disintegration product is being formed in the material. Because the parent elements decay so slowly, this rate is essentially constant for most terrestrial samples and is directly proportional to the concentration of these elements.

In the application of Eq. (1) to rocks and minerals, three basic requirements must be fulfilled. These have been discussed in detail elsewhere[8] and are summarized for the present purpose in Fig. 3. The age methods and the materials to which they are applicable fall into two groups as the result of these requirements. In general, the lead method is applicable only to radioactive minerals and the helium method only to selected rocks and minerals. The reason for this division is apparent from Fig. 4.

### Helium Method

Only recently has sufficient attention been given to the requirements outlined in Fig. 3. Accordingly, most of the helium ages reported in the literature are now known to be unreliable.[8,18] The major sources of this difficulty have been the analytical techniques and the recently demonstrated leakage of helium from certain common rock minerals.[16] Reliable measurements on a routine basis now appear possible. However, the retentivity of minerals for helium has been found to be extremely variable and is of paramount importance in the application of this method.

Although it has not been definitely established that magnetite retains all its helium, there are a number of indications which suggest this possibility. From tests on several common mineral types, magnetite has been found to possess the highest specific retentivity. Helium age ratios for a series of magnetites ranging in geologic age from pre-Cambrian to mid-Tertiary with few exceptions show the proper sequence.[17] Within the small experimental uncertainty of the measurements the same helium age ratio was obtained for a series of Triassic magnetites from widely separated localities and containing a broad range

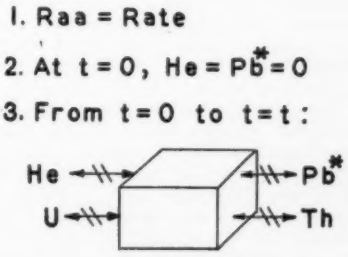


FIG. 3. *Requirements for age measurements by radioactivity.* The observed radioactivity, Raa, must accurately represent the rate of production of He or Pb* in the material. Hence, requirement (1) implies both reliable measurement and representative sampling. (2) At the time of solidification or crystallization, $t=0$, the rock or mineral contained no helium or radiogenic lead. (3) No addition or subtraction of these disintegration products or their sources has occurred during the geological history of the material, i.e., from $t=0$ to the present time, $t=t$.

of helium and radioactive contents.[16] In this connection it is particularly pertinent that the proportions of radium and thorium in these specimens varied considerably.

Accordingly, as a tentative referent, magnetite has been adopted for helium age studies, and considerable progress has been made already in the establishment of a geologic time scale based on measurements of this mineral. The results to date are summarized in Fig. 5 and are compared with the best available lead age ratios on radioactive minerals.

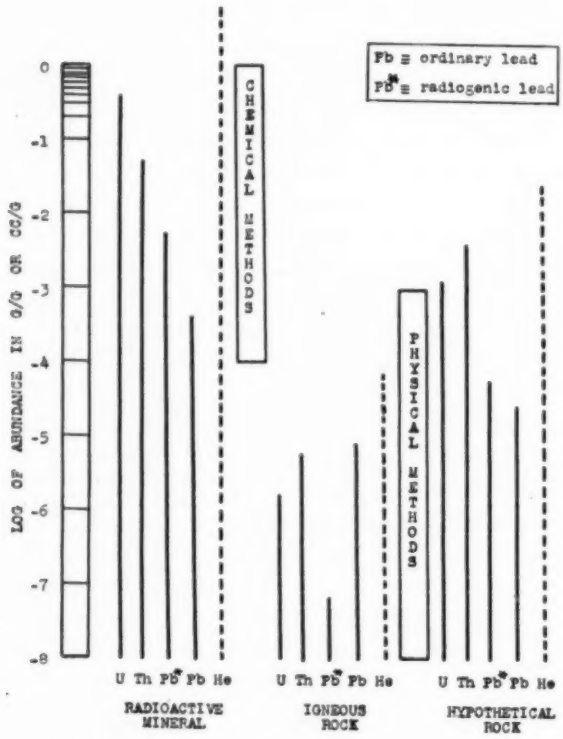


FIG. 4. *Representative radioactive content and decay products of terrestrial materials.* The amounts of radiogenic lead (Pb*) and helium (He) generated in 100 million years by the representative uranium (U) and thorium (Th) contents and the amounts of ordinary lead (Pb) to be expected are indicated. The lead content of such a radioactive mineral can be separated quantitatively by the usual chemical techniques and measured gravimetrically. The lead content of ordinary rocks is considerably beyond the range of chemical methods. Similarly the uranium and thorium content of radioactive minerals can be determined by chemical means, but the content of these elements in ordinary rocks requires sensitive physical detection methods for measurement. The helium content, corresponding to chemically separable quantities of radiogenic lead, is so great that some loss is inevitable. Accordingly, helium ratios on radioactive minerals can represent only minimal age values and cannot be compared directly with corresponding lead ratios. It is conceivable that a material may be found with an intermediate composition, such as the hypothetical rock, that would be suitable for both the lead and helium age methods. Thus far a direct comparison of this type has not been made.

## Lead Method

In the case of radioactive minerals, the denominator of Eq. (1) is based on chemical analyses of U and Th together with the decay constants of these elements.* While the lead can also be separated and determined chemically, it is necessary to identify the proportions of ordinary lead, Pb, and radiogenic lead, Pb*, since only the latter may be used as the numerator of the age equation. Three methods have been used: 1. atomic weight determination, 2. mass spectrographic determination of the abundance of the lead isotopes, 204, 206, 207 and 208, and 3. a determination similar to (2) based on the hyperfine structure of the lead spectrum. The mass spectrographic method yields the highest accuracy and offers a number of other advantages.†

Assuming reliable analytical results, what are the limitations imposed by the fundamental requirements discussed above as applied to the lead method? If any alteration, such as the leaching out of the parent elements, U and Th, has occurred, the calculated rate of production of lead will not be representative of the rate which existed during the lifetime of the mineral. Because the internal radiations shatter radioactive minerals, these materials are particularly susceptible to leaching and replacement by hydrothermal agencies. The extent to which alteration affects the validity of the measurements has not been thoroughly established. Some minerals with considerable evidence of alteration show consistent age measurements, while others with much less apparent change yield obviously unreliable ratios. Accordingly, the practice has been to select minerals, whenever possible, which show the least alteration, but to base the final acceptance of the results on their compatibility with other lead age measurements rather than on any absolute criterion. This procedure is an unfortunate one, but appears to be the only method

* The researches of Kovarik and Adams (reference 19) are largely responsible for the reduction of the uncertainty in the knowledge of $\lambda_U$ and $\lambda_{Th}$.

† Following Aston's initial investigations (reference 20) Nier (reference 21) has made a systematic study of a number of leads separated from radioactive minerals by Baxter and others.

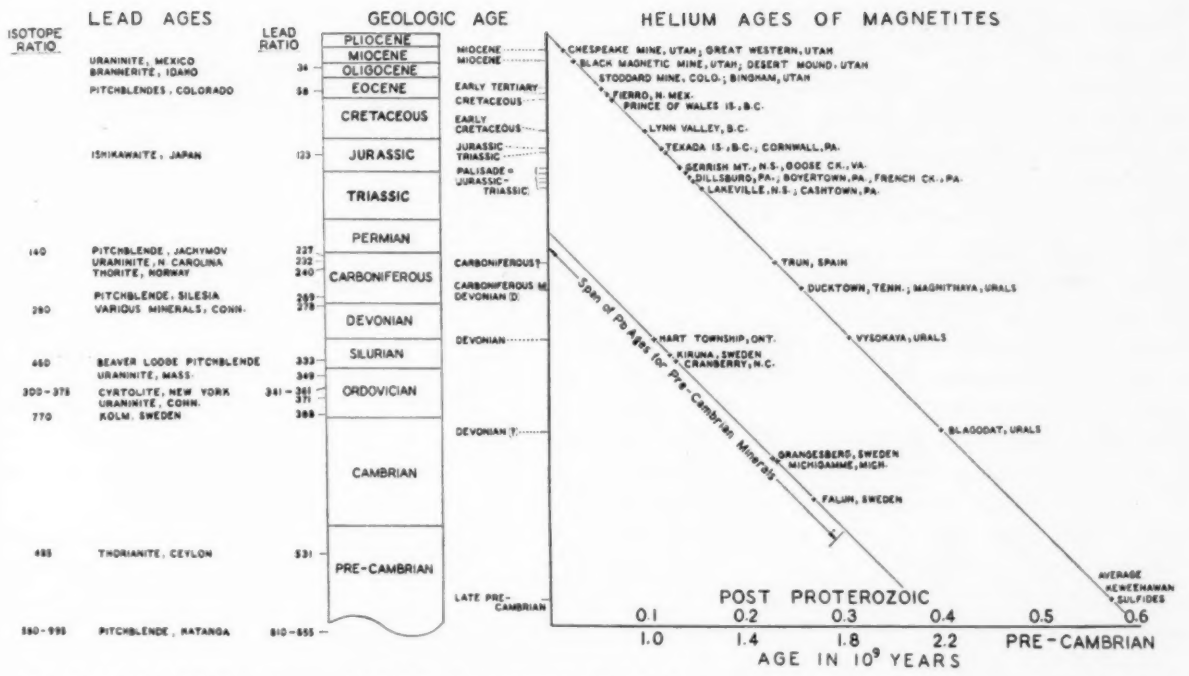


FIG. 5. *Lead and helium time scales.* While the sequence of geologic periods is well-established from paleontologic evidence, radioactive methods provide the only quantitative estimate of their length. The time scale shown is based largely on lead ratio ages, see Eq. (1). Support for the essential correctness of this distribution is provided by the helium ages on numerous magnetites and a few sulfides shown on the right (references 16 and 17). The observed age for the upper group of these minerals is indicated immediately below on the upper (post Proterozoic) scale of abscissas, while the corresponding geologic assignments are shown on the scale of ordinates. It is seen that with the exception of the Blagodat specimen, which is a questionable Devonian, the agreement with the lead ratio time scale is quite good. The isotope ratio, based on the systematic variation of AcD/RaG with time, in some instances is quite different from the lead ratio on the same radioactive mineral (reference 21). More consistent agreement between these two independent lead methods is observed for older minerals (reference 21). These data have not been included because of the geologic uncertainty in comparing helium ages in the earlier Pre-Cambrian.

available at present. A similar procedure is necessary in the study of magnetites. However, the mutual compatibility of these helium age measurements can be determined more reliably than similar comparisons for radioactive minerals, because there are far more magnetite samples available and their geologic sequence is more clearly established.

## GEOPHYSICS

### Well Logging

Schlumberger and associates[22] have established practical methods of measuring the electrical characteristics of subsurface formations. The two most useful electrical parameters are the impedance or resistivity and the natural potential. From empirical study, it has been found that oil bearing sand often can be distinguished from salt-water bearing sand, and the common sedimentary rocks, such as limestone, shale, and sandstone, generally can be identified without expensive subsurface sampling. While the electrical methods fill an important need in petroleum geology, they cannot be used on cased wells. Some nuclear radiations, on the other hand, can penetrate casing.*

For many years ionization chambers and quantum counters have been used to determine the $\gamma$-ray activity of terrestrial materials, but the extension of these techniques to well logging is a recent development. Spak (1937)[23] first reported this application using a Geiger-Müller counter. He credits Gorkov with making the original suggestion some three years earlier. Independently, Howell and his collaborators (1935)[24] applied high pressure ionization chambers for drill hole $\gamma$-ray measurements. These earlier techniques have been ingeniously improved by

* Essentially all completed wells contain one or more liners of jointed steel pipe called casing.

Howell and Frosch[25] and by Scherbatskoy, Westby, and Fearon.[26, 27] Duplicable $\gamma$-logs, both of cased and uncased wells, can now be recorded continuously at logging speeds up to thirty feet per minute. Examples of the types of records obtained are given in Fig. 6.

Because the radioactive content of sedimentary rocks varies roughly with type—for example pure sandstones and limestones are low while shales are relatively high—there is a correlation between electrical logs and $\gamma$-logs. Thus this newer technique inherits considerable geological information that has accrued from the extensive application of electrical methods. Some idea of the degree of correlation between the methods can be obtained from Fig. 7. It is not to be implied that $\gamma$-logs replace electrical logs. Instead the methods are supplementary and provide the geophysicist with a number of different parameters from which to deduce the stratigraphy of subsurface formations.

In addition to this more general application, $\gamma$-logs afford a means of locating cement behind oil well casing that is not subject to the limitations of the older temperature method. It is customary to cement the casing when reducing the size of the drill hole or when shutting off undesirable water flowage from the penetrated formation. Cement is pumped down and flows around the casing and into the surrounding formations for a generally unknown distance and height. Howell and Frosch[25] have shown that the inclusion of only about 0.5 percent carnotite, or any other equally radioactive mineral, in the cement allows the position and relative thickness of the cement behind the casing to be determined with considerable accuracy. Examples of this application are shown in Fig. 8.

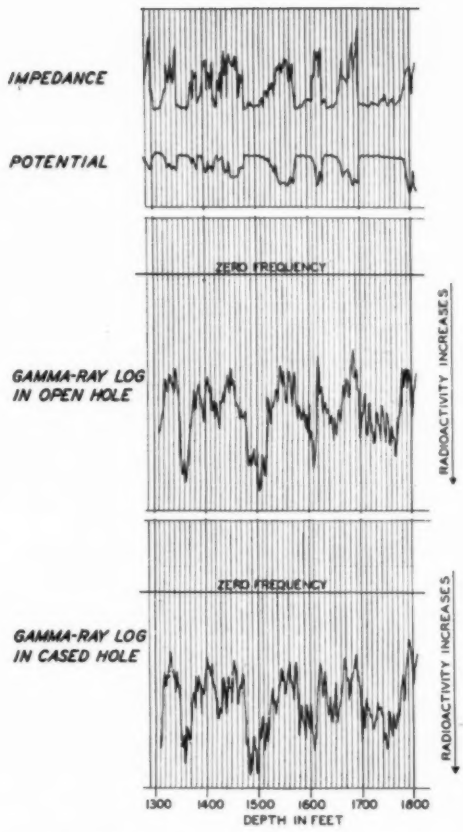


FIG. 6. *Electrical and gamma-ray logs.* The upper traces indicate impedance and potential measurements on a portion of an uncased well. The lower traces are $\gamma$-logs in the same well made before and after casing. (After Howell.)

## Earth Heat

As Slichter[28] has recently shown, the observed surface heat flows establish definite upper limits to the total heat generation which may exist within about 100 or 200 kilometers of the surface of the earth. On the basis of early measurements, it appeared that the rate of generation of heat by the radioactive elements was so great that a stable crust could hardly exist. Accordingly, volcanism, diastrophism, and other dynamic processes were considered by some investigators to be manifestations of the transfer of this excess energy to the surface where it could be radiated into space. A rapid decrease in radioactive content with depth was also postulated; an effect supported to some extent by experimental evidence but not to a sufficient degree to be entirely convincing.

As indicated in the preceding section on age measurements, many of the earlier terrestrial radioactivity measurements are of qualitative value only and are subject to a significant downward revision. The evidence which led to this change has been presented in detail elsewhere.[7, 10] The immediate geophysical importance of this revision is that it allows the existence of a stable crust of a thickness indicated by seismic studies and leaves sufficient additional radioactive material for the underlying mantle and core not to be entirely devoid of these elements.

Because of the large thermal inertia of the earth and the only approximate knowledge of the

heat flux to the surface, thermal conditions below about 200 kilometers are shrouded in mystery. In fact it appears impossible without the aid of as yet unknown devices to determine whether the earth is heating or cooling at depth.

### Exploration

Numerous attempts have been made to correlate surface observations of radioactivity with subsurface features. These measurements have been of two types: (1) determinations of variations in $\gamma$-ray intensity, and (2) surveys of the radioactivity of soil gases.

A few feet of overburden suffice to reduce the $\gamma$-ray intensity from underlying rocks to an undetectable level. Hence, observed variations on the surface are likely the result of local changes in the radioactivity of the soil rather than the result of structural changes below. Some success has been reported[29] in the location of radioactive mineral deposits by $\gamma$-ray measurements. However, the detector must be quite close to the ore body before a significant increase is observable.

The free radon content of soil gases is likewise a function of the features of the soil rather than of the underlying rocks. For example, Clark and Botset[30] observed a rather close correlation between the radon and the heavy mineral content of soil. Unless a subsurface fault exists in materials of widely different radioactive content, no significant change in the radon content of the overlying soil is to be expected. In general few geologically informative data have accrued from surface radioactivity observations although measurements of this type have been of considerable value in studies of the cosmic radiation.

## GEOCHEMISTRY

### General Statement

The less abundant elements can often be used as geochemical tracers of the reactions which have taken place in the formation of terrestrial materials. Quantitative spectroscopic methods are finding increased application in the study of the less abundant stable elements. The radioactive elements can be measured when present in spectroscopically and chemically undetectable amounts. Applications of these two physical techniques have already added considerably to the knowledge of geochemistry. Future researches undoubtedly will greatly extend this knowledge.

### Oceanography

Although oceanographic radioactive relations have been studied for over three decades, only within the last few years have sufficiently accurate measurements been made to allow reliable conclusions to be drawn. An attempt has been made to summarize the more useful data in the schematic diagram of Fig. 9. The disintegration of continental rocks by erosion transfers the

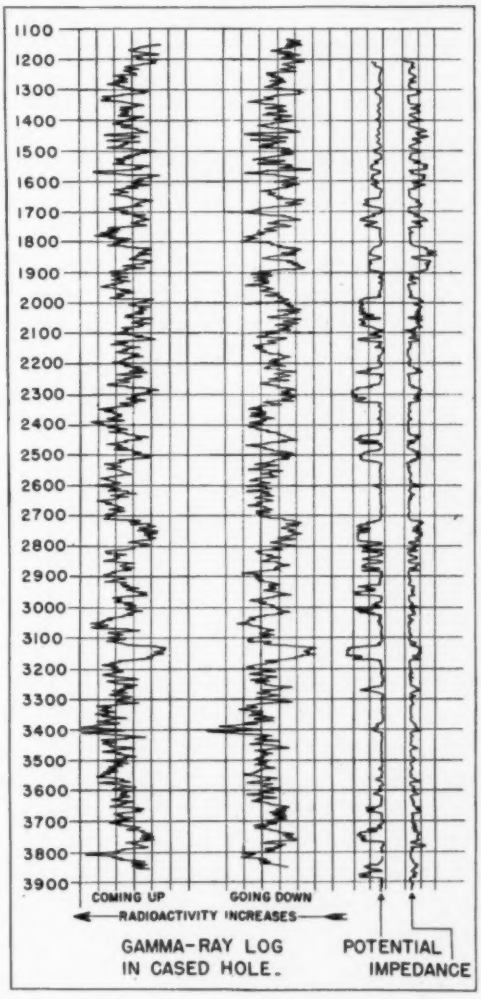


FIG. 7. *Correlation between electrical logs and gamma-logs.* The gamma-logs were made while lowering the detection apparatus and again while removing it. The two directions are seen to give substantially the same results within the statistical fluctuations. Numerous correlations are observed between the $\gamma$-logs and the electrical logs, major ones being at 2700–2800, 3125–3175, 3400, and 3800 feet. (After Howell.)

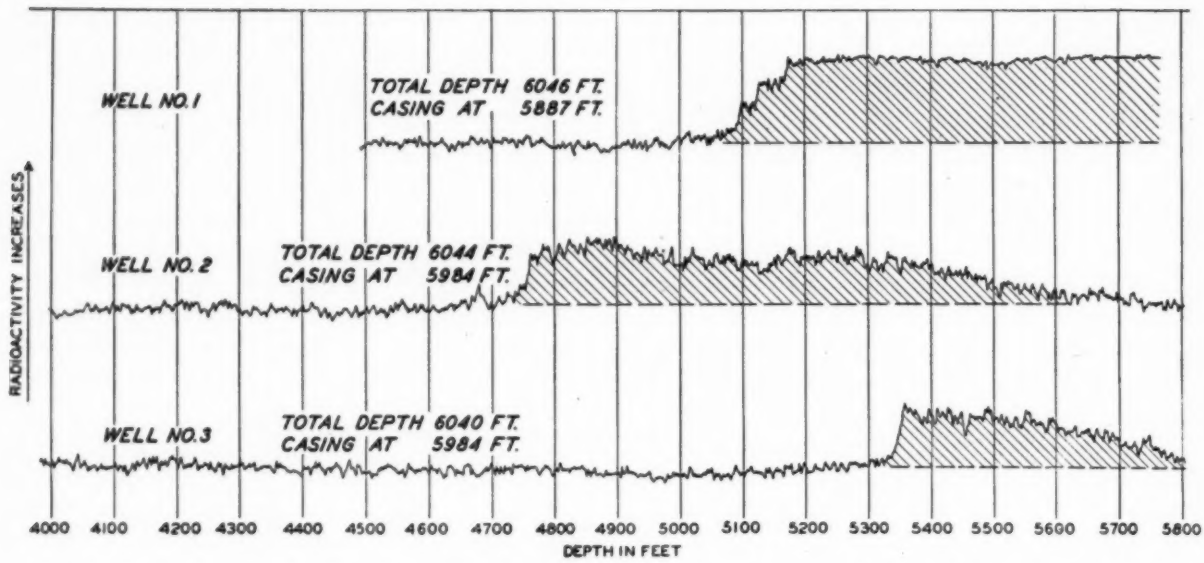
WELL NO.1
TOTAL DEPTH 6046 FT.
CASING AT 5887 FT.
WELL NO.2
TOTAL DEPTH 6044 FT.
CASING AT 5984 FT.
WELL NO.3
TOTAL DEPTH 6040 FT.
CASING AT 5984 FT.
RADIOACTIVITY INCREASES
4000 4100 4200 4300 4400 4500 4600 4700 4800 4900 5000 5100 5200 5300 5400 5500 5600 5700 5800
DEPTH IN FEET

FIG. 8. *Gamma-logs reveal radioactive cement.* The shaded area is proportional to the quantity of cement behind the casing in each of the three wells. The marked differences observed serve to indicate the efficacy of the cementing operations. (After Howell and Frosch.)

radioactive elements from the land to the sea. The clastic materials are deposited near shore with little change in composition. However, the elements dissolved out of the rocks or in colloidal suspension are subject to precipitation according to their individual chemical properties and the nature of the environment.

From the measurements it is inferred that thorium and ionium (being isotopic) are precipitated, together with manganese and ferric iron,* in the region of slightly basic conditions near shore. Since uranium is not precipitated under these conditions, unusually high Th/U ratios should obtain in these sediments. Such marine basins are considered the most likely regions for the formation of source beds of petroleum. The evidence, therefore, suggests that petroleum may originate in rocks with high Th/U ratios. No direct verification of this hypothesis has appeared though there is indirect supporting evidence from the low Th/U ratio observed for sea water at a distance from shore. It is hoped that research now in progress will cast some light on this interesting problem.

## Mineralization

As we have seen, alpha-radiation produces discoloration in certain minerals, biotite and fluorite in particular. Because the range of natural $\alpha$-rays is only a few tens of micra in these minerals, this pleochroic effect is restricted to a microscopic region surrounding the $\alpha$-emitter. In the course of extensive studies of these "pleochroic haloes," Henderson and co-workers[5] discovered a number of unusual types, presumably formed by the radiations from radioactive elements in solution moving through veinlets in the minerals. Many of these haloes are extinct, i.e., they no longer contain active material. However, a permanent, photographic-like record remains to provide information concerning movement of radioactive solutions that occurred millions of years ago. The conclusions to be drawn from these vestiges of the past are not unexpected from related knowledge, but such haloes provide unique, graphic evidence of the microscopic processes of solution movement and deserve more detailed geologic consideration.

Beginning with Mügge's[36] original autoradiographs of radioactive minerals, the photographic action of radiations from radioactive substances has been used widely to determine the distribution of uranium and thorium in terrestrial materials. The locus of the active atoms and qualitative estimates of their concentrations can be obtained quite readily by this method. This information is of interest in understanding the

* The limiting concentration of ferric ions is about $10^{-10}$ o/oo.

modes of formation of radioactive minerals and the subsequent alteration that may have occurred. The latter is of value in determining the suitability of the mineral for lead age studies (see page 280). More recently the photographic technique has been extended to ores of ordinarily stable elements.[37, 38]

Because of their lack of charge, neutrons are able to penetrate the densest matter and coalesce with the nuclei of practically all elements. If a given element has a sufficiently large capture cross section for neutrons and in addition yields a radioactive product, it is possible to determine the distribution and concentration of the element from the radiations emitted. Samples of rock or ore are bombarded by stray, slow neutrons from the cyclotron, while other research is in progress, then removed and placed in direct contact with a photographic film. The autoradiograph produced by the $\beta$-radiation reveals the locus and relative concentration of the active element.[37] When correlated with petrographic study, new information is obtained concerning the genesis of minerals. Manganese, gold, tungsten, copper, arsenic, sodium, potassium, and phosphorus are particularly well suited to this type of investigation.[38] Examples of the autoradiographs obtained are given in Fig. 10. Since many of the elements have characteristic rates of decay, the identity of the active atoms can often be obtained from counter measurements of the material. When combined with similar measurements on known concentrations, the method can be used as a semi-quantitative assay of the ore. The more common elements, such as silicon, oxygen, aluminum, and sulfur, are activated relatively little and hence do not interfere with the application of these techniques.

In the lead age method the abundance of lead isotopes varies with the proportion of uranium and thorium in the mineral, the age of the mineral and the amount of ordinary lead present. Until recently it was assumed that all ordinary lead was composed of a fixed proportion of isotopes.* Nier[39] has shown that there is a small but definite variation in the relative abundance of the lead isotopes that may be of considerable significance in tracing the origin of primary lead ores. Thus far these observations have not received adequate geologic interpretation.

Still more uncertain is the anomalous occurrence of excess helium in certain minerals, beryls and sylvines in particular. Fay, Gluckauf, and Paneth[40] have demonstrated that this helium is not attributable to nuclear disintegration by $\gamma$-rays of the beryllium in the beryls. Were it not for the apparent correlation with age,[41] the excess helium could be considered as a product of magmatic differentiation. It is conceivable that the helium in these minerals contains an unusually high proportion of the recently discovered[42] stable isotope, $He^3$. As yet no isotopic abundance measurements have been made. This tantalizing problem remains for future solution.

### Isotopic Variations

The variation in abundance of lead isotopes in ordinary lead has been considered in the preceding section. Similar variations also have been observed in a number of the lighter elements.

Following the discovery of deuterium ($H^2$) numerous determinations of the density of waters from various sources were made.[43] Variations in density were commonly observed, some being as high as 20 parts per million, i.e., $\gamma = 20$. These differences were attributed to supposed variations in the $H^1/H^2$ ratio, presumably due to differences in the rates of diffusion in nature. However, Dole and his associates[44] have demonstrated conclusively that the observed differences are largely the result of faulty laboratory purification and preparation of the water. After eliminating uncertainties from this source, only minor differences in density are observed and these are due primarily to isotopic variations in oxygen rather than in hydrogen. Geologically the significance of such variations, therefore, is much less than was previously supposed.

The abundance of $He^3$ atoms in atmospheric helium is only about one per million $He^4$. For this reason discovery of the lighter isotope was delayed until application of the cyclotron as a high intensity mass spectrometer.[42] Since $He^3$ must be lost from the earth's atmosphere more readily than $He^4$, terrestrial helium would be expected to have a higher concentration of the lighter isotope than atmospheric helium. While

* This conclusion was based on the apparent constant atomic weight of ordinary leads and the lack of variations in other heavy elements. Specific definitions of the various forms of lead are included in reference 8, pp. 531–532.

only a few measurements have been made, the opposite appears to be the case. Helium from natural gases contains only about one-tenth as much $He^3$ as atmospheric helium. A likely explanation is that terrestrial helium shows a greater dilution by radiogenic $He^4$ of the primordial helium, which presumably contained $He^3$ as one of its components in a somewhat higher proportion than is now found in helium from either source. An alternate possibility is that $He^3$ is formed in the atmosphere by an unknown nuclear reaction involving cosmic radiation.

Nier and his associates[45] have established variations up to 5 percent in the $C^{12}/C^{13}$ abundance ratio of carbon obtained from several natural sources of widely different geologic age and geographic origin. No trends with age were found. Plant spores, algae, petroleum, bituminous shales, torbanite, and kerosene shales have relatively higher ratios than limestones, zeolitic calcite,

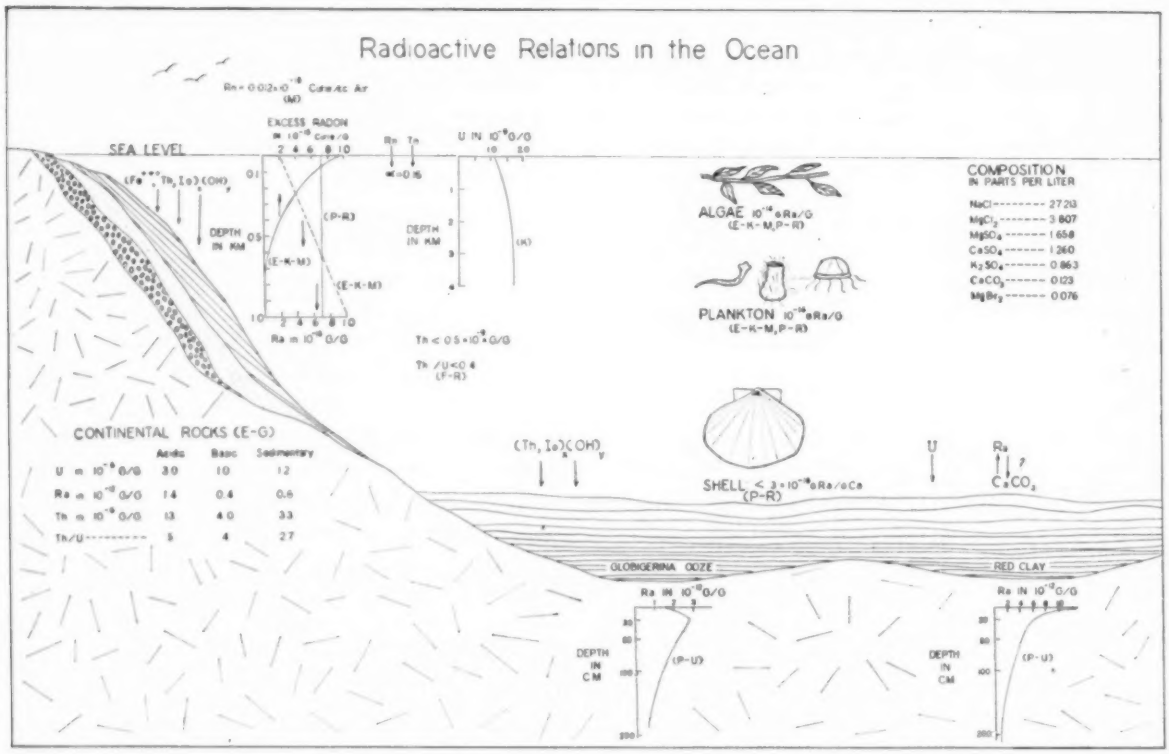


FIG. 9. *Radioactive relations in the ocean.* Considerable selection of data on the basis of evident reliability has been made. Individual investigations are designated as follows: (E-G) Evans and Goodman (reference 7), (E-K-M) Evans, Kip, and Moberg (reference 31), (F-R) Foyn and Rona (reference 32), (K) Karlik (reference 32), (M) Mauchly (reference 33), (P-R) Pettersson and Rona (reference 32), and (P-U) Piggot and Urry (reference 34). The composition of sea water is from the *Challenger* expedition as reported by Posnjak (reference 35). (E-K-M) observed a decrease in excess radon, i.e., above equilibrium amount, with depth and an increase in radium content as shown in the upper left graph. (P-R) did not confirm the latter effect, although their observed average radium content, $0.7\times10^{-16}$ g/g is in good agreement with that of (E-K-M). A slight increase in uranium content with depth was observed by (K) as shown in the adjacent graph. $U/Ra=2.84\times10^6$ at equilibrium. The available evidence indicates the lack of radioactive equilibrium in sea water and that radium is being precipitated in excess of uranium. The lower graphs represent the interesting observations of (P-U) on bottom core samples collected by the ingenious mechanism developed by Piggot. These results clearly show the lack of radioactive equilibrium near the top of these sediments. Two extremes are observed; the usual case very likely is a combination of these two. Excess precipitation of ionium (and hence likewise its isotope thorium) relative to radium and uranium occurs in globigerina oozes, while excess radium relative to ionium and of the latter relative to uranium occurs in red clays. The variation of the content of these elements with depth in the cores follows closely the decay curves. Thus a constant rate of deposition is indicated, and a means of estimating this rate likewise is made available. From the above measurements, it is inferred that thorium and ionium are precipitated (together with manganese and ferric iron) in the region of slightly basic conditions near shore. Since uranium is not precipitated under similar circumstances, unusually high Th/U ratios ($\gg4$) should characterize these sediments. Algae and plankton possess the ability to concentrate radium more than 100-fold above the concentration of the water in which they grow. Conversely, calcareous shells select calcium in preference to radium over 1000-fold. These interesting biochemical mechanisms await explanation. The emanation content of air over the ocean apparently is due to the exhalation of radon from sea water, which has a Henry's law coefficient, $\alpha$, of 0.16.

marine shell, and sea water. Since the $C^{12}/C^{13}$ ratio would be expected to remain substantially the same in a given life cycle, these observations are of value in unravelling the genesis of certain terrestrial materials. The data support independent evidence for the geologic origins of petroleums and limestones.

Early mass spectrographic measurements[46] were able to show that there were no large scale variations in the abundance of oxygen isotopes in various natural substances. However, these observations were not capable of detecting a difference of less than about 2.5 percent in the $O^{18}/O^{16}$ ratio, this ratio being very close to 1/500. Because the oxygen in carbonate rocks and iron oxide ores is easily recovered in the form of water and density measurements on the water can be made with high precision, Dole and Slobod[47] were able to study the isotopic abundance of oxygen in these materials from widely different geologic horizons. No significant difference was observed between the oldest rocks (Grenville marble) and the youngest (clam shells), from which it is concluded tentatively that "there has been no change in the isotopic composition of the oxygen in the oceans (from which these rocks were precipitated) over a period greater than a billion years." This is in agreement with Nier and Gulbransen's observations[45] on the lack of any significant variation in the carbon isotopes from similar sources. The oxygen in certain cuprite ores[50] and in iron ores of Keewatin and Middle Huronian ages was found to have the same isotopic composition as in normal water, which is significantly different from atmospheric oxygen. From this it is concluded that these ores were probably formed by precipitation from water, substantiating the general opinion of geologists. The excessive density of the water prepared from fossil type Silurian ores is attributed to the presence of carbonates which are shown to have slightly higher proportions of the heavier isotope.

Potassium is made up of three isotopes of atomic weights 39, 40, and 41 in relative abundances of about 8300, 1, and 585, respectively. $K^{40}$ is $\beta$-radioactive* with a half-period of $1.6 \pm 0.3 \times 10^9$ yr. The other isotopes are stable. Brewer[48] has studied the isotopic ratio, $K^{39}/K^{40}$, in various minerals, in plants, and in animal tissues. In general no significant variation has been observed for mineral potassium. On the other hand, it is claimed that plant tissues exhibit appreciable variations and usually have the abundance ratio of the soil in which they grow, while kelp and other seaweeds show a preference for the heavier isotope. Because of the widespread distribution of potassium and its biologic as well as geologic significance, it would be of interest to have these interesting observations substantiated by further studies.

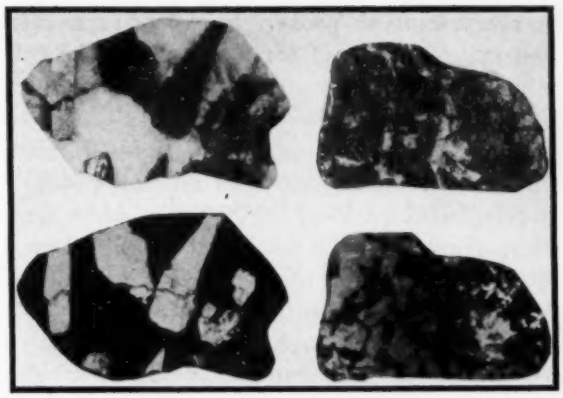

FIG. 10. *Autoradiographs of ores.* The distribution of tungsten in the Spanish wolframite ore (upper left) is indicated by the relative brightness in the print prepared from the autoradiograph, as shown immediately below. The $\beta$-rays from $W^{187}$ ($T = 24$ hr.) are largely responsible for the photographic action. Similarly the $\beta$-rays from $Au^{198}$ ($T = 2.7$ days) reveal the distribution of gold in a sample of Cripple Creek ore activated by slow neutrons. The brightest areas in the photograph (lower right) correspond to native gold, the gray areas to calaverite (gold telluride). The dark regions in both lower prints correspond to quartz which is activated relatively little.

Schumb, Evans, and Leaders[49] have shown that potassium separated from the Pultusk meteorite has the same $K^{40}/K$ ratio as terrestrial potassium within an experimental uncertainty of about 3 percent. This research was undertaken in an attempt to use potassium as an index of the age of meteorites.

## FUTURE APPLICATIONS

An extension of the helium method of age determination to minerals other than magnetite already has begun. This should allow a broader application of the method particularly if sedi-

* Potassium is also $\gamma$-radioactive with approximately 3 $\gamma$'s per 100 $\beta$'s. The $\gamma$-rays presumably result from $K$-electron capture by $K^{40}$ see reference 8, p. 538 for discussion.

mentary minerals prove reliable. The separation and measurement of rock magnetite and other minerals will enable a more complete time scale to be established after which this physical tool can be used to solve many stratigraphic problems. Future extension of the lead method should be largely based on $Pb^{207}/Pb^{206}$ ratios. More direct comparisons between the helium and lead methods are needed since the ultimate success of both depends upon their mutual agreement.

A new era in petroleum prospecting should result from an understanding of the origin of oil. Nuclear physics may well be of aid in solving this complex problem. Unless the present emergency makes it impossible, a systematic study of the genesis of petroleum will begin this year under the sponsorship of the American Petroleum Institute.

The calibration of $\gamma$-ray logs would make available a wealth of geochemical and geophysical data on sedimentary rocks.* While terrestrial radioactivity measurements appear incapable of casting further light on the thermal state of the earth at depths, many important local and near surface problems depend upon this information. Hence, further geothermal radioactivity measurements would be of value, particularly if these were correlated directly with diffusivity and geothermal gradient measurements. The future should also see an extension of the application of neutrons in geophysics. Already the relative scattering coefficients of neutrons appear to be useful in well-logging.[50] The results of this type of survey reveal the relative hydrogen content (largely in the form of water) in the formations. By extending the neutron induced activity method to rocks, an indication of their mineral and fluid contents could be obtained. This application awaits the development of compact, intense neutron sources.

Further knowledge of the variations in the abundance of isotopes in nature and of the distribution of radioactive elements in rocks and minerals should lead to a better understanding of the fundamental processes of geochemistry. There is considerable evidence that unknown radioactive elements, possibly an entire new series,[51] may be present in highly differentiated terrestrial materials. The origin of helium-bearing gases has received only speculative explanation. This problem deserves further attention, particularly in view of the recently discovered light isotope of helium.

Now that agreement among different investigators has been attained in oceanographic radioactivity, whole new fields have been opened for research. The rate of deposition of deep sea sediments can be determined from the degree of radioactive equilibrium between the geologically short-lived elements and their parents. There is every reason to suppose that a similar technique would be applicable to near shore and continental sediments. Artificial radioactive tracers are being used extensively in biology and medicine. Certain organisms are known to concentrate radium in preference to its chemical homologs. Further study of the mechanism of this and related processes should be of value not only in biology but in understanding the role of these organisms in the formation of sedimentary rocks. The radioactivity of potassium affords a means of studying its importance in the precipitation and consolidation of clays.

All in all, it seems certain that in the future the newest developments of physics, especially those exemplified by progress in the understanding of the atomic nucleus, will find ever increasing application in the earth sciences.


## ACKNOWLEDGMENTS

This paper is a direct outgrowth of the Conference on Applied Nuclear Physics held at the Massachusetts Institute of Technology during the fall of 1940 under the sponsorship of the American Institute of Physics. The author is indebted to the numerous speakers and discussers for most of the material herein summarized. He particularly wishes to thank Dr. Lynn G. Howell for permission to reproduce a number of the figures, Dr. P. M. Hurley for the use of unpublished data, and both of these colleagues and Dr. Malcolm Dole for their criticism of the manuscript. The support of the Geological Society of America is gratefully acknowledged.


* *Added in proof:* A beginning in this direction has just been reported by Pontecorvo, Geophys. **7**, 90–94 (1942), but the sensitivity of his instrument is only sufficient to measure sediments containing $>5\times10^{-12}$ g Ra/g or its equivalent.

## BIBLIOGRAPHY


**Radioactivity of Terrestrial Materials**

(1) R. A. Daly, *Igneous Rocks and the Depths of the Earth* (McGraw-Hill, 1933).
(2) N. L. Bowen, *The Evolution of the Igneous Rocks* (Princeton Press, 1928).
(3) V. M. Goldschmidt, J. Chem. Soc. (London) 655–673 (1937). E. S. Larsen and N. B. Keevil, Am. J. Sci. **240**, 204–215 (1942).
(4) C. S. Piggot and H. E. Merwin, Am. J. Sci. **A35**, 227–229 (1938).
(5) G. H. Henderson *et al.*, Proc. Roy. Soc. **A173**, 238–264 (1939).
(6) M. Perey, J. de phys. et rad. **10**, 435–440 (1939).
(7) R. D. Evans and C. Goodman, Bull. Geol. Soc. Am. **52**, 459–490 (1941).
(8) C. Goodman and R. D. Evans, Bull. Geol. Soc. Am. **52**, 491–544 (1941).
(9) Evans, Goodman, Keevil, Lane, and Urry, Phys. Rev. **55**, 931–946 (1939).
(10) C. Goodman and R. D. Evans, Trans. Am. Geophys. Union, 544–547 (1941).
(11) Curtiss, Goodman, Kovarik, Lind, Piggot, and Evans, Phys. Rev. **57**, 457L (1940).
(12) F. F. Grout, *Petrography and Petrology* (McGraw-Hill, 1932).
(13) A. O. Nier, Phys. Rev. **50**, 1041–1045 (1936).
(14) G. Hevesy, *Chem. Analysis by X-Rays and Its Applications* (McGraw-Hill, 1932).
(15) T. R. Wilkins and A. J. Dempster, Phys. Rev. **54**, 315A (1938).

**Geochronology**

(16) P. M. Hurley and C. Goodman, Bull. Geol. Soc. Am. **52**, 545–560 (1941).
(17) P. M. Hurley and C. Goodman, Bull. Geol. Soc. Am. **52**, 1909A (1941).
(18) N. B. Keevil, University of Toronto Series (1941).
(19) A. F. Kovarik and N. I. Adams, Phys. Rev. **54**, 413–421 (1938); J. App. Phys. **12**, 296A (1941).
(20) F. W. Aston, Nature **123**, 313 (1929); Proc. Roy. Soc. **A140**, 535–543 (1933).
(21) A. O. Nier, Phys. Rev. **55**, 153–163 (1939), **60**, 112–116 (1941).

**Geophysics**

(22) C. and M. Schlumberger and E. G. Leonardon, A. I. M. E. Geophys. Pros. 269 (1934).
(23) A. Spak, Comptes rendus (Doklady) (USSR) **16**, 109 (1937).
(24) L. G. Howell and A. Frosch, Geophys. **4**, 106–114 (1939).
(25) L. G. Howell and A. Frosch, A. I. M. M. E. Tech. Pub. **1113**, 1–8 (Nov. 1939).
(26) G. H. Westby and S. A. Scherbatskoy, Oil and Gas J. (Feb. 22, 1940).
(27) W. G. Green and R. E. Fearon, Geophys. **5**, 272–283 (1940).
(28) L. B. Slichter, Bull. Geol. Soc. Am. **52**, 561–600 (1941).
(29) R. Ambronn, *Elements of Geophysics* (McGraw-Hill, 1928).
(30) R. W. Clark and H. G. Botset, Bull. Am. Assoc. Petrol. Geol. **16**, 1349–56 (1932).

**Geochemistry**

(31) Evans, Kip, and Moberg, Am. J. Sci. **36**, 241–259 (1938).
(32) Foyn, Karlik, Pettersson, and Rona, A series of four papers (Meddlelanden Fran Oceanografiska Institutet I Goteberg 2) Femte Följden **B6**, 1–44 (1939).
(33) S. J. Mauchly, Terr. Mag. **29**, 187–194 (1924).
(34) C. S. Piggot and W. D. Urry, The latest of a series of five papers, contains references to the earlier ones, Am. J. Sci. **240**, 93–103 (1942).
(35) E. Posnjak, Am. J. Sci. **238**, 562 (1940).
(36) O. Mügge, Zentralbl. Mineralogie **71**, 144–147 (1909).
(37) C. Goodman and D. C. Picton, Phys. Rev. **60**, 688L (1941).
(38) C. Goodman and G. A. Thompson, Bull. Geol. Soc Am. **52**, 1905A (1941).
(39) A. O. Nier, J. Am. Chem. Soc. **60**, 1571–1576 (1938); Phys. Rev. **60**, 112–116 (1941).
(40) Fay, Gluckauf, and Paneth, Proc. Roy. Soc. **A165**, 238–246 (1938).
(41) Rayleigh, Proc. Roy. Soc. **A142**, 370 (1933).
(42) L. W. Alvarez and R. Cornog, Phys. Rev. **56**, 613L (1939).
(43) E. H. Riesenfeld and T. L. Chang, Naturwiss. **24**, 616–618 (1936), general summary
(44) M. Dole, J. Chem. Phys. **4**, 268–275 (1936).
(45) A. O. Nier and F. A. Gulbransen, J. Am. Chem. Soc. **61**, 697–698 (1939).
(46) Manian, Urey, and Bleakney, J. Am. Chem. Soc. **56**, 2601–2609 (1934).
(47) M. Dole and R. J. Slobod, J. Am. Chem. Soc. **62**, 471–479 (1940).
(48) A. K. Brewer, J. Am. Chem. Soc. **58**, 365–372 (1936).
(49) Schumb, Evans, and Leaders, J. Am. Chem. Soc. **63**, 1203–1205 (1941).
(50) W. H. Hall and C. Hochanadel, J. Am. Chem. Soc. **62**, 3259 (1940).

**General**

(51) B. Pontecorvo, "Neutron well-logging," Oil and Gas J. (Feb. 18, 1941).
(52) W. Wahl, "A new radioactive series," Science **93**, 16–17 (1941).

H. V. Ellsworth, "Rare element minerals of Canada," Econ. Geol. Series No. 11 (1932); J. Noetzlin, "Volcanism and nuclear chemistry," Comptes rendus **208**, 1662–1664 (1939); A. Holmes, *Age of the Earth* (Thomas Nelson and Sons, 1937); National Research Council, "Age of the earth," Bull. 80 (1931).

# Frictional Phenomena. IX

BY ANDREW GEMANT
*The Detroit Edison Company, Detroit, Michigan*

## Chapter IX. Applications of Liquid Viscosity to Electrical Insulating Liquids, Particularly in High Voltage Cables

***Abstract***

THIS chapter deals with: (1) mechanical processes involving viscosity, particularly (a) impregnation, (b) breathing, (c) oil migration with respect to high voltage cables; (2) chemical processes involving viscosity, such as (a) Voltol process, (b) wax formation in cables, (c) polymerization of styrene; (3) electrical conductivity. With regard to the latter, the fundamental quantities, besides viscosity, that determine the conductivity are discussed, together with the various experimental methods whose interpretation allows the quantities in question to be computed.

### *36. Mechanical Processes and Viscosity*

There are three fields in which liquid viscosity has to be considered in connection with liquid dielectrics. One of these is that of mechanical processes, particularly dynamic ones, concerned with motions of the liquid. Another is that of chemical processes, often accompanied by a change of viscosity. A third is that of electrical conductivity, controlled among other factors by the viscosity of the medium. All these are dealt with briefly in this chapter.

Let us begin with the motion of insulating liquids. There are several electrical devices in which some kind of liquid motion takes place, but according to the nature of this monograph, aimed more at a logical and constructive presentation than at completeness, only one device, i.e. high voltage cables, will be considered as an illustration. There are several different phases in manufacture and operation that are of interest in this respect.

(a) *Impregnation.*—The insulation of high voltage cables consists of paper strips wound around the central copper conductor, the body of paper being afterwards impregnated with oil. The most usual impregnation process is carried out by winding the cable (copper conductor plus paper) around a drum, placing the assembly in a tank and, as a first step, evacuating the whole system. After that, oil is allowed to enter the tank. During this phase of the process oil will penetrate, at least to a large extent, into the pores of the paper chiefly by means of capillary forces. The paper will be partially impregnated, the rest of the pores being filled with gas under reduced pressure attained during this phase. Finally hydraulic pressure will drive the oil completely into the pores and other capillary spaces left between the paper strips. Only a minute amount (less than 0.5 percent) of gas space under atmospheric pressure (so-called voids) will be left over.

The speed of the impregnation process is that of a viscous flow. By Eq. (13) a resistance value $R$ was defined for any sort of channel, through which flow takes place under any driving force. For a single circular capillary tube it was $R=8\eta/r^4$. The resistance $R$ is the product of the viscosity of the medium (here the oil) and a geometric factor, depending upon the configuration of the channel or channel-system. The value of $R$ for papers is determined by apparatus originally introduced by Emanueli[1] and similar to that described in connection with sound absorbing materials in Section 17 (c). The geometric factor mentioned is independent of the nature of the medium, as long as no change of the structure, such as swelling of fibers, takes place. The resistance of the paper insulation (Fig. 63) is less than that of a single layer times the number of layers, because a certain leakage path exists along the spaces (so-called butt spaces) left between neighboring turns of the same layer and along the narrow space left between neighboring turns of subsequent layers (see the dotted line in Fig. 63).

The lower the viscosity of the oil, therefore, and the more porous the paper, the faster will be

the impregnation. However, in the usual cable design fairly viscous oils (about 20 poise at room temperature) have to be used for several reasons, partly discussed below under (c) Migration. The porosity, on the other hand, is required to be low, since the electrical strength increases with decreasing porosity. These features, then, slow down impregnation considerably, for which reason the temperature is raised to around 115°C, and the viscosity lowered to the order of 0.3 poise. On the basis of this low viscosity level, impregnation is completed in about 48 hours. It should be recalled once more that the driving force during the first part of impregnation is chiefly the

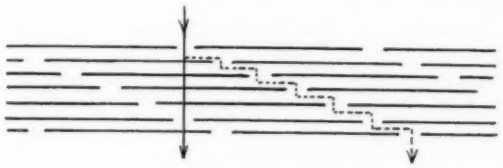

FIG. 63. Diagram of oil flow through paper insulation.

capillary force, the external pressure acting only in the second phase of the process. The applicability of the equations of viscous flow is, however, independent of the nature of the driving force.

In recent years a large number of new cable constructions have been suggested and adopted. In contradistinction to these new types the usual one is called, although not very correctly, "solid"-type cable, since its insulation, paper completely impregnated with a viscous oil, behaves in several respects like a solid. One of the new types, the Beaver-type cable,[2] consists of paper tapes that are preimpregnated with a very viscous oil and thus requires no impregnation after taping. The interstices left between the individual tapes are then filled with nitrogen gas under a pressure of 200 lb. per sq. in. This type is mentioned not because of its manifold advantages, which do not interest us here, but because it does away with the impregnation of the whole cable which, as indicated above, is a fairly difficult process, particularly if the degree of impregnation is required to be as high as possible. The impregnation of single paper tapes can be completed much faster and more completely, owing to the low value of the resistance *R*.

(b) *Breathing.*—The viscosity of the impregnating oil or compound (so-called if mixed with resin) has an essential influence not only on the impregnation of the cable, but also on its operation. During operation the cable undergoes daily load cycles, both the amperage and temperature varying in a cyclic manner. During a temperature rise the oil expands, during a drop it contracts, and this motion is called breathing.

This cyclic process in itself is reversible, thus harmless. Unfortunately, another irreversible, thus harmful, process follows in its trail. The sheath of the cable, made of lead because its flexibility and plasticity are desirable in the manufacture, handling, and installation of the cable, follows the expansion of the oil by a plastic expansion, but does not follow the contraction. The reason is that during expansion the pressure difference inside and outside the sheath is higher than the yield value of lead (see Chapter XII); thus the lead will flow. During contraction of the oil the lead sheath does not follow because the pressure difference inside and outside, usually around 10, or at the most 15 pounds, is lower than the yield value. Hence the contraction of the oil in the space inside the sheath that has at this point a practically constant volume (the expansion coefficient of the lead being around ten times smaller than that of the oil) will initiate a displacement of the oil through the paper, resulting in the formation of voids, or at least leaving behind some poorly impregnated layers of paper. Because of the ensuing gaseous ionization in these voids these occurrences are highly undesirable.

The actual process during this cooling period depends largely upon the viscosity of the oil. Cooling starts from the outside, thus a considerable temperature gradient exists in the radial direction. Because of the large temperature coefficient of the viscosity of heavy oils and compounds used in "solid" type cables, the outer part of the insulation will have a higher viscosity than the inner parts near the copper conductor.

This viscosity gradient will determine to a certain extent the location of the displacement just mentioned, in that flow through the papers within the inner half of the insulation is doubtless greatly facilitated as compared with that in the outer parts. In agreement with this conclusion it is found that the majority of voids and dry

spots are located in the inner half of the insulation. This is undesirable because the field intensity near the conductor is substantially higher than near the sheath, and thus the probability of ionization and subsequent deterioration is high.

There are several designs to counteract this unwanted occurrence. A recent one is that by W. A. Del Mar,[3] utilizing two different types of paper, a more porous one for the inner layers, and a denser one, possessing a higher modulus of elasticity, for the outer layers. The compressive action of the latter prevents to a certain extent void formation in the neighborhood of the conductor.

A more radical departure from the "solid" cable is the compression cable,[4,5] the principle of which is that the whole cable is placed in a steel or a second lead pipe, the interspace containing gas of 200 lb. per sq. in. This pressure makes the lead sheath collapse during the cooling period, so that the mechanism of void formation as determined by the viscous properties of the oil cannot become effective. Usually an oval-shaped cross section (Fig. 64) is an added feature of the compression cable. When the internal pressure increases because of heating, the sheath will not expand uniformly as a circular lead sheath would

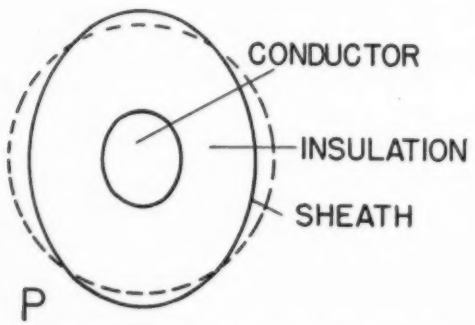


FIG. 64. Breathing of a compression type cable.

do, but will undergo a deformation, assuming a shape of lesser eccentricity (dotted line), thus accommodating a larger volume of oil. Upon cooling, the external pressure will flatten the cross section to its original shape, which thus appears to hinge on four points like *P* in the figure.

(c) *Migration.*—A third way in which viscosity plays a dominating role is in connection with the position of cables, as in hilly country or at terminals, where a gradient of elevation exists. In such cases a pressure head acts along the cable and a flow of oil will take place longitudinally (not radially as in the previous cases). Again the rate of migration will be determined by

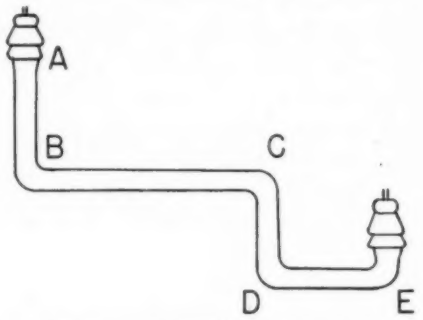


FIG. 65. Diagram illustrating oil migration in cables, according to Scott.

the viscosity, and thus, since migration is evidently undesirable, compounds of high viscosity at operating temperatures (up to 70°C) are selected as impregnants.

T. R. Scott[6] among others carried out considerable work in this field, and the effects of migration can best be illustrated in Fig. 65. It shows diagrammatically a cable running vertically at sections *A–B* and *C–D*, and horizontally at *B–C* and *D–E*. The cable is terminated at both ends by so-called potheads that contain either gas cushions or bellows, allowing a free inflow and outflow of compound. The pressure heads *A–B* and *C–D* cause the oil to migrate longitudinally from left to right, involving a decrease of pressure in the pothead *A* and an increase at *E*.

The flow along *B–C* is determined by pressure head *A–B* and the resistance of the length *B–C*; similarly the flow in *D–E* is determined by the pressure head *C–D* and the resistance *D–E*. If we assume that *B–C* is much longer than *D–E*, then the resistances of the respective branches are in the same ratio and the respective flows are in an inverse ratio. The result of this difference, the two pressure heads being equal, is an excess of the outflow at *C* over the inflow at the same point —in other words, a formation of voids.

Scott also carried out actual measurements of the value of *R* per centimeter of cable. The flow takes place along the conductor and below the

TABLE X. Flow resistance of cable conductors in longitudinal direction, according to Scott.

| Cross section of stranded conductor, sq. cm | Flow resistance, $R$ per cm cable in c.g.s. units |
|---|---|
| 1.0 | 35,000 |
| 1.3 | 20,000 |
| 1.6 | 12,000 |
| 2.0 | 8,000 |

sheath. Values of $R$ for stranded conductors of varying cross section are shown in Table X.

An effective method of preventing longitudinal viscous flow of the compound in cables is the application of so-called stop joints. It is common practice to limit individual lengths of cable to about 300 feet and join these lengths together. It is possible to use a solid or plastic type of insulating material in the joints that will prevent a free flow of the compound through the joint. Thus migration is restricted to individual sections, and cannot assume high values.

Scott suggests the use of polymeric styrene in stop joints. Paper strips are previously impregnated with the monomer, then polymerized and separated. Such papers are then used in preparing the joint in a cold process, so-called since no subsequent polymerization by heat is required. The single styrenated paper of 5-mil thickness has a breakdown strength of 1500 volts per mil. Such tapes are now produced on a commercial scale.

### *37. Chemical Processes and Viscosity*

A second field relating to insulating liquids in which viscosity plays an essential role is that of certain chemical processes the course of which can be followed by noting the increase in viscosity. The chemical processes are condensation and polymerization, the latter having been discussed already in Section 30. Both of these processes are accompanied by an increase of the molecular weight, the former with and the latter without an evolution of hydrogen gas.

Reverting to Section 21, it was shown that the constant $B$ of Eq. (68) increases with the molar heat of vaporization, thus with the molecular weight. It is essentially the same $B$ constant that at ordinary temperature determines the variation of $\eta$ in a given series of materials, as can be seen from Fig. 31, where the height of the lines increases with their slope. Thus it can be concluded that the viscosity of a substance will increase with an increasing degree of polymerization. This relation, by the way, should not be confused with the similar relation of Staudinger (Section 30) concerned with colloidal solutions of macromolecular substances. In the present case we deal with homogeneous liquids, although it cannot be denied that in certain instances both mechanisms might act together.

Several interesting examples can be quoted to illustrate the significance of the above-mentioned relation.

(a) In the so-called "Voltol process"[7] an industrial application of the phenomenon was attempted. Lubricating oils (see Chapter X) must have a certain minimum viscosity and the Voltol process is aimed at producing such oils from low viscosity materials by means of an electric discharge in hydrogen gas at reduced pressure. Thus the molecular weight of mineral oils could be raised from 400 to 650. Viscosity of around 0.15 poise could be raised to about 3. The processes involved seem to be both condensation and polymerization.

(b) In high voltage cables a similar process takes place, wherever voids are present between

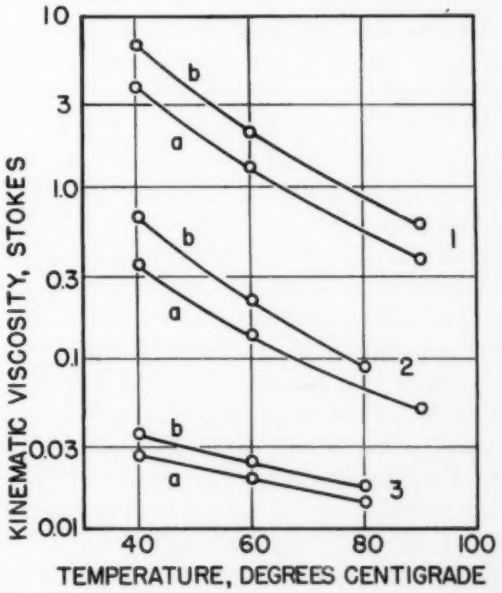


FIG. 66. Viscosity *vs.* temperature of hydrocarbons (after Sticher and Thomas). (a) Before bombardment; (b) after bombardment. (1) Synthetic oil; (2) synthetic turpentine polymer; (3) *n*-hexadecene.

layers of impregnated paper. In such voids gaseous ionization takes place, and this discharge process polymerizes the oil. The result is the formation of highly viscous and finally solid wax-like products. The present writer has described several methods[8] for the study of this process. A recent interesting study was published by Sticher and Thomas,[9] attempting a quantitative evaluation of the chemical changes. Also they extend the research to compounds of known chemical constitution. From among the many results of this research one particular item of interest is presented here. Figure 66 shows the viscosity as a function of temperature of three particular liquids (*a*) before bombardment (*b*) after bombardment at 60 cycles for four hours. The liquids are specified in the caption to the figure. It can be seen that about 50 percent increase in viscosity has occurred during four hours of treatment. In contradiction to the Voltol process the changes in high voltage cables are not welcome, since they are signs of a progressive deterioration of the insulation. According to Sticher and coworkers[9a] and to Shanklin,[10] however, wax formation might lead to self-healing and stabilization in certain cases, as in the low gas-pressure cable, operating at around 15 lb. per sq. in. gauge pressure. In both instances quoted, viscosity increases as the molecular weight increases, and is a good measure of the progress of the chemical reaction.

(c) A third interesting example is polystyrene, of which mention was made in Section 36 in connection with Scott's work on terminals and joints. The polymerization of monostyrene has become a process of considerable technical importance, and thus it is of interest that its progress can be followed by viscosity measurements as in the foregoing cases.

Polymerization of the monomer occurs fairly easily, in fact, much too easily for shipping and storing of the material, during which time a polymerization is unwanted. It was found that certain added materials act as inhibitors. The monomer then can be stored without any difficulty. It is of interest to find out how such a monomer polymerizes if it is heated to the proper temperature. This comparison can be made easily by following the changes in viscosity with time. Such data of Scott are shown in Fig. 67 for

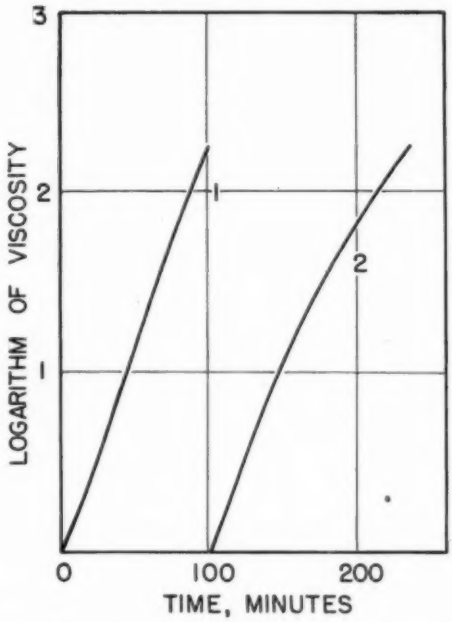


FIG. 67. Viscosity of styrene *vs.* time of polymerization, after Scott. (1) Pure styrene; (2) styrene+0.05 percent quinone.

a heating temperature of 120°C. While curve 1 refers to the pure monomer, curve 2 refers to styrene to which was added 0.05 percent of quinone as inhibitor. It can be seen that an induction period of 100 minutes elapses before the process starts, but after that the rate of the reaction is the same as for the pure material. The change of viscosity in this case is considerable, 1 : 100 in 100 minutes.

If too much inhibitor has been added, it is necessary to remove it by means of a distillation process before polymerization will start. Addition of only small amounts is, therefore, necessary if the optimum results are to be obtained.

### *38. Electrical Conductivity and Viscosity*

The third field relating to insulating liquids in connection with viscous processes is their electrical conductivity. It is a long established fact that the term "insulating" does not mean zero conduction of current; it serves only to designate a range of conductivity sufficiently low for the currents not to cause any serious disturbance from the standpoint of the electrical apparatus in which the liquid is used. The small current across the liquid in these cases is an unwanted occurrence only if it increases with time, since

it then might reach a level causing interference with the chief function of the appliance. Thus the concept "insulating" is purely relative as it depends upon the appliance in question. In a rough way, however, it is useful to consider liquids of a conductivity of an order less than $10^{-10}$ mho/cm as "insulating."

The discussion to be presented in this section will be only sketchy, since there are many other detailed and complete treatments on the subject. First the fundamental equation controlling ionic mobility will be discussed, and it will be shown how the latter depends upon the viscosity of the liquid. The viscosity is, however, only one factor in the electrical conductivity since the latter depends also upon the concentration, charge, and size of the ions. Considering the importance of the question, a little digression along these lines will be made to point out the experimental methods for determining all fundamental factors involved.

In order to fix our ideas, the general case will be considered in which at least one of the two ions present (cations and anions) are large colloidal aggregates. This is indicated in Fig. 68 for the case of large anions, assumed to contain five (generally $z$) elementary units $e$ of electricity. The cations can be large, too, or small as shown

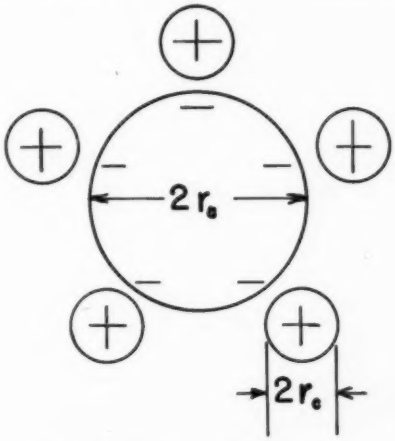


FIG. 68. Diagram of colloidal ion.

in Fig. 68, carrying only one unit each. The number of such composite units per cm³ should be $n$. The radii of the two types of ions are $r_a$ and $r_c$, respectively.

The conductivity $\sigma$ is the total charge flowing through 1 cm² during 1 sec. if unit field strength is applied. The charge involved in each unit shown in Fig. 68 is $ze$; thus the charge per cm³ is $nze$. We now define ionic mobilities $m_a$ and $m_c$ such as to give the absolute velocities in unit field strength. The two ions having opposite signs, their opposite velocities have to be added if the total charge flowing across 1 cm² is to be computed. Thus a prism of base 1 and height $(m_c+m_a)$ will be displaced across 1 cm² during 1 sec. The charge contained in this prism is $nze(m_c+m_a)$; thus

$$\sigma = nze(m_c+m_a). \tag{104}$$

It now remains to determine the mobilities. In Section 26 Stokes' equation was discussed (Eq. (78)), as giving the viscous resistance of a sphere in a liquid. Although it is strictly valid only for spheres much larger than the molecules of the liquid, Einstein suggested its use for ions as well, and this conception proved to be quite fruitful. The electric force acting on the anion, for instance, is $ze$ if the field strength is unity; thus the condition for equilibrium will be:

$$ze = 6\pi\eta r_a u;$$

hence, the mobility:

$$m_a = ze/6\pi\eta r_a. \tag{105}$$

A similar equation with $z=1$ will be valid for the cations of Fig. 68. In these equations $\eta$ is the viscosity of the medium.

Equations (104) and (105) give the electrical conductivity as a function of the viscosity of the liquid and the number, charge, and size of the ions.

The correctness of Eq. (105) as to the influence of $\eta$ has been proved by several means. One of the proofs is the so-called Walden rule, stating that the mobility of ions is inversely proportional to the viscosity of the solvent, a rule found empirically before the theoretical Eq. (105) was established. Table XI, after data of Ulich,[11] gives the mobilities $m$ and the products $m\eta$ for a few ions in different organic solvents. While the constancy of the product $m\eta$ for the ion $N(C_2H_5)_4^+$ is quite remarkable, the agreement is less close for the other ions, but sufficient to show the validity in respect to $\eta$ of Eq. (105).

Another way of checking the viscosity relation is by varying the temperature. In this regard the

TABLE XI. Ionic mobilities at 25°C after Ulich.

| Solvent | $100\eta$ | | $N(C_2H_5)_4^+$ | $N(CH_3)_4^+$ | $Na^+$ | $J^-$ |
|---|---|---|---|---|---|---|
| Methyl alcohol | 0.545 | $m$ | 54 | 65 | 46 | 61 |
| | | $m\eta$ | 0.294 | 0.354 | 0.251 | 0.332 |
| Ethyl alcohol | 1.087 | $m$ | 27.2 | 29.2 | 21.9 | 26.3 |
| | | $m\eta$ | 0.295 | 0.317 | 0.238 | 0.285 |
| Acetone | 0.316 | $m$ | 93.1 | 102.8 | 68.6 | 115.9 |
| | | $m\eta$ | 0.294 | 0.325 | 0.217 | 0.366 |
| Furfural | 1.494 | $m$ | 19.6 | | 12.7 | 28.4 |
| | | $m\eta$ | 0.293 | | 0.190 | 0.424 |
| Aceto-nitrile | 0.346 | $m$ | 85 | | 81 | 109 |
| | | $m\eta$ | 0.294 | | 0.28 | 0.38 |
| Epichlor-hydrine | 1.03 | $m$ | 28.6 | 32.8 | | 35.4 |
| | | $m\eta$ | 0.295 | 0.338 | | 0.365 |
| Pyridine | 0.890 | $m$ | 35 | | 25 | 47 |
| | | $m\eta$ | 0.294 | | 0.22 | 0.42 |

fact has to be borne in mind that the temperature affects not only the viscosity $\eta$ but also the other characteristic quantities, $n$, $r$, and $z$; thus the final effect upon $\sigma$ might be very complicated indeed. However, in certain simple systems it could be proved without doubt that $\sigma$ varies with the temperature inversely to $\eta$, the product $\sigma\eta$ being constant. The validity of this relation is known from experience with aqueous solutions of totally dissociated electrolytes, and has been established experimentally for insulating oils by J. B. Whitehead[12] and co-workers.

On the basis of this relation, several conclusions can be drawn. One is of a general and practical nature, simply stating that in selecting insulating oils for cables or other high voltage equipment, oils of higher viscosity should be given preference, from the standpoint of conductivity, since, other properties being constant, the conductivity will decrease with increasing viscosity. Of course, other factors often will decide the choice in a contrary direction, for instance, mechanical considerations, as shown in Section 36, or chemical stability both with regard to electronic bombardment and oxidation. The chemical stability does not depend directly upon viscosity, but since more viscous oils have a higher molecular weight, and since this, to a certain degree, is an indication of lesser stability, there is sometimes an inverse correlation between viscosity and chemical stability.

Another consequence of the $\sigma(\eta)$ relation is of a quantitative nature. If measurements of both $\sigma$ and $\eta$ are taken, for a series of oil samples or for a series of temperatures, it is possible to carry out an analysis of the data by considering the product $(\sigma\eta)$. In doing this the viscosity effect is, so to speak, eliminated and only the other effects upon $\sigma$ are left. If, for instance, it is assumed that $r$ and $z$ remain constant, the change of the product $(\sigma\eta)$ will tell us directly how $n$, the concentration of the particles, changes owing to varying electrolytic dissociation. If, on the other hand, there is additional information to the effect that electrolytic dissociation is complete, thus constant, then the variation of $(\sigma\eta)$ is a measure of the changes occurring in $z$ and $r$ because of ionic association. In the general case both the degree of electrolytic dissociation and the degree of ionic association will change. The reason is that an ionic association (formation of complex colloidal ions) reduces the concentration of single ions, and thus shifts the electrolytic equilibrium

$$\text{undissociated molecule} \rightleftarrows \text{single ions}$$

in the direction of the upper arrow.

Such a case can be seen in Fig. 69, referring to the equivalent conductance of tetraisoamylammonium nitrate in dioxane-water mixtures at

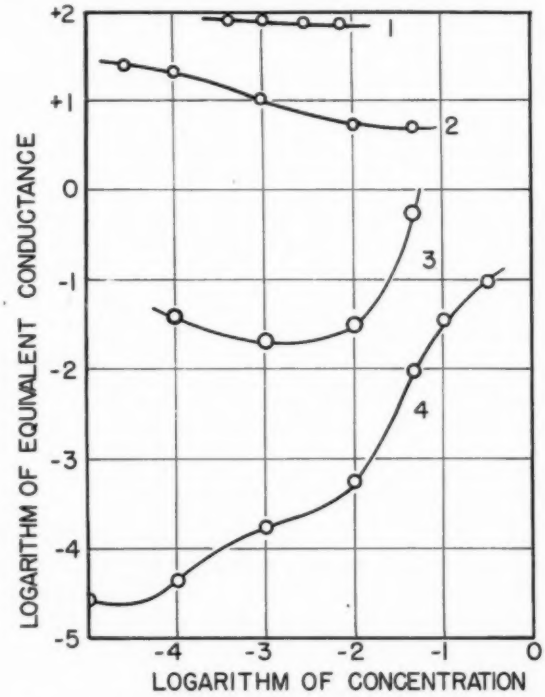


FIG. 69. Equivalent conductance of tetraisoamylammonium nitrate *vs.* concentration, after Kraus and Fuoss. Solvent: water-dioxane mixtures: (1) pure water; (2) 85 percent dioxane; (3) 96 percent dioxane; (4) pure dioxane.

25°C, obtained by Kraus and Fuoss.[13] The equivalent conductance $\Lambda$, defined by

$$\Lambda = 1000\sigma/c, \qquad (106)$$

where $c$ = concentration in equivalents per liter, is useful in comparing solutions of different concentration, since it gives the conductance per unit concentration, and thus depends on the secondary changes in $n$, $r$, and $z$, as caused by a change in the total concentration. Thus, for a totally dissociated electrolyte, $\Lambda$ should be independent of the concentration (disregarding the so-called Debye effect), whereas for weak electrolytes, having a finite dissociation constant, $\Lambda$ should decrease with increasing concentration.

Figure 69 indicates several curves referring to increasing percentage of dioxane and decreasing dielectric constant. Whereas $\Lambda$ for water as solvent is constant, it decreases for a mixture containing 85 percent dioxane. Thus it appears that the electrolyte is strong in water and weak in dioxane. However, the curve for 96 percent dioxane goes through a minimum, and that for 100 percent dioxane increases practically through its whole course. The explanation for this increase, according to Bjerrum,[14] as well as to Kraus and Fuoss, is the formation of triple ions by means of an association of single ions and undissociated molecules. This process shifts the electrolytic equilibrium towards increased dissociation, thus increasing the total number of ions.

The process illustrated by this case is probably very general in insulating liquids (characterized by low dielectric constants) and an analysis of data on $\sigma$, in which the first step is the building of the product $(\sigma\eta)$, will be helpful in discovering similar occurrences. The plots of the product $(\sigma\eta)$ *versus* temperature in the quoted work of Whitehead often show deviations from a horizontal line for reasons similar to those just discussed.

Balsbaugh and co-workers,[15] conducting very extensive researches on deterioration of oils, also analyze their recent data, first reducing the conductivity values to the product $(\sigma\eta)$.

Caution is required in interpreting $\sigma$ *vs.* temperature curves on oils when extended to the very low temperatures at which the oil gradually solidifies. The oil first becomes a gel, as described in Chapter VIII, in separating into a

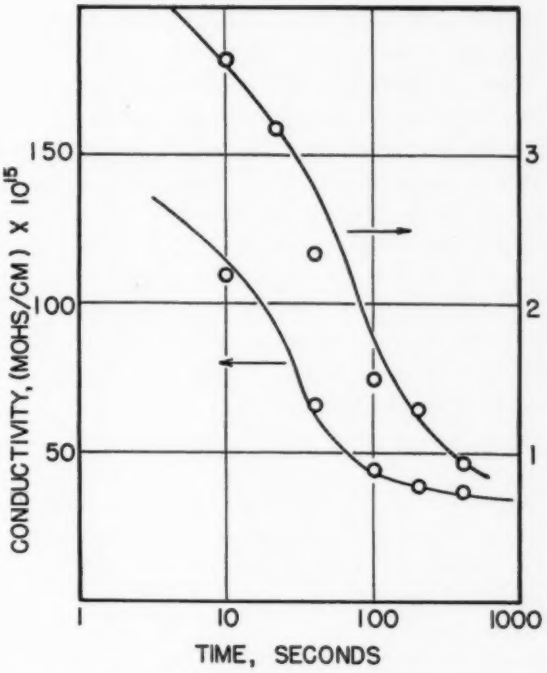


FIG. 70. Conductivity *vs.* time obtained from transients on two particular oils after J. B. Whitehead. ○ Experimental points. Full lines computed after an equation of Gemant.

liquid and a crystalline phase. The electrical conductivity of such a heterogeneous system is then a sum of the two components, to be calculated with due regard to the geometric shape of the two phases. In such instances unusual $\sigma$-temperature curves are obtained, as shown and analyzed by the writer[16] who found that the conductivity of oils passes through a minimum with decreasing temperature. Similar curves were obtained by W. Jackson for paraffin wax.

Several investigators prefer the measurement of $\sigma$ by means of alternating voltages instead of d.c. voltages. In such cases specific a.c. losses, which generally show more or less sharp peaks at certain critical frequencies, are superimposed upon the d.c. conductivity. If a.c. data are obtained, it is useful to attempt a separation of d.c. and specific a.c. losses, before conclusions regarding the nature of ions are drawn. Such separation can be made if $\sigma$ *vs.* frequency is measured up to fairly low frequencies, and $\sigma$ is then extrapolated towards zero frequency. In homogeneous liquids such precaution is not necessary, as specific losses at power and acoustical frequencies are zero; thus the correct d.c.

conductivity can be measured by means of alternating current.

Definite deviations from this simple behavior occur if the frequency is approaching radio-frequencies and higher. In such cases rotation of dipolar constituents causes specific losses at certain characteristic frequencies. This subject will not be pursued here; more will be said about it in connection with solids in Chapter XIV of this monograph. It will suffice to point out that the characteristic frequency $f_0$ is connected with the viscosity $\eta$ of the liquid by the relation deduced by Debye

$$f_0 = kT/4\pi\eta r^3, \qquad (107)$$

where $r$ = radius of dipolar molecule. Measurement of $f_0$ and knowledge of the viscosity allow the radius of the rotating molecules to be computed.

The measured a.c. conductivity differs from the d.c. value also in cases of inhomogeneity in both a sol and a gel. An interpretation of results in these cases might be very involved, but enlightening if successful. Inhomogeneous systems of this kind were successfully investigated in a series of papers by J. D. Piper and coworkers[17] on the conductivity of insulating liquids to which electrolytes of known chemical constitution and in controlled amounts were added.

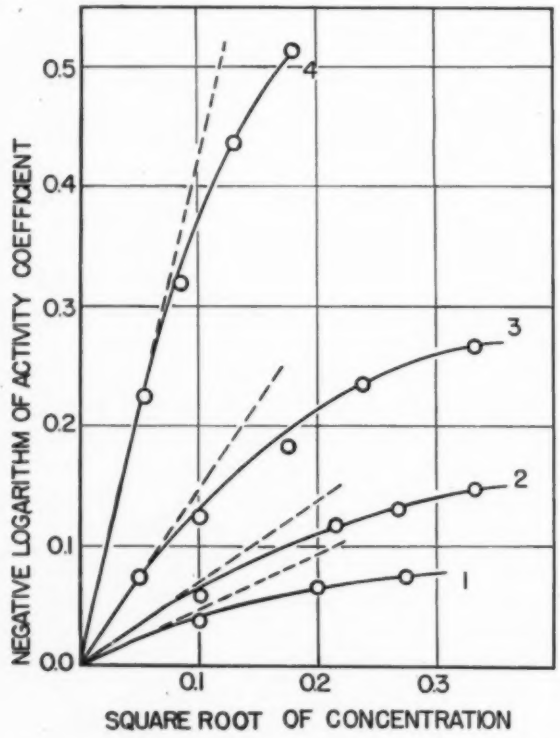


FIG. 71. Activity coefficient *vs.* concentration of hydrochloric acid in water-dioxane mixtures, after Harned and Morrison. (1) Pure water; (2) 20 percent dioxane; (3) 45 percent dioxane; (4) 70 percent dioxane.

Besides d.c. and a.c. measurements of conductivity a third method is sometimes used with success, i.e., transient measurement. Carried out some time ago by J. B. Whitehead, and recently by the Balsbaugh group, it proved very useful. The writer[18] tried to compute absolute mobilities from such current-time curves. An equation was set up, describing the characteristic decrease of conductivity with time on the basis of an accumulation of ions near the electrodes. Figure 70 shows two experimental curves obtained by Whitehead on two particular oils. The corresponding full lines are drawn according to the equation mentioned, which then allows the mobilities of the cations and anions to be computed. In case of the lower curve the two mobilities obtained were: $3.1\times10^{-7}$ and $0.37\times10^{-7}$ cm/sec. per volt/cm. Knowing the viscosity (1.1 poise) and assuming $z=1$, the two radii computed from Eq. (105) are $2.5\times10^{-7}$ and $2.1\times10^{-6}$ cm. From Eq. (104), again assuming $z=1$, the number of charge units becomes $2\times10^{12}$ per cm$^3$.

Thus, the role of viscosity in the electrical conductivity of insulating liquids has been demonstrated in this section, showing that a number of other factors, too, are involved in establishing a definite conductivity. Because of the relatively large numbers of variables, conductivity and viscosity measurements of the type described are not sufficient for the evaluation of all the data. It will be imperative to use entirely different methods as well.

The ultracentrifuge, so useful in the field of synthetic polymers (Section 30) for evaluating particle sizes, does not hold out much hope in this connection, because of the small number of charge carriers. The use of the electron microscope may be more feasible, because the visibility of the particles might allow by some means an identification of the ions among other neutral particles. The success of the instrument in other fields—viruses,[19] for instance—certainly invites

its use in the present problem as well. If the migration in an electrical field could be observed under the instrument—a technique yet to be developed, but not essentially impossible—then the mobility $m$ and radius $r$, and thus the charge $z$, would become known, at least for particles above a certain size.

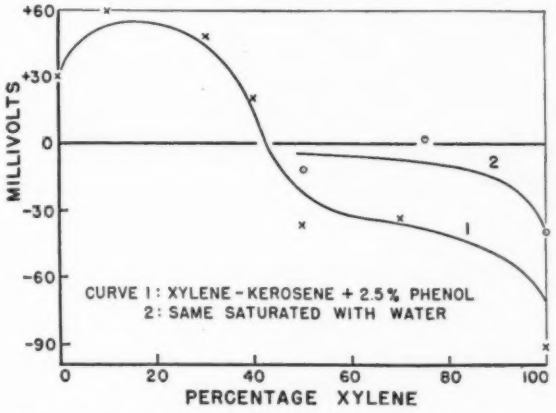


FIG. 72. E.m.f.'s of cells containing boundaries copper-copper oleate solutions in insulating liquids, after Gemant.

Another method that in certain instances would give directly the last remaining variable, namely the number of particles $n$, is the electrochemical potentiometric method. In aqueous and alcoholic solutions this method gives excellent results. It measures specifically the concentration, more rigorously: activity of certain ions, according to the reversible electrode used. In the cell

platinum (hydrogen)/liquid containing
hydrochloric acid in solution/
(silver chloride) silver,

for instance, the hydrogen ion activity can be obtained by measuring the e.m.f. of the cell. Figure 71 after Harned and Morrison[20] should serve as an indication that precision data can be obtained on dioxane-water solvents of dielectric constants as low as 17.7. The data deduced from e.m.f. measurements on the cell above connect the logarithm of the activity coefficient $f$ (a measure of the Debye effect) with the concentration. The dotted lines refer to coefficients computed from equations valid for dilute solutions, the agreement with experiment being very good. With such data on hand the $p$H of any HCl solution in the dioxane-solvents, in other words the number $n$ for the $H^+$ and $Cl'$ ions, can be obtained by means of an e.m.f. measurement.

The writer[21] tried to obtain reproducible e.m.f. data on liquids of even lower dielectric constant. Figure 72 refers to the cell copper/liquid/liquid (copper oleate)/copper in xylene-kerosene-phenol mixtures (positive if right end of cell is positive). An interpretation of these data particularly of the reversed (negative) e.m.f.'s has not yet been accomplished. A continuation of this research with better defined systems is now under way, and the transference number (ratio of ionic mobilities) is computed from data on concentration cells using solvents of a dielectric constant as low as 2.7.

## *Bibliography for Chapter IX*


1. L. Emanueli, *High Voltage Cables* (Chapman, 1929).
2. C. J. Beaver and E. L. Davey, Conf. Internat. Gr. Rés. Elect., No. 208 (1939).
3. Wm. A. Del Mar, Trans. A. I. E. E. **60**, 206 (1941).
4. P. V. Hunter, P. Dunsheath, and L. G. Brazier, Conf. Internat. Gr. Rés. Elect., No. 204 (1939).
5. K. S. Wyatt and F. W. Main, Conf. Internat, Gr. Rés. Elect., No. 235 (1939).
6. T. R. Scott and J. K. Webb, Elec. Communication **16**, 276 (1938); and **17**, 88 (1938).
7. G. Glockler and S. C. Lind, *Electrochemistry of Gases and Other Dielectrics* (Wiley, 1939).
8. Andrew Gemant, World Power **21**, 235 (1934).
9. Joseph Sticher and D. E. F. Thomas, Trans. A. I. E. E. **58**, 709 (1939).

9a. Joseph Sticher, D. E. F. Thomas, C. D. Robb, and F. M. Hull, *The Effect of Corona Discharge on Cable Insulation*, National Research Council meeting, Pittsburgh, (Nov. 1938).

10. G. B. Shanklin, Trans. A. I. E. E. **58**, 307 (1939).
11. H. Ulich, Trans. Faraday Soc. **23**, 388 (1927).
12. J. B. Whitehead, *Impregnated Paper Insulation* (Wiley, 1935).
13. C. A. Kraus and R. M. Fuoss, J. Am. Chem. Soc. **55**, 21 (1933).
14. See, for instance, D. A. McInnes, *The Principles of Electrochemistry* (Reinhold, 1939).
15. J. C. Balsbaugh, A. H. Howell, and A. G. Assaf, Ind. Eng. Chem. **32**, 1497 (1940).
16. Andrew Gemant, J. Petrol Technol. **22**, 646 (1936).
17. J. D. Piper, C. C. Smith, N. A. Kerstein, and A. G. Fleiger, Ind. Eng. Chem. **32**, 1510 (1940).
18. Andrew Gemant, Phys. Rev. **58**, 904 (1940).
19. W. M. Stanley, *Problems and Trends in Virus Research* (University of Pennsylvania Press, 1941), p. 15.
20. H. S. Harned and J. O. Morrison, J. Am. Chem. Soc. **58**, 1908 (1936).
21. Andrew Gemant, Trans. Electrochem. Soc. **78**, 49 (1940).

# Bactericidal Radiation

BY A. PAULUS

*Westinghouse Electric and Manufacturing Company, Lamp Division, Pittsburgh, Pennsylvania*

SCIENCE is gradually selecting and studying various groups of waves in the electromagnetic spectrum. These groups are studied for the purpose of finding their characteristics and their application to human welfare. While the electromagnetic spectrum extends to and beyond the infinitely short cosmic waves on one side and through the visible and heat regions and radio waves of various lengths on the other side, consideration is here given to a small group of waves in the ultraviolet region (Fig. 1).

Just as visible light is made up of different wave-lengths which are separated by a prism into the rainbow colors, so the ultraviolet region may be separated into groups which have widely differing effects. Beyond the visible, the group of waves of 4000 to about 3300 angstroms are chemically active, affect photographic plates and, in common with still shorter wave-lengths, cause fluorescent and phosphorescent materials to glow.

A second group measuring 3300 to 2850 angstroms are biologically effective causing erythemal and tanning reactions, increasing vitamin D, and preventing rickets. The effective bactericidal wave-lengths 2850 to 2000 angstroms have been receiving much attention during the past few years as the development of suitable generators makes possible the practical application of bactericidal radiations.

Below 2000 angstroms is a group of wave-lengths which produce ozone in the air. A small proportion of these ozone producing waves, together with the more active bactericidal waves, produces the best conditions for the destruction of bacteria and mold.

## EFFECT OF ULTRAVIOLET ON BACTERIA

In 1877 Downes and Blunt showed that bacteria were killed by sunlight. The lethal effect was attributed to mild and extended oxidation or in short to heat. Later the killing effect was attributed to the production of hydrogen peroxide in the aqueous media. Both these early theories have been disproved by experiments in which the lethal effect was produced independently of heating or oxygen and where the chemical action in the media was negligible. As a result of studies by Clark, Norton, and others and confirmed by Bayne, Jones, and Van der Lingen, it has been generally accepted that the bactericidal effect of selected wave-lengths of

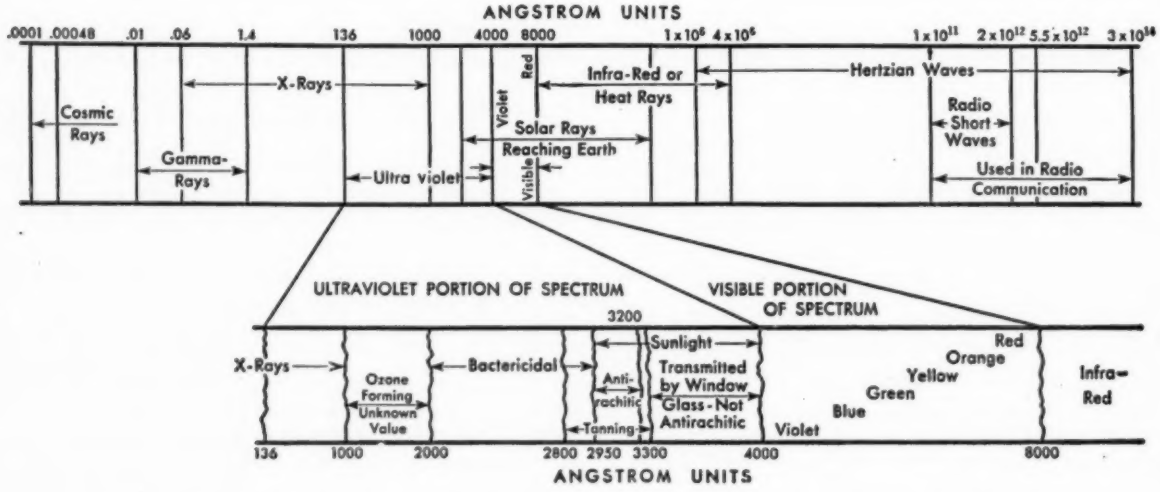


FIG. 1. The radiant energy spectrum. The Sterilamp is an efficient generator of radiation in the bactericidal band of the ultraviolet spectrum.

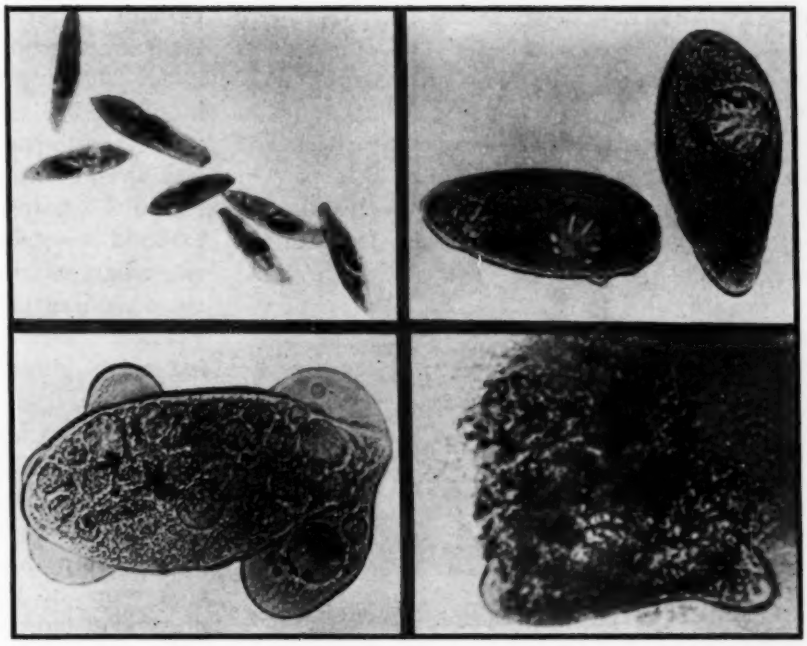

FIG. 2. Progressive stages in the killing of bacteria by short-wave radiation. At the upper left are normal paramecia. At the upper right are two paramecia after thirty seconds of irradiation, showing distension just beginning. Distension continues in the third view, followed by bursting of the cell wall. Death of a bacterium is caused by a change in the osmotic tension of the cell wall, which causes the organism to swell and break, as shown in the lower right-hand corner.

ultraviolet is the result of direct photo-chemical action on the organisms. The disintegration of micro-organisms under radiations, principally of 2537 angstroms, is shown in Fig. 2, where paramecia which are single cell organisms found in stagnant water, are exposed to the radiations from a Sterilamp. The picture shows how the radiations cause the organism to swell, blister, and finally disintegrate. Bacteria are so small that the changes which take place because of irradiation cannot be shown by an ordinary microscope, but they are probably similar to the changes in the much larger paramecia.

## ULTRAVIOLET GENERATORS

The sun is considered the only natural source of ultraviolet but only a small part of the short wave-lengths reach the earth because of the filtering action of the atmosphere. The shortest wave-lengths which can penetrate the atmospheric blanket measure about 2900 angstroms, and the amount of this radiation is only about one millionth as great as that at 3130 angstroms. The ultraviolet radiation from the sun in the bactericidal region is great enough to have been noted, but it is weak when compared to the output of many artificial sources.

Practically all artificial sources of ultraviolet radiation, with the exception of the carbon or iron electrode arc lamps, have one element in common—mercury vapor. Electrical discharges through mercury vapor produce more radiation in the ultraviolet region than similar discharges through any other known vapor or gas. The earliest and best known source of ultraviolet is the quartz mercury arc lamp which has an envelope of fused quartz and at least one electrode of mercury. The output of ultraviolet can be shifted by varying the temperature and pressure of the mercury vapor. Increasing the temperature and pressure produces more of the longer wave-lengths and the high pressure mercury lamp becomes an efficient source of visible light. If the pressure is kept low, that is, if it can be measured by a few millimeters of mercury column, the radiation produced by an electric current is very largely in the bactericidal region with maximum output at 2537 angstrom units.

These low temperature, low pressure conditions are inherent in the Sterilamp, Fig. 3, and make it an efficient bactericidal agent, which is inexpensive to operate, has long life with small change in output, does not heat up the surrounding air, and gives wide distribution of radiation. The glass tube which forms the lamp is made of glass which cuts off the radiation slightly below 2000 angstroms, thus limiting the production of

ozone so that the concentration does not rise to more than one part in three or four million parts of air. It is also true that radiation of 2537 angstroms breaks up ozone and thus acts as an automatic regulator of ozone concentrations. The slight amount of ozone developed is helpful in controlling the development of mold and bacteria in spaces which are shaded from direct radiation.

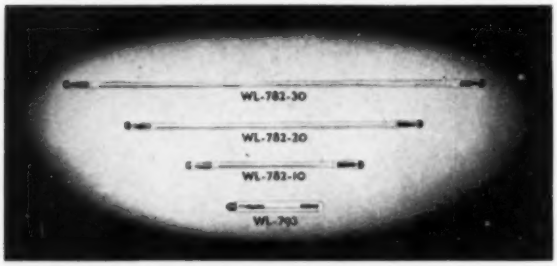


FIG. 3. Sterilamps.

The electrical discharge in a Sterilamp is between unheated electrodes, because this permits simple construction of the lamp and the current controlling transformer, permits control of the output of the lamp by changing the primary voltage of the transformer, makes a lamp which will operate satisfactorily under varying temperature conditions, and will have a long effective life. Deterioration of output comes gradually because of changes in the glass known as solarization and to a slight extent to blackening of the tube by vaporization of the electrode material.

## MEASUREMENT OF ULTRAVIOLET

Much of the recent advance in the application of ultraviolet radiation is due to improvements in the equipment and methods for measuring the different groups of wave-lengths in the ultraviolet spectrum. Three photo-cells developed by Dr. H. C. Rentschler, head of Westinghouse Research Department, cover the principal groups of wave-lengths in the ultraviolet spectrum. For measurement of the almost complete ultraviolet region there is a photo-cell having a thorium cathode which is responsive to a spectral range from 3750 angstroms to about 200 angstroms, with a maximum response at 2600 angstroms. Another photo-cell, made up with a tantalum cathode, responds to wave-lengths from 2950 to 2000 angstroms with maximum sensitivity at about 2400 angstroms. This photo-cell is useful in measuring the bactericidal region of ultraviolet as it is not sensitive to the wave-lengths near the visible edge of the ultraviolet spectrum. A third photo-cell, with a platinum coated cathode, is not affected by radiations above 2000 angstroms and, therefore, is capable of measuring the wave-lengths which produce ozone in the air.

The ultraviolet radiations in the regions affecting these photo-cells cause a minute electric current to flow through the tube and charge a condenser which discharges through a relay tube which in turn causes a larger condenser to discharge through the coil of a relay which operates a counting mechanism with an audible click. After discharge, the condensers again charge up and the action is repeated as long as ultraviolet light reaches the electrodes and current flows through the photo-cell. As each click represents a definite amount of ultraviolet radiation for which there is no generally accepted unit, the meter is called a click meter (Fig. 4). Each click may represent any desired quantity of radiation by varying the size of the condenser in the circuit of the photo-tube. However, the standard meter is calibrated so that one click represents 220 micro-watt seconds.

FIG. 4. The new Westinghouse portable a.c. ultraviolet meter. Shown at the left is the photo-tube in its separate housing, which fits into the front compartment of the carrying case when not in use.

Another small indicating meter is an adaptation of the foot candle meter. A filter which cuts out about 95 percent of the visible light but permits passage of ultraviolet is placed over the window of the meter, and a fluorescent screen is placed next to the filter. Ultraviolet light which strikes the screen is converted into visible light and acts on the light sensitive cell which operates the pointer. This meter is very convenient for testing ultraviolet sources, such as the Sterilamp, which give off little heat but it is not reliable for hot sources, as the cell is sensitive to heat as well as light, and the meter must be placed very close to or in contact with the lamp to get a reading.

## APPLICATIONS OF STERILAMPS

The development of an ultraviolet generator which operates at temperatures only a few degrees above the surrounding air requires but a small amount of power, has a fairly uniform output and long life, opens up almost unlimited possibilities for usefulness. Early applications of Sterilamps were for the preservation of meat held in refrigerators. The radiations are effective in preventing or greatly reducing the development of mold and slime during the storage and marketing periods. Installations of Sterilamps in retail meat stores reduce trimming losses and, in case of failure of the refrigeration equipment, insure against meat spoilage until repairs can be made. Displays in refrigerated cases are protected from contamination by air-borne organisms, and the sales appeal is strengthened. The meat packer and wholesaler use Sterilamps to keep their products free of organisms which cause spoilage and thus supply the retail trade with meats having low bacterial contamination and, consequently, of superior keeping qualities and flavor (Fig. 5). Protection of meat in this way has made economically possible the tenderizing of beef in a few days at temperatures of 60°F or more. Thus, only about one-tenth of the time is required by this new and patented process compared to the former methods of aging at about 34°F.

FIG. 5. Beef may be made uniformly tender and palatable in three days in this room. Weekly capacity of meat tenderizing in this room by the Westinghouse Tenderay Process is approximately 144,000 pounds. The ultraviolet lamps on the ceiling bathe the meat and air in the room with invisible rays deadly to mold and bacteria, hence prevent spoilage. A relative humidity kept at 90 percent prevents dehydration, which causes shrinkage and loss of juiciness in meat. A temperature of 60°F speeds up the natural chemical reactions which break down tough tissues and bring about tenderizing. Those elements, together with a scientifically predetermined technique in handling, make up the Tenderay Process.

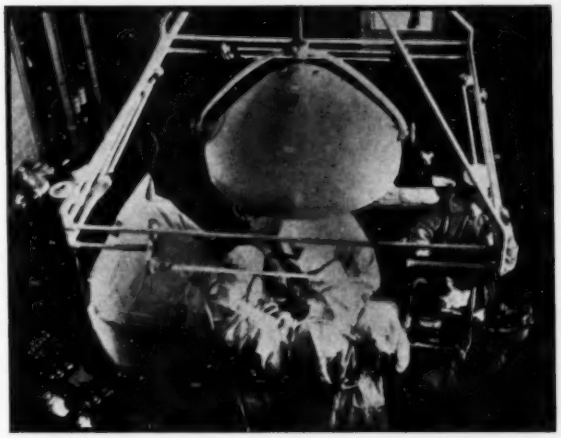

FIG. 6. Sterilamps mounted above the operating table in this operating room in the Duke Hospital, Durham, North Carolina, reduce bacterial count in the air and provide a virtually sterile environment on and around the operating site.

In hospital operating rooms, Sterilamps are mounted over the operating table (Fig. 6) to reduce the danger of infection of surgical wounds by organisms floating in the air or exhaled by the operating staff. The records in more than 4000 operations in one hospital show that in 1782 operations performed without radiation there resulted 207 infections and six deaths, while 2463 operations of the same types resulted in only six infections and no deaths. Time required for healing was also reduced by more than half.

In wards and nurseries the use of ultraviolet radiation has reduced spread of infectious diseases from person to person. Evidence has also been accumulated to show that selected radiation in schools and offices has reduced or eliminated the spread of colds and other diseases which have a tendency to become epidemic.

Sterilamps have been applied in dairy barns, poultry houses, breweries, bottlers, bakeries, pharmaceutical houses, air conditioning systems, and many other places. A new industry has thus been developed that has as its primary purpose the protection of products and people from the unseen dangers ever present in the air.

# Résumés of Recent Research

**Statistical Theory of Rubber** During the past several years considerable attention has been paid to the behavior of rubber-like materials. Recently F. T. Wall[1] developed a statistical theory which accounts for some of the properties of rubber. This theory postulates that rubber is made up of very long chain molecules which, because of rotation about the carbon-carbon valence bonds, can assume various shapes.

In Fig. 1 are illustrated three possible shapes for some relatively short molecules. In that diagram the $x$ values are the components of the distances between the ends of the molecules along the direction in which the rubber is to be stretched. It is then recognized that the distribution of these $x$ values will be subject to the normal probability distribution function, represented by curve $S$ in Fig. 2. It will be observed that most of the molecules have small $x$ values and that only a few are in a straightened out condition.

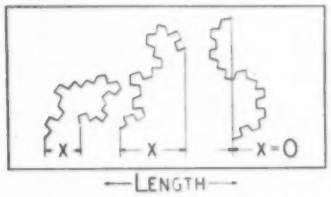


FIG. 1. Plane projections for rubber-like molecules.

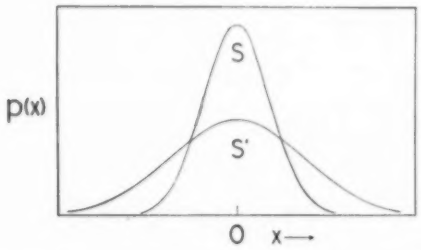


FIG. 2. $S$: Distribution function for unstretched rubber. $S'$: Distribution function for stretched rubber with 100 percent elongation.

When a macroscopic piece of rubber is stretched, the distribution $S$ will also be stretched into a new distribution $S'$ (Fig. 2). The statistical problem which Wall then solved involved the calculation of the probability of finding the system with a distribution $S'$ when its most probable distribution is $S$. This result he related to the entropy of stretching in accordance with the statistical theory of entropy. Then by well-known thermodynamic equations he deduced an equation of state for a cylindrical piece of rubber, namely:

$$\tau = \frac{NkT}{l_0}\left(\frac{l}{l_0} - \frac{l_0}{l}\right),$$

where $\tau$ is the tension of the rubber, $N$ the number of molecules, $k$ the Boltzmann constant, $T$ the absolute temperature, $l_0$ the length of the unstretched rubber, and $l$ the length under a tension $\tau$. It was observed that this equation agrees better with observation than some other equations and that it applies to compression as well as to extension.

**Industrial Noises and Industrial Deafness** The importance of occupational deafness becomes obvious when the hearing loss among boilermakers is compared (Fig. 1) to the so-called "normal" hearing loss of the average population (as measured by the Bell Telephone Laboratories at the 1939 World's Fairs).

In recent years a survey was conducted in France with the purpose of determining if there was any relationship between the intensity and the frequency distribution of industrial noises

[1] F. T. Wall, J. Chem. Phys. **10**, 132 (1942).

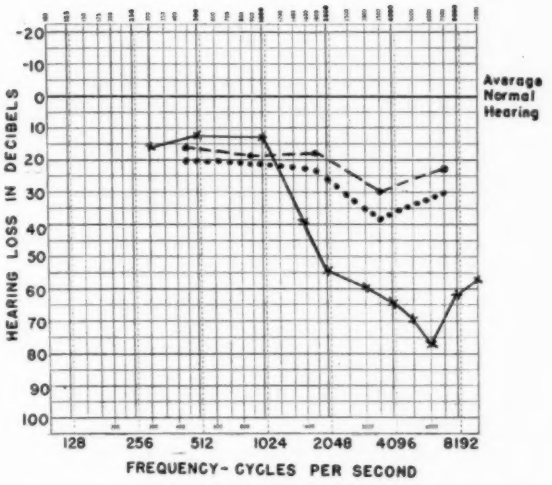


FIG. 1. Comparison between "normal" and industrial hearing loss. —— Permanent hearing loss among boilermakers after more than 15 years of employment. – – – Average hearing loss in 40–49 year age group of the general population. .... Average hearing loss in 50–59 year age group of the general population.

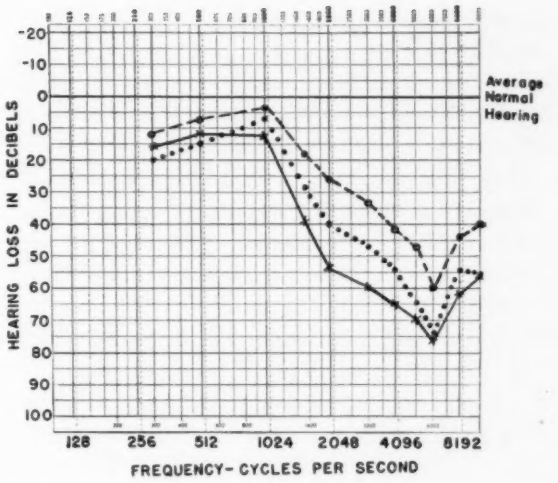


FIG. 2. Hearing loss among various categories of personnel after 15 years of employment. —— Boilermakers (average noise level: 90 db). .... Black- and ironsmiths (average noise level: 80 db). – – – Machinists (average noise level: 75 db).

and the hearing loss commonly encountered among industrial workers.*

It was possible to show some degree of correlation between the average noise level and the temporary and permanent hearing losses. This is illustrated by Fig. 2 which shows furthermore how the permanent hearing loss is almost completely localized in the region above 1500 cycles (with the maximum loss occurring at 6000 cycles), while the most important components of industrial noises are usually to be found below this frequency limit. The very small permanent loss for low frequencies points to a very rapid recuperation from temporary losses in this region. This is in marked contrast to what happens in the higher frequency range where some correlation is found to exist between the temporary and permanent losses.

While the mechanism responsible for the high frequency deafness as a consequence of exposure to low frequency noise is still unknown, the phenomenon in itself is significant. Inasmuch as the particular high frequency range for which the permanent hearing loss will be maximum is also the one which is first affected by noise deafness, it becomes possible to detect at an early stage the danger of impending deafness among industrial workers, aviators, etc. It would seem desirable that this localized hearing loss caused by industrial noises should be taken into account in the design of ear defenders.

**City Noise*** The many mechanical devices that were invented during the '20's, which increased efficiency and output, so intrigued the general public at first that they did not realize the damage that was being done to their health by the noise inherent in the operation of these many mechanical devices. The noise of the automatic riveter, the compressed air drill, the subway turnstile, to mention but a few of the newer devices, was added to the clamor of the elevated, subway, and surface cars, screeching brakes, terrifying automobile horns, chain driven trucks, and all the other noises encountered in a large industrial community.

As these noises continued to multiply the public became conscious of the effects of noise upon their nervous systems, with the result that complaints from citizens began to pile up in the Health Department. However, because there was no scientific evidence that noise was harmful, the Department of Health had little success when

* Some of the results of this investigation were published in an article by W. A. Rosenblith, J. Acous. Soc. Am. **13**, 220 (1942).

* Shirley W. Wynne, J. Acous. Soc. Am. **13**, 214 (1942).

persons making unnecessary noises were summoned to Court.

In 1929 the then Commissioner of Health, Dr. Shirley W. Wynne, appointed a committee made up of outstanding men in the various professions—physicians, lawyers, automotive engineers, and acoustical engineers—to make a study of noise. The physicians were asked to study the effects of noise upon the human system. Experiments were carried out which proved that intercranial pressure was increased fourfold, blood pressure was raised, heart action was made irregular, and hearing was damaged. The engineers measured the amount of noise made by automobiles, elevated and subway trains, and suggested practical measures for lessening these noises. Many of these recommendations have been carried out. The lawyers devised a city ordinance which would, if enacted into the law, make possible the infliction of small fines, and yet provide for the expeditious handling of violators of the ordinance. Because of lack of public sentiment the ordinance was not enacted.

The results of this study proved that noise is detrimental to health, that it interferes with the efficiency of workers, and that most noise can be prevented.

The general public lacks an appreciation of the effect of noise upon the human organism, and until they have been educated and public opinion aroused, little progress will be made in abating unnecessary noises.

# New Books

## Theory of Gaseous Conduction and Electronics

By Frederick A. Maxfield and R. Ralph Benedict. Pp. 483+xiv, Figs. 241, 15×23 cm. McGraw-Hill Book Company, Inc., New York, 1941. Price $4.50.

A new book, especially in as rapidly developing a field as that of conduction in gases, must be catalogued either as suited to the needs of the undergraduate being introduced to the subject, or as essentially a reference for those who have already mastered its fundamentals. This book, intended as an undergraduate text, actually succeeds in being something of a compromise: there are both explanations suited to the undergraduate, and tabulations and calculation methods which form a convenient reference for the expert.

The thoroughness with which the most diverse aspects of the subject are gone into (nine pages of discussion are given, for example, of the Fermi-Dirac statistics of electrons in metals) is praiseworthy, but might discourage students not well grounded in mathematics and electricity. This difficulty would be heightened by the use of m.k.s. units in schools using pre-requisite physics texts based on the c.g.s. system. Qualitative explanations are, however, also abundant and well-written. The value of the book as a text is much enhanced by a large choice of problems.

The authors have placed most of their emphasis on theoretical principles, although recently published experimental material has not been neglected. In regard to applications, even such relatively recent developments as double-grid thyratrons, oil-poor circuit breakers, and fluorescent lamps are discussed.

One disadvantage of this book as a reference is that sources of material presented are at times difficult to find. In setting forth the fundamental principles involved in gaseous discharges and showing how these apply to a great variety of commercial devices, however, the authors have achieved a high degree of success. The book is recommended for both engineers and physicists interested in conduction in gases.

John E. White
*University of Pittsburgh*

## Temperature Measurement and Control

By Robert L. Weber. Pp. 430+x, Figs. 183, 15½×22 cm. The Blakiston Company, Philadelphia, 1941. Price $4.00.

This book presents the material on temperature measurement offered to students with one year of physics at The Pennsylvania State College. The volume contains, in addition to the descriptions of methods of temperature measurements, a sufficiently detailed discussion of the basic theory to give the student an adequate background. For those who prefer to approach the subject of heat from the standpoint of temperature measurements the book will serve as a good basic text. References at the end of each chapter are a guide to more detailed discussion of the material. A set of problems will be found at the end of many chapters.

The book is divided into two parts. The first deals with the general theory and the second constitutes a laboratory guide. While the reviewer prefers to have the experiments dispersed throughout the body of the text so that the demarcation between the theory and the laboratory work is less obvious, he recognizes that this is just an opinion and is likely to cause confusion unless sufficient equipment is available so that the two can be coordinated closely.

The book is a valuable addition to the textbook material on the subject. The diagrams are excellent. The type and binding are good, but the paper shows too much glare for comfort.

H. B. Wahlin
*University of Wisconsin*

# Here and There

### Recruiting Continues for Technologists

About a year ago the Federal Civil Service Commission began a recruiting drive for technologists. The number of persons on the employment lists now established is not sufficient for today's wartime needs. Accordingly, the Commission has recently reissued the announcement of these opportunities for Government employment with slightly modified requirements. Salaries for the positions range from $2000 to $5600 a year. Applications may be filed until further notice with the Commission's Washington office.

By technologist the Commission means a person experienced in "the necessary production, engineering, and scientific research work essential for the successful operation of an industrial plant, where such plant operation is based upon a thorough and expert knowledge of a branch of an applied science," such as explosives, fuels, plastics, rubber, minerals, or textiles.

For the Junior positions ($2000 a year), applicants will no longer have to take a written test, and, as before, no written test will be given for the higher positions. The maximum age limit for all the grades has been raised to 60 years.

Copies of the announcement (No. 188), and the forms for applying, may be obtained at first- and second-class post offices, or from the Civil Service Commission, Washington, D. C.

★

### Bulletin of Mathematical Biophysics

The June, 1942 issue of the *Bulletin of Mathematical Biophysics*, edited by N. Rashevsky and published by the University of Chicago Press, will contain the following articles:

**A Mathematical Analysis of Elongation and Constriction in Cell Division,** H. D. LANDAHL.

**A Fundamental Form for the Differential Equation of Colonial and Organism Growth,** NATHAN W. SHOCK AND MANUEL F. MORALES.

**A Note on the Diffusion of Electrolytes in Cells,** ALSTON S. HOUSEHOLDER AND ROBERT R. WILLIAMSON.

**Periodic Phenomena in the Interaction of Two Neurons,** GEORGE SACHER.

**A Theory of Electrical Polarity in Cells,** ROBERT R. WILLIAMSON AND INGRAM BLOCH.

**An Alternate Approach to the Mathematical Biophysics of Perception of Combinations of Musical Tones,** N. RASHEVSKY.

★

### Charles A. Coffin Fellowships

The General Electric Company has announced the winners of the fellowships granted annually by the Charles A. Coffin Foundation to enable outstanding young graduates to continue or undertake research work in educational institutions either in this country or abroad. The fields in which awards are made include electricity, physics, and physical chemistry. This year's successful applicants are:

Boris D. Abramis, University of California, to continue at same school the theoretical and experimental study of hyper-frequency wave guides; Robert W. Hull, Yale University, to study at Massachusetts Institute of Technology the chemical nature of thermionic emitters, such as oxide cathodes, and the effects of impurities on their properties; Edward R. Kane, Union College, to conduct at Massachusetts Institute of Technology an experimental study of the absolute temperature scale; Hershel Markovitz, University of Pittsburgh, to attend Columbia University to work on the theory of the use of the distribution functions in calculating the thermodynamic properties of liquids; and Arthur E. Snowdon, Carnegie Institute of Technology, to study at the same school the design of variable, smooth model transmission line.

★

### Recent Appointment

Dr. Louis M. Heil, research associate in science at the University of Chicago, has been appointed Head of the Department of Physics at Cooper Union with the rank of full professor. He succeeds Professor Albert Ball, who will retire on June 30.

Emmett M. Irwin, consulting engineer and chief electrical engineer in charge of design and construction of all controls and drives for the 200-inch telescope being constructed at Palomar Mountain, California, has been placed in charge of the newly created Pacific Coast Branch of the Waugh Laboratories of New York.

★

### Necrology

Sir William Bragg, Director of the Davy-Faraday Research Laboratory, Fullerian Professor of Chemistry and Director of the Royal Institution, London, and President of the Royal Society from 1935 to 1940, died on March 13 in his eightieth year.

★

### Calendar of Meetings

**May**

11–13 American Institute of Chemical Engineers, Boston, Massachusetts
15–16 Acoustical Society of America, Ann Arbor, Michigan
31–June 5 Society of Automotive Engineers, White Sulphur Springs, West Virginia

**June**

8–11 American Society of Mechanical Engineers, Cleveland, Ohio
8–12 American Medical Association, Atlantic City, New Jersey
15–20 American Association for the Advancement of Science, Salt Lake City, Utah
16 American Association of Physics Teachers, Salt Lake City, Utah
18–20 National Colloid Symposium, Boulder, Colorado
22–26 American Institute of Electrical Engineers, Chicago, Illinois
25–27 American Physical Society, State College, Pennsylvania
25–27 American Association of Physics Teachers, State College, Pennsylvania
29–July 1 Institute of Radio Engineers, Cleveland, Ohio
29–July 1 American Society of Heating and Ventilating Engineers, St. Paul, Minnesota

**July**

11 American Physical Society, Pacific Coast, Berkeley, California
22–24 American Society of Civil Engineers, Spokane, Washington

**September**

7– 9 Mathematical Association of America, Ithaca, New York
7–11 American Chemical Society, Buffalo, New York
8–11 American Mathematical Society, Ithaca, New York
9–11 American Institute of Electrical Engineers, Vancouver, B. C.

# Contributed Original Research

## On the State of Stress in Thick Bars‡

M. M. Frocht[1] and M. M. Leven[2]
*Carnegie Institute of Technology, Pittsburgh, Pennsylvania*
(Received February 2, 1942)

The view is now generally held that in bars containing circular holes or other discontinuities the state of stress ceases to be two-dimensional when the ratio of the radius of the hole $r$ to the thickness of the bar $t$ is less than unity. It is further believed that the factor of stress concentration in thick bars is materially smaller than in thin bars. This view also forms the basis for the doubts which have arisen regarding the reliability of certain theoretical work on stress concentrations produced by very small holes. In this paper results are reported from a photoelastic investigation using both elastic and frozen (see reference 4, Chapter 10) stress patterns and showing that the present point of view is erroneous. Experimental results show that no deviation from a state of plane stress can be found in bars with central circular holes when $r/t$ is of the order of magnitude of about $\frac{1}{4}$ instead of unity. Experiments further show that the factors of stress concentration remain essentially the same in thick as in thin bars. The present work may also be taken as experimental corroboration of the theoretical value for the factor of stress concentration obtained by Neuber for a very small hole in a bar in tension or compression.

IN the theory of elasticity two types of two-dimensional problems are recognized: one of plane stress and one of plane strain. A state of plane stress is approached in a very thin bar without discontinuities in tension or compression and a state of plane strain is approached in the central transverse section of an infinitely long cylinder subjected to uniform loading along a line parallel to its axis.

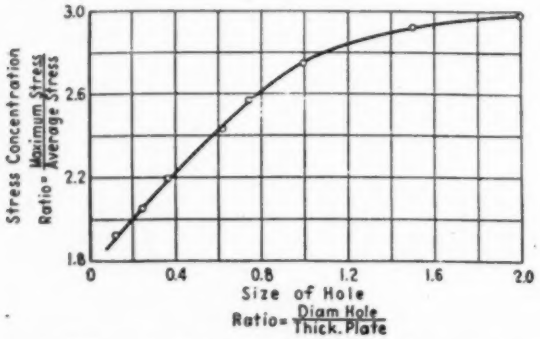


FIG. 1. Effect of thickness upon factor of stress concentration in which $2r/D$ is kept constant (Vose).

When a thin bar in tension has a discontinuity, such as a hole, groove, or fillet the state of stress may be affected by the discontinuity. It is both of theoretical and practical interest to examine the effect of the thickness on the state of stress resulting from such discontinuities.

A survey of the literature shows that at least one experimental attempt to answer this question was made in recent years. In 1935 Vose[3] published a curve purporting to show the effect of the thickness of a bar with a circular hole upon the factors of stress concentrations, and he concluded that there is a pronounced reduction in the factor of stress concentration as the thickness increases.

Vose's results are shown in Fig. 1. It is seen, for example, that for a hole in a bar in tension the factor of stress concentration drops from nearly 3.00 to 1.90 as $2r/t$ varies from 2.00 to approximately 0.1, the reduction being 37 percent.

As far back as 1935 the authors had reason to

‡ Presented at the Fourteenth Semi-Annual Eastern Photoelasticity Conference, held at Yale University, New Haven, Connecticut, December 6, 1941, under the auspices of the Civil and Mechanical Engineering Departments.

[1] Associate Professor of Mechanics in charge of Photoelastic Laboratory, Carnegie Institute of Technology, Pittsburgh, Pennsylvania.

[2] Mechanician and Research Assistant, Photoelastic Laboratory, Carnegie Institute of Technology, Pittsburgh, Pennsylvania.

[3] See R. W. Vose, "An application of the interferometer strain gage in photoelasticity," J. App. Mech. **57**, A-101 (1935).

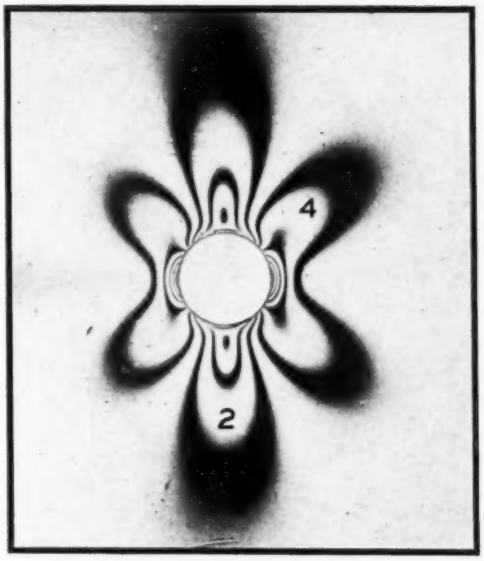


Dimensions:

| | | |
|---|---|---|
| $2r = 0.189''$ | $2r/D = 0.140$ | $P = 298$ lbs. |
| $D = 1.355''$ | $2r/t = 0.223$ | Min. area $= 0.945$ sq. in |
| $d = 1.166''$ | | $s_{Av} = 316$ psi. |
| $t = 0.811''$ | | $2F = 106$ psi. |
| | | $n_{Av} = 2.98$ fringes |

$n_{max} = 8.00$; $k = 8.00/2.98 = 2.68$; $k$ (from curve) $= 2.55$.
Error $= +5$ percent.

FIG. 2. Thick bar with central circular hole subjected to pure tension.

TABLE I.

| Type of stresses | Diameter of hole $2r$ in. | Width of bar $D$ in. | Thickness of bar $t$ in. | $2r/D$ | $2r/t$ | Factor of stress concentration $k$ | Factor of stress concentration for thin plates $k_0$ | $k/k_0$ |
|---|---|---|---|---|---|---|---|---|
| Elastic room temp. | 0.189 | 0.632 | 0.640 | 0.300 | 0.295 | 2.32 | 2.29 | 1.01 |
| Elastic room temp. | 0.158 | 1.540 | 0.811 | 0.102 | 0.195 | 2.44 | 2.62 | 0.93 |
| Elastic room temp. | 0.189 | 1.355 | 0.811 | 0.140 | 0.223 | 2.68 | 2.55 | 1.05 |
| Frozen 260°F | 0.212 | 1.342 | 0.805 | 0.158 | 0.263 | 2.43[a] | 2.52 | 0.965 |
| Frozen 260°F | 0.212 | 1.342 | 0.805 | 0.158 | 0.263 | 2.53[b] | 2.52 | 1.00 |

[a] From central slice 0.392″ thick.
[b] From central slice 0.275″ thick.

doubt Vose's conclusion. In our studies of stress concentrations carried on at that time, plates from $\frac{3}{16}''$ to $\frac{3}{8}''$ thick were used, and no effect of the thickness of the plate on the factors of stress concentration was found even for grooves $\frac{1}{16}''$ in radius.

Vose's conclusions have been accepted by J. N. Goodier[4] who in reviewing Neuber's book *Kerbspannungslehre* states: "When the radius of the hole, or in notches, the radius of the curvature, is small, it is likely in photoelastic models to be of the same order as the thickness of the plate. The state of stress is then no longer even approximately two-dimensional, as Vose has recently pointed out." Goodier makes this the basis for a likelihood "to resist the author's [Neuber's] conclusion that his final formulas are satisfactorily confirmed."

According to this view, it would follow that in a $\frac{1}{4}''$ plate three-dimensional effects exist around a central circular hole $\frac{1}{2}''$ in diameter, or to take a more extreme case, in order to eliminate three-dimensional stresses around a $\frac{1}{8}''$ hole in tension the bar would have to be thinner than $\frac{1}{16}$ of an inch.

The purpose of the present paper is to present the results from a recent photoelastic investigation of this problem using thicker bars, and the newer method of frozen stress patterns, as well as elastic stress patterns at room temperature.

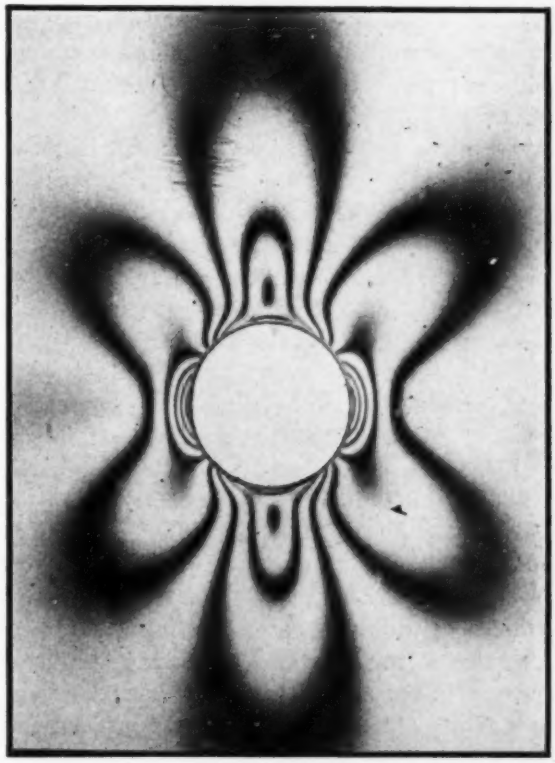

FIG. 2(a). Enlargement of central portion of Fig. 2.

[4] J. App. Mech. pp. A-188, 189 (December, 1937).

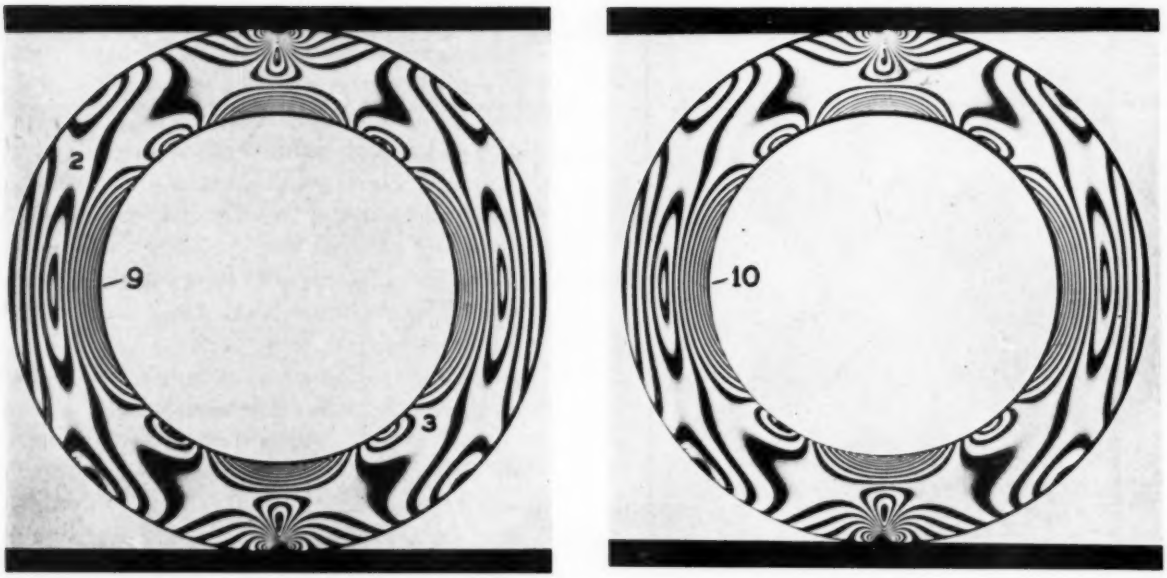


(a) (b)

FIG. 3. (a). Space effect distributed. (b). Space effect eliminated from left and lower parts.

## THICK RECTANGULAR BAR. ELASTIC PATTERNS AT ROOM TEMPERATURES

Table I shows the dimensions of the bars which were pulled in tension by means of axial loads. A typical stress pattern is shown in Fig. 2. Attention is directed to the clear boundary stresses. In view of the relatively great thickness of 0.8 inch the high degree of boundary visibility around the $\frac{3}{16}''$ diameter hole is indeed remarkable. Unless proper precautions are taken it is very easy to lose a fringe or two due to shadows or space effects. This can happen even in thin models with large circular holes, let alone in a bar 0.8″ thick with a small hole. Inspection of Fig. 3 shows one whole fringe was lost because of faulty technique in the polariscope. Thus in Fig. 3(a) the maximum fringe order is 9 whereas in Fig. 3(b) it is 10.[5]

Table I shows the resulting factors of stress concentration based on elastic patterns at room temperature. The values of these factors are seen to fluctuate about the corresponding value of the factor for a thin plate. The average value is, however, in very good agreement with the value for a thin plate. These fluctuations indicate

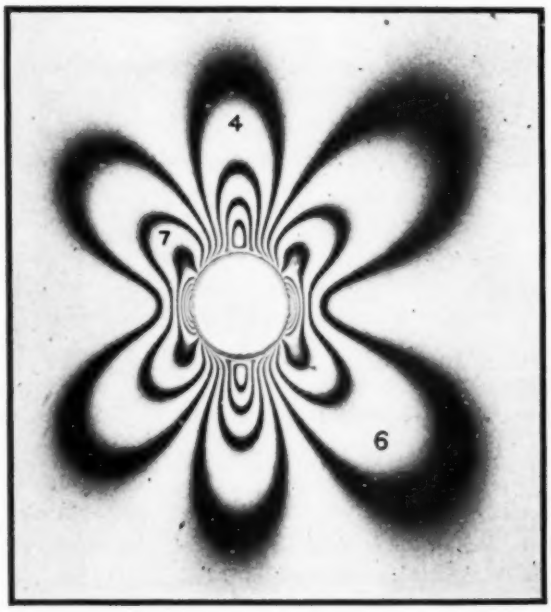


| Original dimensions: | Final dimensions: | $P=21.2$ lbs. |
|---|---|---|
| $2r=0.189''$ | $r'=0.106''$ | Min. area $=0.931$ sq. in. |
| $D=1.355''$ | $D'=1.342''$ | $s_{Av}=22.8$ psi. |
| $d=1.166''$ | $d'=1.157''$ | $2F=3.97$ psi. |
| $t=0.811''$ | $t'=0.805''$ | $n_{Av}=5.74$ fringes |
| | $2r'/D'=0.158$ | $k$ (from 2 dimens. curve) |
| | $2r'/t'=0.263$ | $=2.52$ |

FIG. 4. Thick bar with small circular hole in pure tension (frozen stresses viewed through Halowax oil).

[5] The proper technique for revealing boundary stresses is discussed in detail, Max M. Frocht, *Photoelasticity* (John Wiley & Sons, Inc., New York), Vol. 1, Chapter 11, pp. 370, 376.

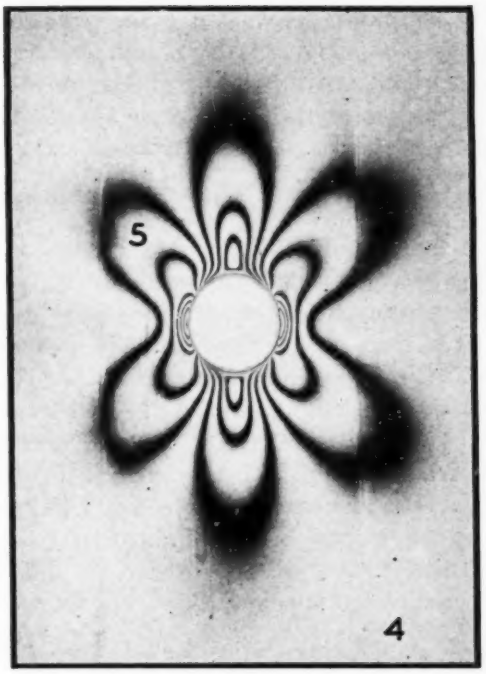


Final dimensions:

| | |
|---|---|
| $r' = 0.106''$ | $P = 21.2$ lbs. |
| $D' = 1.342''$ | $s_{Av} = 22.8$ psi. |
| $d' = 1.157''$ | $2F = 5.23$ psi. |
| $t' = 0.612''$ | $n_{Av} = 4.355$ fringes |

$n_{max} = 9.87$; $k = 9.87/4.355 = 2.27$.

FIG. 5. Thick bar with small circular hole in pure tension (frozen stresses viewed through Halowax oil). Plate thinned down from 0.805″ to 0.612″.

possibly that the pin through which the load was applied deflected considerably as the loads were increased and bore on, or came in contact with, different parts of the bar.

The above results are obviously at variance with those obtained by Vose. The difference is in all probability due to the particular method employed for determining the boundary stresses. It has been pointed out by several observers that lateral deformations cannot be used as a measure of the sum of the principal stresses in thick bars, and Vose seems to have relied mainly upon such deformations.[6] Additional errors are introduced by the fact that the needles of the interferometer can never be placed right at the boundary.

The elastic stress patterns by themselves do not provide, however, sufficient evidence to warrant a conclusion regarding the distribution of the stresses in the bar as a function of thickness. Strictly interpreted they furnish only data for the integrated effect, but they do not specifically tell us how the stresses vary from layer to layer. In order to answer this question a photoelastic stress pattern was frozen into a bar 0.8″ thick, and this bar was subsequently milled down in several stages to give thinner bars of 0.612″, 0.392″, and 0.275″, respectively. The milling was done equally from both sides so that each thinner bar represents a central section of the original bar. The corresponding stress patterns are shown in Figs. 4–7. Curves of $(p-q)$ in fringes per inch of thickness were plotted for several sections. Figure 8 shows one set of these curves from which the values of the fringe order $n$ at a particular point could be obtained as a function of thickness $t$. The results are shown in Fig. 9. Inspection of these curves shows that the inner layers carry a somewhat greater stress per inch of thickness than the outer layers of the bar. The curves are, however, straight over the middle half approximately, and the maximum deviation from the straight line does not exceed 12 percent.

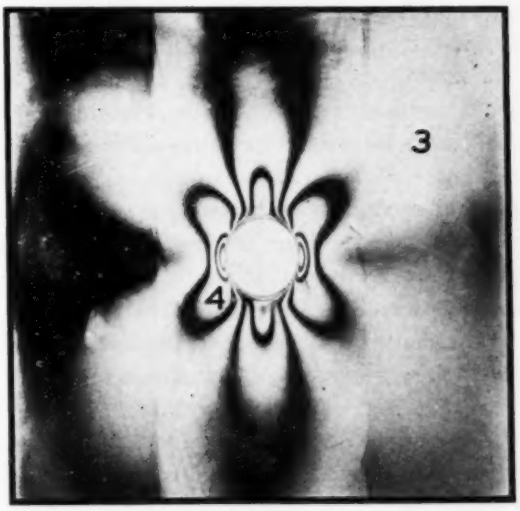


Final dimensions:

| | |
|---|---|
| $r' = 0.106''$ | $s_{Av} = 22.8$ psi. |
| $D' = 1.342''$ | $2F = 8.16$ psi. |
| $d' = 1.157''$ | $n_{Av} = 2.79$ fringes |
| $t' = 0.392''$ | |

$n_{max} = 6.75$; $k = 6.75/2.79 = 2.43$.

FIG. 6. Thick bar with small circular hole in pure tension (frozen stresses viewed through Halowax oil). Plate thinned down from 0.805″ to 0.392″.

[6] This point was stressed by Dr. D. C. Drucker from Cornell University in his oral discussion of the present paper.

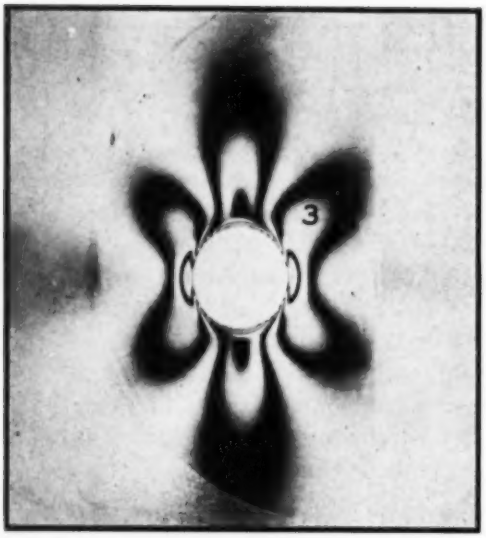


Final dimensions:

| | |
|---|---|
| $r' = 0.106''$ | $P = 21.20$ lbs. |
| $D' = 1.342''$ | $s_{Av} = 22.8$ psi. |
| $d' = 1.157''$ | $2F = 11.62$ psi. |
| $t' = 0.275''$ | $n_{Av} = 1.96$ fringes |

$n_{max} = 5.00$; $k = 5.00/1.96 = 2.54$.

FIG. 7. Thick bar with small circular hole in pure tension (frozen stresses viewed through Halowax oil). Plate thinned down from 0.805″ to 0.275″.

## FACTORS OF STRESS CONCENTRATION

It should be observed that the frozen stress patterns introduce greater difficulties into the problem of stress concentration as compared with the elastic patterns at room temperature. First, the deformation becomes rather large and the shape of the transverse hole is materially changed; second, the process of annealing or freezing produces edge effects which are most undesirable as they destroy the boundary visibility, which is so essential to the accurate determination of stress concentrations. Nevertheless, the results from the frozen stress pattern are interesting and corroborating. Since the curves of Fig. 9 show that the greatest stresses exist in the central part of the bar we determine the maximum stresses around the hole from the stress patterns for the inside sections. This gives factors of stress concentration of 2.43 and 2.53 as compared with 2.52 for a thin plate of the same face dimensions,[7] as shown in Table I.

In view of the difficulties pointed out above these results may be taken to represent good support for a conclusion that the factor of stress concentration in the thick bar is essentially the same as in thin bars having the same ratio $2r/D$.

## THICK BAR WITH LARGE RIVET OR PIN

A bar 0.8″ thick and $1\frac{3}{8}$″ wide was pulled by means of a pin 1.00″ in diameter and a photoelastic stress pattern was frozen into it. The bar was then milled down equally from both sides to give several thinner bars. A typical frozen stress pattern is shown in Fig. 10. Curves of $(p-q)$ were plotted for the different bars from which the resulting curve of the fringe order $n$ *vs.* thickness $t$ was obtained. This turned out to be a straight line, indicating that the small disturbances observed when the hole was small are here altogether absent.

## CONCLUSIONS

1. Experiments show that in thick bars with circular holes the inner layers carry a somewhat greater stress than the outer layers. This is shown by the frozen stress patterns and the curves of the fringe order $n$ *vs.* thickness $t$.

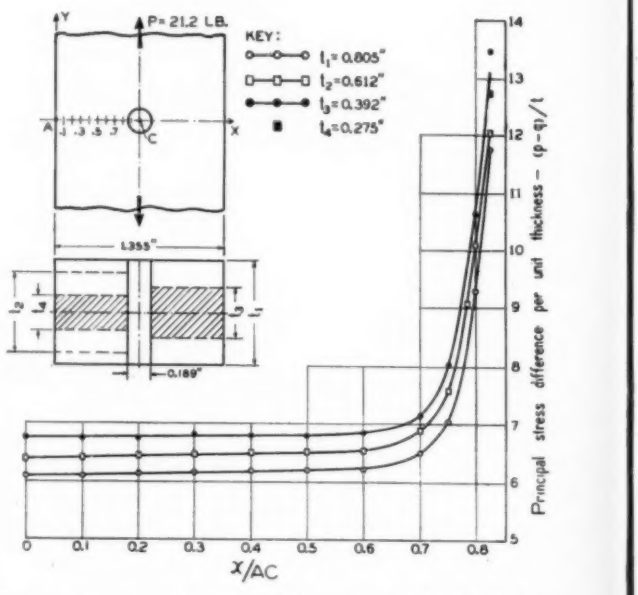


FIG. 8. Curves of $(p-q)$ in fringes per inch of thickness across $AC$, for slices of different thicknesses.

[7] Two-dimensional factors of stress concentration can be found in the following: N. C. Riggs and M. M. Frocht, *Strength of Materials*, chapter 13 (The Ronald Press Company, New York); M. M. Frocht, "Photoelastic studies in stress concentrations," Mech. Eng. J. A. S. M. E. (August, 1936).

2. The variations in the stresses are, however, small and do not exceed 12 percent.

3. Vose's conclusions regarding the effect of the thickness upon the factors of stress concentration are definitely not substantiated by our work. The curve published by him and shown in Fig. 1 is believed to be in error.

4. Factors of stress concentration for small holes in thick bars do not differ by more than 5 percent from the corresponding factors in a thin plate.

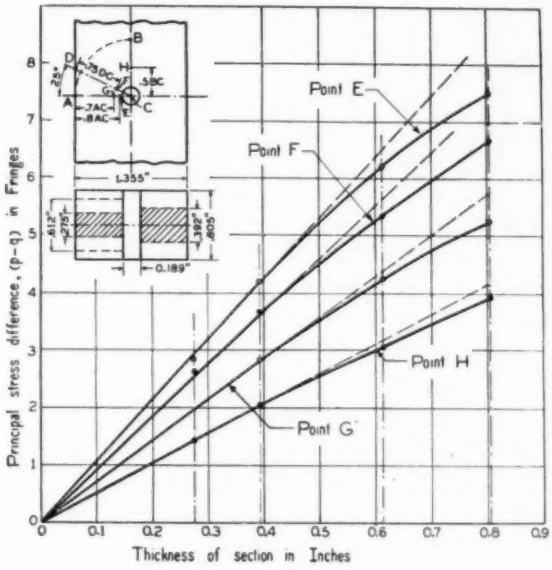


FIG. 9. Curves of fringe order *vs.* thickness, based on curves such as shown in Fig. 8. To illustrate, the curve for point $G$ is obtained by taking the fringe order $n_1$ from Fig. 8 and multiplying it by the thickness. Thus at point $G$ where $x/AC=0.7$ and $t=0.392''$, $n=n_1t=7.2\times0.392=2.82$. Similarly, at point $G$ for $t=0.612''$, $n=n_1t=6.90\times0.612=4.22$.

5. When the hole becomes large, as in the case of the single rivet or pin, experimental data fail to show any influence of thickness, indicating that the important element is the ratio of the dimensions rather than the absolute dimensions which determine the state of stress.

6. For practical design purposes the state of stress in thick bars may be assumed to be the same as in thin bars and the factors of stress concentrations although somewhat reduced approach the same values as for thin bars.

| Original dimensions: | Final dimensions: | $P=21.2$ lbs. |
|---|---|---|
| $2r=1.004''$ | $2r'=1.178''$ | $s_{Av}=77.9$ psi. |
| $D=1.360''$ | $D'=1.330''$ | $2F=5.08$ psi. |
| $2r/D=0.739$ | $d'=0.340''$ | $n_{Av}=15.3$ fringes |
| | $t'=0.630''$ | |
| | $2r'/D'=0.885$ | |

$n_{max}=27$; $k=27/15.3=1.77$; $k$ (from 2-dimens. curve) $=1.80$.

FIG. 10. Head of thick bar strained with a single large central rivet (frozen stresses viewed through Halowax oil). Bar thinned down from 0.800" to 0.630".

7. The experiments may be interpreted as substantiating Neuber's theoretical conclusion regarding stress concentrations produced by very small holes.

# Measurement of the Initial Inner Permeability of Iron over a Wide Radiofrequency Range

ROBERT W. WOODS*
*Department of Physics, The University of Chicago, Chicago, Illinois*
(Received January 20, 1942)

Previous investigations on the variation with frequency of the initial inner permeability $\mu_L$ of iron reveals great disparity of results. In this experiment certain refinements of technique and of analysis have been introduced which make the accuracy adequate for comparison with theory. The method used was to determine the change in resonant frequency of a coil and condenser combination caused by insertion of a permeable sample in the field of the coil. This change in frequency is interpreted as being caused by change of flux through the coil. The same iron wire had been measured previously over a different frequency range by other men working in this laboratory. The value of $\mu_L$ was found to be $\sim$60 over the frequency range from 30 kc to 40 mc showing no dispersion region between these limits. Results of this method are compared with those of other methods.

## I. INTRODUCTION

THE most commonly used method for measuring the initial permeability of ferromagnetic materials at ordinary radiofrequencies has been to measure radiofrequency resistance. The permeability $\mu_R$ calculated from these data, called the outer or resistive permeability, is different in value from the inner or inductive permeability $\mu_L$.

Kreielsheimer[1] calculated values of $\mu_L$ from his measurements of resistance for the range from 40 meters to 1000 meters. Several investigators[2] have calculated $\mu_L$ from inductance measurements for frequencies above 100 megacycles but the methods employed have in general not been applicable at lower frequencies. Wait[3] using a method due to Belz,[4] obtained some values which he called "apparent permeability." These values, while probably adequate as a check on the reported[5] anomalous behavior of $\mu_L$ in the 100-meter region, was, by reason of inadequate analysis, only about one-tenth of the probable value of $\mu_L$.

In view of the low accuracy of these results it was decided to calculate $\mu_L$ over a more extended range and with more adequate analysis, from measurements of inductance. The sample of iron was a single strand of the same wire used by Glatthart.[6]

## II. METHOD

To measure the permeability $\mu_L$ at frequency $f$ the iron wire sample was placed symmetrically along the axis of the coil (Fig. 1) in the frequency control tank circuit of a stabilized[7] oscillator.

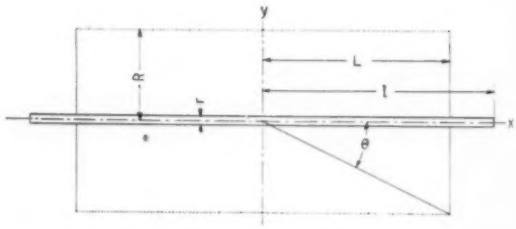


FIG. 1. Longitudinal section of coil.

The frequency $f$ was measured. Figure 2 is a diagram of the measurement circuit. The Franklin oscillator[8] was employed because the coil in this oscillator has one side grounded, and no part of the d.c. grid or plate current flows through the coil as in the electron coupled oscillator. The other oscillator which provided the heterodyne was an electron coupled oscil-

* Now at Union College, Lincoln, Nebraska.
[1] K. Kreielsheimer, Ann. d. Physik **17**, 293 (1933).
[2] J. B. Hoag and H. Jones, Phys. Rev. **42**, 571 (1932); J. L. Glatthart, Phys. Rev. **55**, 833 (1939); G. Potapenko and R. Sanger, Zeits. f. Physik **104**, 779 (1937).
[3] G. R. Wait, Phys. Rev. **29**, 566 (1927); **32**, 967 (1928).
[4] M. H. Belz, Phil. Mag. **44**, 479 (1922); M. H. Belz, Proc. Camb. Phil. Soc. **21**, 52 (1922).
[5] B. Wedensky and K. Theodortshik, Physik. Zeits. **24**, 216 (1923); W. Kartschagin, Ann. d. Physik **67**, 325 (1922).
[6] J. L. Glatthart, Phys. Rev. **55**, 833 (1939).
[7] C. D. Perrine, Radio p. 14 (June, 1939); L. Norton, Radio p. 11 (July, 1939); C. E. Berry, Radio p. 50 (November, 1939); L. Norton, Radio p. 41 (January, 1940); G. F. Lampkin, Proc. I.R.E. **149** (March, 1939).
[8] L. Norton, Radio p. 41 (January, 1940).

lator. Doubling the frequency of both of these oscillators increased their stability and minimized any tendency toward "pulling." The beat frequency output of the mixer was passed through a low pass filter, amplified, and applied to the horizontal plates of an oscilloscope. The Lissajous figure on the screen of the oscilloscope enabled the experimenter to set the 80–120 kc oscillator to an exact multiple of this beat frequency. By zero beating a high harmonic of this last-mentioned oscillator against the accurately calibrated radiofrequency oscillator, it was possible to measure the beat frequency to a high degree of accuracy. The difference between two determinations, once with the iron wire in the coil, and once with a copper wire replacement of the same dimensions gave the value of $df$. The value of $f$ was measured by direct comparison of the frequency of the test oscillator with the calibrated oscillator, again by the zero beat method. These are the only measurements except the dimensions of the coil, length $2L$, radius $R$ and of the sample, length $2l=6$ cm, radius $r=0.0088$ cm.

The values of $\mu_L$ are then calculated from the observed data‡ by the formula

$$\mu_L=[1/Q]\{[2SAdf]/[f(a-U)]\}+P$$

where $A=\pi R^2$ and $a=\pi r^2$; $S$ is a factor which allows for radial variation of the magnetic field $H$ of the coil; $U$ is a factor which allows for reduction of $H$ due to magnetization of the sample; $Q$ is a factor which allows for radial variation of the instantaneous flux density $B$ within the iron sample, due to eddy currents. It is a function of $f$ and of $\mu_L$. $P$ is the analogue for copper of $Q$ for iron.

‡ In order to keep the value of $H$ constant in all measurements it seems that a variable resistor should be placed in the tank circuit and adjusted so that $H$ be kept constant at all frequencies. This was considered and was not done for three reasons: (a) The inclusion of a resistor in the frequency control tank circuit of an oscillator adversely affects the $Q$ of the circuit and decreases the stability of operation. (b) Previous measurements of effective permeability seem to indicate that the permeability does not appreciably increase above the initial value until the value of $H$ exceeds one oersted. (c) Experimentally, at a fixed frequency, changes in the capacity of the feedback condenser within the functional limits, which changed the voltage across the coil, the current through the coil, and consequently the value of $H$, made no appreciable difference in the calculated value of the permeability. The static permeability was determined by the ring-ballistic method and was found to be 108 at 0.22 oersted. This is comparable to the values of effective permeability obtained at radiofrequencies, since even at low frequencies, 60 cycles, the effective permeability obtained by dynamic methods is only a little more than half of the static permeability at initial field strengths. The outer permeability was not measured.

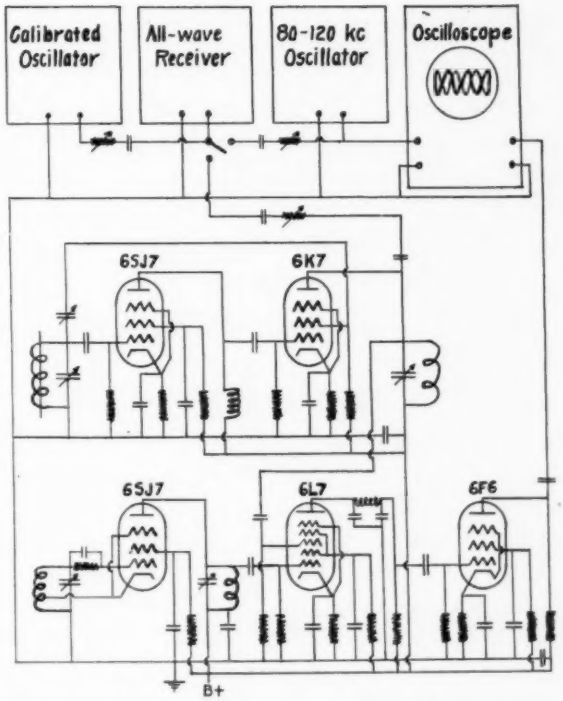


FIG. 2. Measurement circuit. Values of circuit components have purposely been omitted from the diagram because these values of coils, condensers, and chokes had to be changed as the frequency was changed. The resistance values depend on tube characteristics and may be selected from any circuit design tables.

## III. DERIVATION OF EQUATION

From[9]

$$f=[1/2\pi]\sqrt{\{[1/L_eC]-[R/2L_e]^2\}}$$

where $L_e$=effective inductance, $C$=constant tuning capacity, $R$=constant r-f resistance,

$$-2df/f=[dL_e/L_e]\{1-CR^2/[4L_e-CR^2]\}\approx dL_e/L_e$$

since for normal values of $C$, $R$, and $L_e$,

$$CR^2/[4L_e-CR^2]\approx 2.5\times 10^{-5}\ll 1.$$

From[10]

$$L_e=L/[1-4\pi^2f^2LC_0] \quad \text{and} \quad 4\pi^2f^2[C+C_0]=1,$$

where $L$=true inductance and $C_0$=distributed

[9] A. Hund, *Phenomena in High Frequency Systems* (McGraw-Hill, 1936), p. 92.

[10] A. Hund, *High Frequency Measurements* (McGraw-Hill, 1933), p. 243.

capacity,

$$dL/L=[dL_c/L_c]\{C/[C+C_0]\}\approx -2df/f$$

if we neglect the effect of distributed capacity by limiting $C$ to values which are large with respect to $C_0$.

From[11] $N=LI$ where $N$=flux through coil and $I$=current in coil,

$$dL/L=dN/N-dI/I=-2df/f.$$

But

$$dN/N=[\text{final flux}-\text{initial flux}]/[\text{initial flux}]$$
$$=[(N_c+N_m)-(N_i+N_n)]/(N_i+N_n),$$

where $N_c$=flux through copper replacement wire at $x=0$ (Fig. 1)$=aH'_0P$; where $H'_0$=axial field $=K(I+dI)$; $N_i$=flux through iron wire$=\mu aH_0Q$; where $H_0=KI$; $N_m$=flux around copper wire in area $(A-a)=[(SA-a)-U(P-1)]H'_0$; $N_n$ =flux around iron wire in area $(A-a)=[(SA-a)-U(\mu Q-1)]H_0$. The first term of $N_m$ and $N_n$ is the flux that would be caused in $(A-a)$ by the current in the coil. The second term is the reduction of flux due to magnetization of the sample. The factors $S$, $U$, $Q$, $P$ have been defined and will be evaluated later. Substituting and simplifying,

$$2df/f=dI/I-dN/N$$
$$=[(\mu Q-P)(1+dI/I)]/[(\mu Q-1)+SA/(a-U)]$$

or since $dI/I\ll 1$; $df/f\ll 1$; and $2SA/(a-U)\gg 2$;

$$\mu=[1/Q]\{[2SAdf]/[f(a-U)]+P\}.$$

Since $Q$ is a function of $\mu$, $\mu$ may be evaluated by successive approximation.

## IV. EVALUATION OF $S$

The flux in the cross section of a coil is obtained by integrating the field over the cross section. The field is given by Gray[12] for any point in the coil. When $x=0$

$$H=2\pi nI\{2L/\sqrt{(R^2+L^2)}$$
$$+[6R^2Ly^2]/[4\sqrt{(R^2+L^2)^5}]$$
$$+[30RL(3R^2-4L^2)y^4]$$
$$/[64\sqrt{(R^2+L^2)^9}]+\cdots\},$$

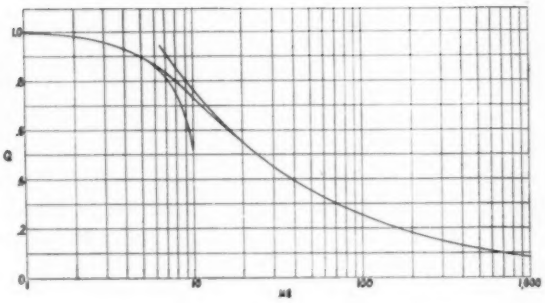

FIG. 3. Variation of flux in sample wire with frequency.

$$N=2\pi\int_r^R Hydy=H_0(AS-aS')$$
$$=H_0(AS-a) \text{ since } S'\approx 1,$$

where

$$S=1+3R^4/[8(R^2+L^2)^2]$$
$$+[5R^5(3R^2-4L^2)]/[64(R^2+L^2)^4]+\cdots.$$

## V. EVALUATION OF $Q$

Berg[13] has shown that the differential equation

$$\partial^2B/\partial y^2+[1/y]\partial B/\partial y=[4\pi\mu/\rho]\partial B/\partial t$$

(where $\rho$=resistivity$=10^4$ e.m.u. for iron, and $y$=radial distance) gives the condition for radial variation of flux density in the iron. We are dealing with a sine wave field caused by a sine wave current in the coil. At small field strengths $B=B_1\cos\omega t+B_2\sin\omega t$, where the phase angle is zero at the surface of the iron and varies radially. The effective value also varies radially from the surface value $B_0$.

The solution of this differential equation is exactly analogous to the solution of the similar equation for skin effect and yields, using the notation employed by Berg,[14]

$$B=[B_0\sqrt{2}/(ber^2\,mr+bei^2\,mr)][(ber\,mr\,ber\,my$$
$$+bei\,mr\,bei\,my)\cos\omega t-(bei\,mr\,ber\,my$$
$$-ber\,mr\,bei\,my)\sin\omega t]$$

where

$$mr=r\sqrt{\{8\pi^2\mu f/\rho\}}=0.78\sqrt{ug}$$

where $g=f\cdot 10^{-6}$ and since $\rho=10^4$ and $r=0.0088$ cm

$$N_i \text{ (instantaneous)}=2\pi\int_0^r Bydy$$

[11] L. Page and N. I. Adams, *Principles of Electricity* (D. Van Nostrand Company, 1931), p. 333.
[12] A. Gray, *Absolute Measurements in Electricity and Magnetism* (Macmillan, 1927), pp. 210 ff.
[13] E. J. Berg, *Electrical Engineering, Advanced Course* (McGraw-Hill, 1916), pp. 151 ff.
[14] Reference 13, pp. 225 ff.

and

$$N_i \text{ (effective)} = [B_0 2\pi r/m]\sqrt{\{[(ber'\, mr)^2 + (bei'\, mr)^2]/[ber^2\, mr + bei^2\, mr]\}}.$$

Using Russell's approximations[15] $N_i = \mu H_0 aQ$, where for values of $mr < 2$

$$Q = 1 - 0.494 \cdot 10^{-2}(\mu g)^2 + 0.419 \cdot 10^{-4}(\mu g)^4 - 0.3918 \cdot 10^{-6}(\mu g)^6 + \cdots$$

and for values of $mr > 4$

$$Q = 2.585/\sqrt{(\mu g)} - 0.581/(\mu g) + 0.1325/\sqrt{(\mu g)^3} + 0.4175/(\mu g)^2 + \cdots.$$

These two expressions for $Q$ have been plotted (Fig. 3) over the ranges for which they give acceptable accuracy and the two curves joined by a smooth curve to provide continuity over the range where neither approximation is satisfactory. Furthermore, since in the derivation of these expressions $\mu$ and $\rho$ occur only as a ratio, the values of $P$ may be read from the same graph by using $5.65g$ instead of $\mu g$ since 5.65 is the ratio of the resistivities of iron and copper.

## VI. EVALUATION OF $U$

Consider a wire of infinite length extending along the axis of the coil (Fig. 1). At a point $x$,[16]

$$N_x = \tfrac{1}{2}\int_0^r (B_{xy} - H_x) y dy = \tfrac{1}{4}(\mu Q - 1) r^2 H_x$$

$$= H_0(\mu Q - 1)[r^2\sqrt{(R^2+L^2)}/(8L)] \times \{(x+L)/\sqrt{[R^2+(x+L)^2]} - (x-L)/\sqrt{[R^2+(x-L)^2]}\}.$$

The surface magnetization in this wire would be

$$D'_x = -dN_x/dx = H_0(\mu Q - 1)[r^2R^2\sqrt{(R^2+L^2)}/(8L)] \times \{1/\sqrt{[R^2+(x-L)^2]^3} - 1/\sqrt{[R^2+(x+L)^2]^3}\}.$$

In addition to this magnetization due to the non-uniform field, in our sample of finite length $2l$, the flux which would otherwise be in the permeable material, beyond $x = l$ will be "reflected" from the "open" end and leak out along the length of the sample in such a manner that the surface magnetization due to this "reflected" flux is proportional[17] to $x$ and to $H_x$; i.e., $D''_x = C_1 x H_x$ in which $C_1$ may be evaluated from

$$\int_0^l D''_x dx = N_l;$$

($N_l$ for the wire of infinite length). The total surface density of magnetization then

$$D_x = D'_x + D''_x = -dN_x/dx + C_1 x H_x = (uQ-1)H_0 \cdot f(x),$$

$$f(x) = C_2\{1/\sqrt{[R^2+(x-L)^2]^3} - 1/\sqrt{[R^2+(x+L)^2]^3}\} + C_3\{x(x+L)/\sqrt{[R^2+(x+L)^2]} - x(x-L)/\sqrt{[R^2+(x-L)^2]}\},$$

$$C_2 = r^2R^2\sqrt{(R^2+L^2)}/8L$$

and

$$C_3 = C_1C_2/[r^2R^2(\mu Q - 1)].$$

It is apparent that these constants must be evaluated for each coil and each sample. It is also evident that the surface magnetization will be different for each coil and each sample. Figure 4 shows the surface magnetization factor $f(x)$ for the single sample used in each of the several coils. Furthermore $f(x)$ is independent of the material and of the frequency, being a function of coil and sample dimensions only.

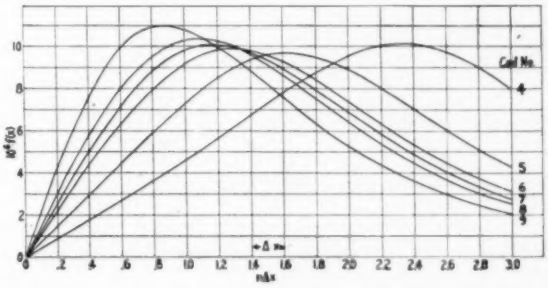


FIG. 4. Surface magnetization of sample in one set of coils.

The reduction of the field of the coil at a point $(0, y)$ due to this surface magnetization

$$H'' = 2\int_0^l D_x x dx/\sqrt{(x^2+y^2)^3}$$

($y$ is not a function of $x$). With the expression for $D_x$ as derived above, this integral becomes a very complicated one involving the use of

[15] A. Russell, Phil. Mag. **17**, 528 (1909).
[16] Reference 12, pp. 210 ff.
[17] J. A. Ewing, *Magnetic Induction in Iron and Other Materials* (Electrician Publishing Company, 1892), pp. 25 ff.

TABLE I. Coil data.

| Coil number | Winding | Radius (cm) | Half-length (cm) | Turns | $S$ | $U$ |
|---|---|---|---|---|---|---|
| 1 | Double layer | 1.85 | 2.855 | 170 | 1.031 | 85.6 |
| 2 | Single layer | 1.85 | 2.855 | 120 | 1.031 | 85.6 |
| 3 | Single layer | 1.85 | 1.905 | 75 | 1.084 | 95.5 |
| 4 | Single layer | 1.56 | 2.38 | 52 | 1.034 | 74.8 |
| 5 | Single layer | 1.56 | 1.59 | 33 | 1.087 | 81.5 |
| 6 | Single layer | 1.56 | 1.19 | 25 | 1.149 | 88.5 |
| 7 | Single layer | 1.56 | 1.03 | 20 | 1.196 | 95.5 |
| 8 | Single layer | 1.56 | 0.90 | 17 | 1.230 | 99.0 |
| 9 | Single layer | 1.56 | 0.45 | 9 | 1.395 | 115.0 |
| 10 | Spaced turns | 1.61 | 1.27 | 17 | 1.147 | 108.0 |
| 11 | Spaced turns | 1.61 | 1.27 | 11 | 1.147 | 108.0 |

reduction formulas which give a multiplicity of elliptic integrals. Furthermore since subsequent to this integration it will be necessary to integrate with respect to $y$ over the cross section of the coil in order to find the flux reduction, the complexity of rigorous analysis becomes too great. Approximate formulation of $D_z$ allows the integration to be performed quite readily. Approximating $f(x)$ by straight line segments and applying the two point formula several times, the result is:

$$H''=2(\mu Q-1)H_0\int_0^l [f(x)xdx/\sqrt{(x^2+y^2)^3}]$$

$$=2(\mu Q-1)H_0\sum_{n=0}^{n}\{[(f_{(n\Delta x)}-f_{(n-1)\Delta x})/\Delta x]\times\int_{(n-1)\Delta x}^{n\Delta x}[x^2dx/\sqrt{(x^2+y^2)^3}]+[nf_{(n-1)\Delta x}-(n-1)f_{n\Delta x}]\times\int_{(n-1)\Delta x}^{n\Delta x}[xdx/\sqrt{(x^2+y^2)^3}]\}$$

$$=[2(\mu Q-1)H_0/\Delta x](\sum_{n=0}^{n}\{[2f_{(n\Delta x)}-(f_{(n-1)\Delta x}+f_{(n+1)\Delta x})]\log[n\Delta x+\sqrt{(n^2\overline{\Delta x}^2+y^2)}]\}-f_{n\Delta x}\{\log[n\Delta x+\sqrt{(n^2\overline{\Delta x}^2+y^2)}]+[\Delta x/\sqrt{(n^2\overline{\Delta x}^2+y^2)}]\}).$$

Integrating over the area of the coil

$$N''=2\pi\int_0^R H''ydy=(\mu Q-1)H_0U,$$

$$U=(2\pi/\Delta x)(\sum_{n=0}^{n}\{[2f_{(n\Delta x)}-(f_{(n-1)\Delta x}+f_{(n+1)\Delta x})]\cdot[R^2\log(n\Delta x+\sqrt{[n^2\overline{\Delta x}^2+R^2]})-\tfrac{1}{2}(n\Delta x-\sqrt{[n^2\overline{\Delta x}^2+R^2]})^2]\}-f_{n\Delta x}\{R^2\log(n\Delta x+\sqrt{[n^2\overline{\Delta x}^2+R^2]})-\tfrac{1}{2}(n\Delta x-\sqrt{[n^2\overline{\Delta x}^2+R^2]})^2-2\Delta x(n\Delta x-\sqrt{[n^2\overline{\Delta x}^2+R^2]})\}).$$

It is apparent that $U$ is a function of coil and sample dimensions only and is therefore independent of frequency and sample material. It has been evaluated for each coil (Table I).

By evaluating $N''$ for the entire area of the coil, this analysis allows for the reduction in field inside the sample due to magnetization of the sample, since analysis shows it to be of the same order as the field reduction outside the sample. Actually this internal reduction in flux is negligible, due to the small area of the sample.

## VII. CONDITION FOR INITIAL PERMEABILITY

An upper limit is set to the value of tuning capacity by the necessity of keeping the axial field of the coil low enough to insure initial permeability; i.e., $H<1$ oersted. From $H=0.4\pi nI\cos\theta$ (Fig. 1) and $I=E/\omega L=E\sqrt{[C/L]}$

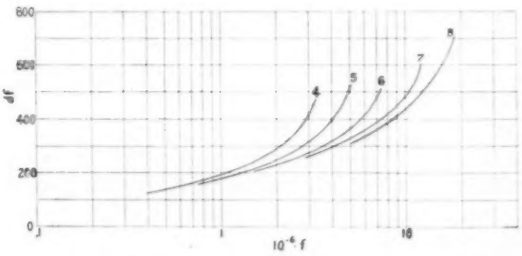


FIG. 5. Observed data for one set of coils.

since $\omega\approx 1/\sqrt{(LC)}$ (where $E$ = resonant voltage and $\omega L$ = reactance of coil ≈ impedance) $H_0=0.4\pi n\cos\theta E\sqrt{(C/L)}<1$ oersted. Oscillograph measurements indicate $E<5$ volts in the oscillators used. For the longest coil using the finest wire this gives $C<100L$; ($C$ in $\mu\mu$f, $L$ in $\mu$h). For the shorter coils using larger wire $C<900L$. This allows the use of very high $C$ circuits, promoting oscillator stability, and extending the usable range of the coil. At low frequencies a

multilayer coil is necessary, $n$ increases, and the maximum $C$ must come down. There is thus a low frequency limit to the application of the method ($\approx$50 kc).

## VIII. DISCUSSION OF RESULTS

The observed data for one set of coils are shown in Fig. 5. These values represent the average of from four to ten individual readings, the probable error of which depends on the frequency, being greater at higher frequencies due to decreased stability of the oscillator. On the average the probable error is less than 2 percent.

A comparative examination of the results of other investigators, listed in the introduction to this report, reveals considerable disparity, the results being scarcely comparable because of differences in sample size and composition, difference in frequency range and differences in method and analysis.

In general, at frequencies below 40 mc and for the limited range of frequency employed by any one investigator, $\mu_L$ as calculated from measures of inductance shows an apparent variation with frequency. This has been due to a use of approximation formulas in the analysis, and to the failure to limit the application of these formulas to the range of frequency where the errors introduced by the approximation would be legitimately negligible. The necessity for this limitation is made visually apparent in Fig. 6 where the dotted portion of each separate curve is that part of the curve discarded because of the aforementioned limitation.

The variation of $\mu_L$ with wave-length is shown in Fig. 6. The permeability $\mu_L$ is practically constant over the entire radiofrequency range from 30 kc to 40 mc. The apparent increase at the high frequency end of the range of each coil is due to the neglect of the distributed capacity factor which is legitimately negligible at lower frequencies.

In the range between 50 kc and 30 kc the apparent increase in $\mu_L$ with decreasing frequency

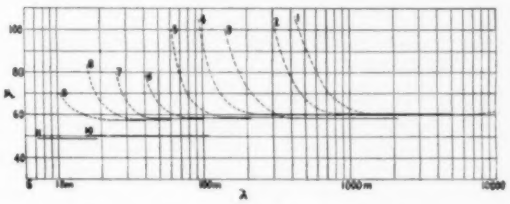

FIG. 6. Variation of $\mu_L$ with wave-length $\lambda$.

is due, in part at least, to an increasing axial field strength, since even with a multi-layer coil the tuning capacity was very large for these low frequencies.

Since coils 10 and 11 were space wound, they had very little distributed capacity, allowing a check on the variation of $\mu_L$ to higher frequency than was possible with a close wound coil. However, the theoretical development of the values of $S$ and $U$ was based on the theory for a close wound coil. This explains the disparity between the results obtained with coils 10 and 11 and those obtained with the other coils. The results with these coils are therefore qualitative only.

The difference in the results from coil to coil is due to departures of the close wound coil from the ideal current sheet and to uncertainty in the approximate evaluation of $U$.

I wish to express my sincere appreciation to Dr. J. Barton Hoag for suggesting the problem, and for his encouragement and kindly advice during the progress of the investigation.

# Demagnetizing Factors of Rods

R. M. Bozorth and D. M. Chapin
*Bell Telephone Laboratories, New York, New York*
(Received March 4, 1942)

A chart is constructed for converting the apparent magnetic permeability to the true permeability of cylinders of any given ratio of length to diameter. The curves are based on previous calculations in which account was taken of the variation of the demagnetizing factor $N$ with permeability, but in which the permeability was assumed constant over any one cylinder. The flux distribution has been determined experimentally in several cylinders, and as the field acting on the specimen is increased from zero, the positions of the effective poles have been found to move toward the middle of the rod until (if the permeability is sufficiently high) they are located about 0.7 of the distance from the middle to the ends, and then to move toward and approach the ends as limits as the permeability declines in high fields.

WHEN using the ballistic galvanometer for making magnetic measurements on cylinders or rods it is common practice to determine directly the "apparent" permeability $\mu'$, equal to the quotient of the flux density $B$ and the applied field strength $H'$. The $B$ is determined at the middle of the rod and $H'$ is calculated simply from the current flowing through the magnetizing solenoid. Then $\mu'$ is converted to the (true) permeability $\mu$ by calculation using the appropriate demagnetizing factor $N$, thus taking account of the field strength produced at the middle of the rod by the rod itself. One purpose of this note is to provide a simple graphical means of converting true to apparent permeability or *vice versa* when the specimens are cylindrical rods of any ratio of length to diameter. The chart shown has already found considerable use in practical problems dealing with such rods.

Other purposes of this report are to record experiments on the distribution of magnetization in several rods, to show how the positions of the poles change with permeability and to compare these findings with theory.

## GRAPHICAL CONVERSION OF μ TO μ′

The demagnetizing factor $N$ is given by

$$H=H'-NI$$

or the equivalent

$$H=H'-(N/4\pi)(B-H),$$

in which $H$ is the (true) field strength, $H'$ the applied field strength equal to that which would exist if the specimen were removed, $I$ the intensity of magnetization and $B$ the flux density measured at the middle of the rod. The $N$ considered here may be termed the ballistic demagnetizing factor to distinguish it from the magnetometric demagnetizing factor which is not multiplied by the $I$ at the middle but by some kind of an average of the intensity of magnetization over the whole bar depending on the position of the magnetometer needle.

The equation given above may be rewritten:

$$\frac{1}{\mu-1}=\frac{1}{\mu'-\mu'/\mu}-\frac{N}{4\pi}$$

or

$$\frac{1}{\mu}\left(1-\frac{N}{4\pi}\right)=\frac{1}{\mu'}-\frac{N}{4\pi},$$

the apparent permeability being defined as $\mu'=B/H'$. In practice sufficient accuracy is always obtained by using the simpler equation:

$$1/\mu=(1/\mu')-(N/4\pi).$$

It is thus possible to plot $\mu$ against $\mu'$ for a cylindrical rod of given dimensional ratio provided $N$ is known, even if $N$ varies with permeability. Such a plot is shown in Fig. 1. The values of $N$ have been taken from the compilations of Stäblein, Schlechtweg, Neumann, and Warmuth[1] and are the results of calculations

[1] H. Neumann, Wiss. Veröff. Siemens-Konz. **10**, 55–71, No. 2 (1931); H. Neumann and K. Warmuth, Wiss. Veröff. Siemens-Konz. **11**, 25–35, No. 2 (1930); F. Stäblein and H. Schlechtweg, Zeits. f. Physik **95**, 630–46 (1935); K. Warmuth, Arch. f. Elektrotech. **30**, 761–79 (1936); **31**, 124–30 (1937) and **33**, 747–63 (1939).

that agree within experimental error with the experimental determinations. The curves of Fig. 1 are corrected for variation of $N$ with $\mu$, the permeability being that corresponding to the $B$ existing at the middle of the rod. The original calculations of $N$ were based on the assumption that $\mu$ is constant over the rod and this may in certain circumstances cause a definite error in the calculated $\mu$ *vs.* $\mu'$ relation.

The values of $N/4\pi$ appropriate for $\mu=\infty$ are plotted, in the upper left-hand portion of Fig. 1, against the dimensional ratio, $m=$length/diameter, of the rod. Since $\mu'=4\pi/N$ when $\mu=\infty$, the scale-reading at the right (for $\mu'$) is the reciprocal of the scale-reading at the left (for $N/4\pi$) for any given horizontal line (ordinate). Also, the asymptote for any given $\mu$ *vs.* $\mu'$ curve ($m=$constant) lies on the same horizontal line as the value of $N/4\pi$ that corresponds to this value of $m$.

The method of using the chart is obvious. Interpolation for values of $m$ not given may be

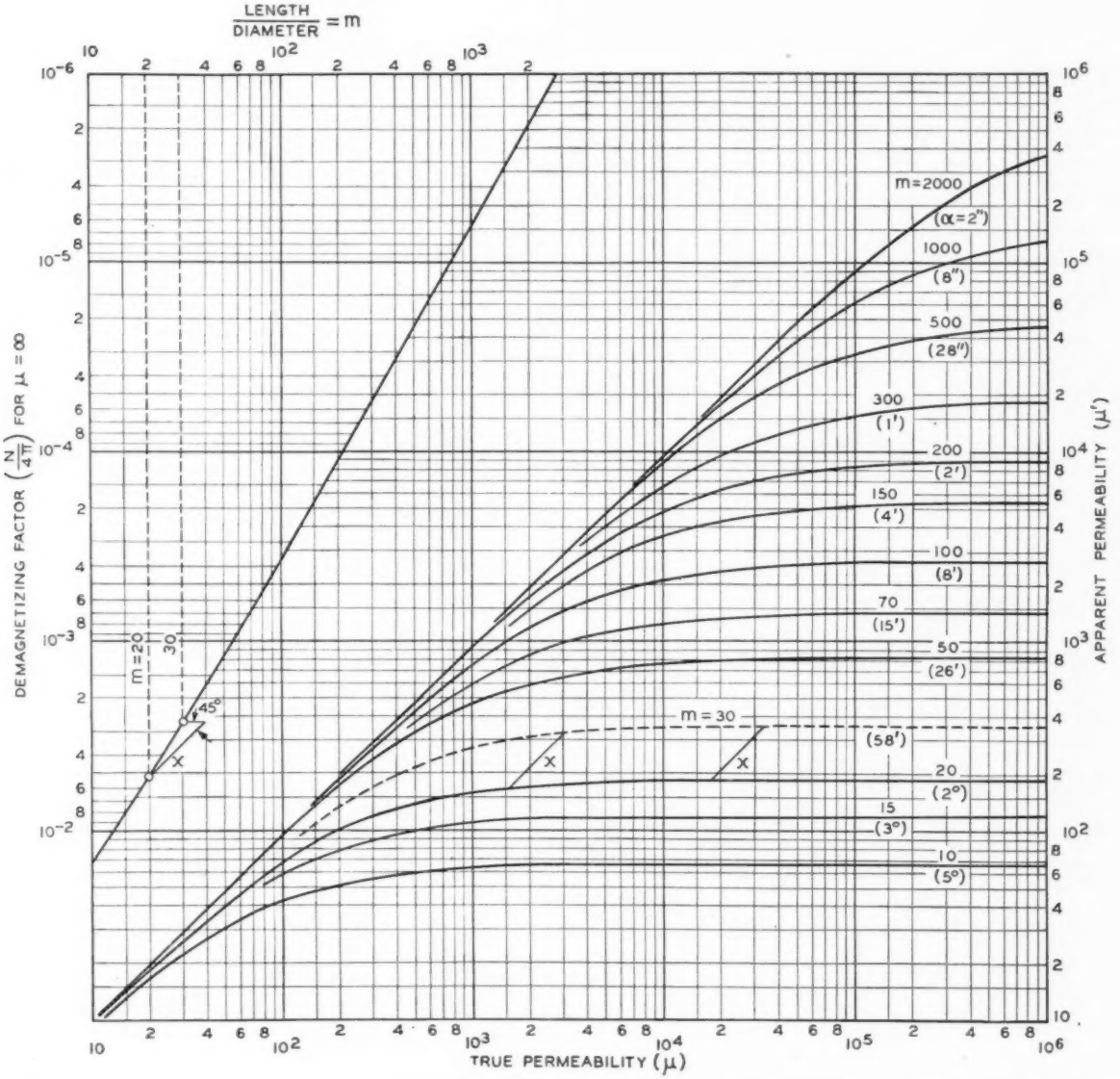


FIG. 1. Relation between apparent permeability $\mu'$ and true permeability $\mu$ of cylinders having any given ratio $m$ of length to diameter. Demagnetizing factors $N$ as defined by $H=H'-NI$, are shown as a function of $m$ for rods having very high permeabilities. The curves may also be used for converting $\mu'$ to $\mu$ for ring specimens in which there is an air gap subtending an angle $\alpha$ at the center of the ring.

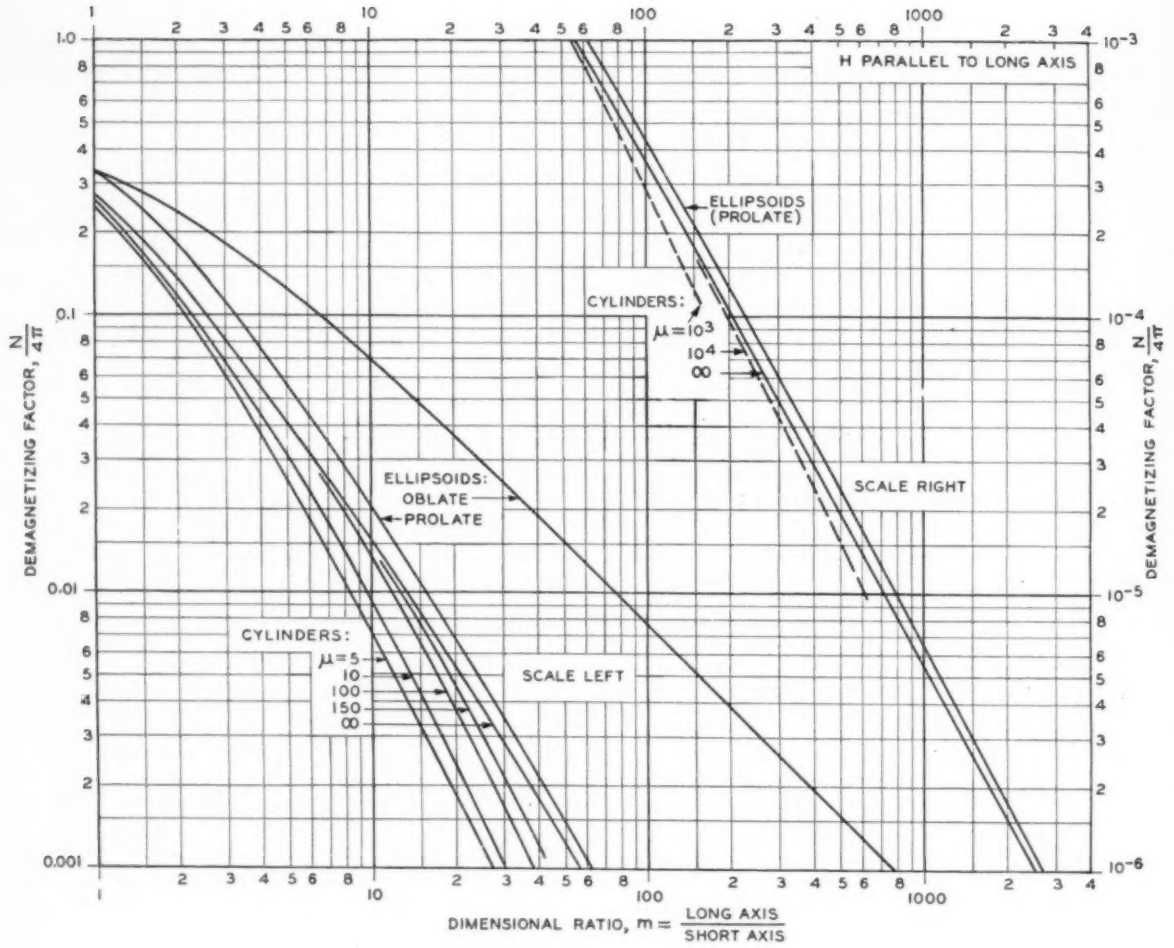


FIG. 2. Demagnetizing factors of ellipsoids and cylinders (see the equations and reference 1).

performed as follows: The appropriate value of $m$ (say, 30) is located on the scale at the top and the corresponding value of $N/4\pi$ (0.0027) found on the curve of $N/4\pi$ *vs.* $m$. The value of $N/4\pi$ is noted also for a nearby value of $m$ for which a $\mu$ *vs.* $\mu'$ curve is drawn (e.g., $m=20$). Horizontal lines are drawn through the points corresponding to these values of $m$ and $N/4\pi$, and the 45° distance $x$ between these lines is determined. The line $x$ of the same length and 45° inclination, may then be drawn from any point on the curve for $m=20$ and will give a point on the curve for $m=30$, as shown by the dotted construction lines on the chart. This method of interpolation is based on the fact that all of the $\mu$ *vs.* $\mu'$ curves are similar, except as influenced by the variation of $N$ with $\mu'$, and differ only by a translation along a line inclined 45° to the axes. The amount of such a displacement at $\mu=\infty$ is obviously the same, on a logarithmic scale, as the displacement made when a point on the $N/4\pi$ *vs.* $m$ curve is moved from one value of $m$ to another; therefore, this is the displacement for all parts of the $\mu$ *vs.* $\mu'$ curve. The slight correction in the interpolation for variation of $N$ with $\mu$ is at all times negligible.

For convenience the demagnetizing factors for oblate and prolate ellipsoids of revolution, and for rods having finite permeabilities, are plotted in Fig. 2. Convenient forms of the equations for accurate calculation of $N/4\pi$ for the ellipsoids are as follows:

(1) For oblate ellipsoid with axes $a=c/m$, $b=c$,

(a) Magnetized parallel to a long axis, $b$ or $c$,

$$\frac{N}{4\pi}=\frac{1}{2}\left[\frac{m^2}{(m^2-1)^{\frac{3}{2}}}\arcsin\frac{(m^2-1)^{\frac{1}{2}}}{m}-\frac{1}{m^2-1}\right],$$

$$\frac{N}{4\pi}=\frac{\pi m-2}{4m^2}\quad\text{if}\quad m\gg 1.$$

(b) Magnetized parallel to the short axis, $a$,

$$\frac{N}{4\pi}=\frac{m^2}{m^2-1}-\frac{m^2}{(m^2-1)^{\frac{3}{2}}}\arcsin\frac{(m^2-1)^{\frac{1}{2}}}{m},$$

$$\frac{N}{4\pi}=1-\frac{\pi}{2m}\quad\text{if}\quad m\gg 1.$$

(2) For prolate ellipsoid with axes $a=mc$, $b=c$,

(a) Magnetized parallel to the long axis, $a$,

$$\frac{N}{4\pi}=\frac{1}{m^2-1}\left\{\frac{m}{2(m^2-1)^{\frac{1}{2}}}\ln\frac{m+(m^2-1)^{\frac{1}{2}}}{m-(m^2-1)^{\frac{1}{2}}}-1\right\},$$

$$\frac{N}{4\pi}=\frac{1}{m^2}(\ln 2m-1)\quad\text{if}\quad m\gg 1.$$

(b) Magnetized parallel to a short axis, $b$ or $c$,

$$\frac{N}{4\pi}=\frac{1}{2}\left\{\frac{m^2}{m^2-1}-\frac{m}{(m^2-1)^{\frac{1}{2}}}\ln\frac{m+(m^2-1)^{\frac{1}{2}}}{m-(m^2-1)^{\frac{1}{2}}}\right\},$$

$$\frac{N}{4\pi}=\frac{1}{2}\left(1-\frac{\ln 2m}{m^2}\right)\quad\text{if}\quad m\gg 1.$$

Neumann and Warmuth[1] give the following formula for calculating $N/4\pi$ for long cylindrical rods having infinite permeability:

$$(N/4\pi)_{\mu=\infty}=(4.02\log_{10}m-0.92)/(2m^2)\quad m\geq 10.$$

It should be remembered that the demagnitizing factors, $N_1$, $N_2$, and $N_3$, in three mutually perpendicular directions in a specimen of any shape add up to $4\pi$:

$$N_1+N_2+N_3=4\pi.$$

From this it follows that the curves of Fig. 2 approach $N/4\pi=1$ as an asymptote as $m$ approaches zero. Also it is convenient to remember that for a thin ring with an air gap that subtends the angle $\alpha$ at the center of the ring, the demagnetizing factor is given simply by

$$N/4\pi=\alpha/360$$

if $\alpha$ is in degrees. Thus for each rod of dimensional ratio $m$, there is a value of $N$ that applies also to a ring having an air gap of angular width $\alpha$. In Fig. 1 these values of $\alpha$ are recorded in parentheses just below the corresponding values of $m$, and the figure may thus be used for ring specimens as well as rods.

## FLUX DISTRIBUTION

In addition to a knowledge of the true permeability of a rod, as determined from $H'$ and from $B$ as measured in a short search coil placed at the middle of a bar, it is often desired to determine this $\mu$ when the search coil covers a considerable portion of the rod or even is longer than the rod. This can be done if the distribution of flux in the rod is known. Flux distribution was determined in two rods having widely different permeabilities but the same diameter (0.97 cm), length (50.6 cm), and dimensional ratio (52.4). Both rods were cut from the same stock of molybdenum permalloy containing 79 percent nickel, 4 percent molybdenum, and the rest iron; one was heat-treated for high permeability while the other was unannealed, as swaged.

Measurements were made with a fluxmeter using a small search coil 2 mm long placed at various positions along the rod. The applied field of given strength $H'$ was reversed in direction to produce the required change in flux. The results are shown in Figs. 3 and 4 in which the flux density $B_l$ at any point along the rod is referred to the density $B$ at the middle. Actually flux-densities are corrected by subtracting $H'$ from each of them; they are in reality $B_l-H'$ and $B-H'$. The abscissa $l/l_0$ is the position of the coil on the rod expressed as the fraction of the distance from the middle to the end. Each curve is marked with the corresponding value of $H'$ and corresponding values of $\mu'$ and $B$ are given in the insert.

The distribution of flux in the annealed rod when the permeability is highest ($H'=5.0$, $\mu'=871$) is nearly parabolic. For comparison, the dotted line of Fig. 3 is drawn as a parabola

cutting the experimental curve at $B_l/B=0.5$. The nearby dashed line is the distribution accurately calculated by Würschmidt[2] under the assumption that $\mu=\infty$; it is nearly parabolic.

The position of the effective pole, given by

$$l_p/l_0=\int_0^\infty \frac{B_l-H'}{B-H'}d\frac{l}{l_0},$$

may be determined* for each of these theoretical curves and for the experimental curves; for the parabolic distribution it lies at $l_p/l_0=0.73$, Würschmidt's distribution gives 0.73, and for these experimental curves $l_p/l_0$ lies between 0.72 and 0.96.

The demagnetizing factor of a rod depends not only on the dimensional ratio and on the permeability, if that is uniform throughout the bar, but also on the variation of permeability if, as is generally the case, it is different in one portion of the rod than in another. It has been reported[3] that the positions of the effective poles move toward the middle of the rod and then outward again as the magnetization is increased from zero, and it has been pointed out[4] that they are nearest the middle when the magnetization is approximately that corresponding to maximum permeability. The more recent calcu-

[2] J. Würschmidt, *Theorie des Entmagnetizierung Factors und der Scherung von Magnetizierungskurven* (Vieweg, Braunschweig, 1925).

* This integral is equal to

$$\int_0^1 \frac{B_l-H}{B-H'}d\frac{l}{l_0} \quad \text{since} \quad \int_0^\infty (H_l-H')d(l/l_0)=0$$

and

$$\int_1^\infty (B_l-H)d(l/l_0)=0,$$

as pointed out to us by Mr. H. J. Williams. In all of our experiments $B-H$ and $B-H'$ (both at the middle of the rod) are indistinguishable.

[3] L. Holborn, Sitz, Preuss. Akad. Wiss. 159–68 (1898); C. G. Lamb, Phil. Mag. **48**, 262–71 (1899).

[4] G. F. C. Searle and T. G. Bedford, Phil. Trans. Roy. Soc. **A198**, 33–104 (1902). For further discussion of change of $N$ with $B$, see E. Dussler, Ann. d. Physik **86**, 66–94 (1928) and D. Foster, Phil. Mag. **8**, 304–13 (1929).

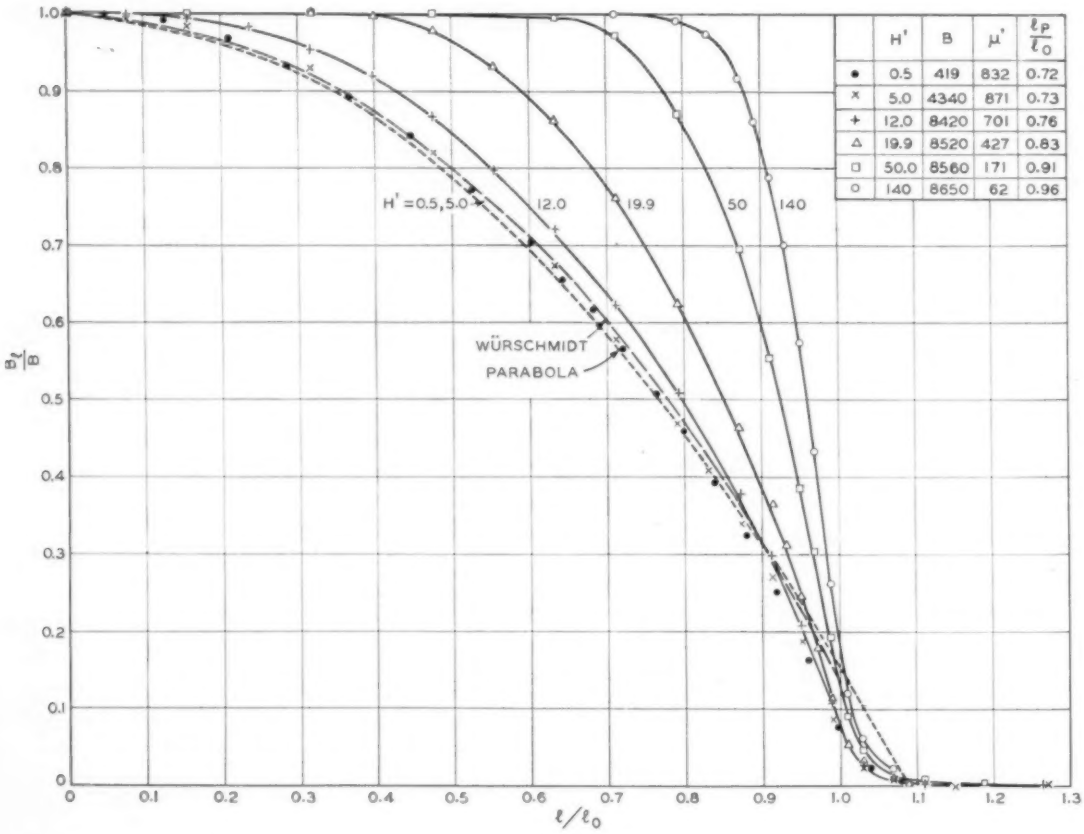


FIG. 3. Distribution of flux in rod of annealed permalloy having dimensional ratio $m=52.4$. Values of $B$, $H'$, $\mu'$ and $l_p/l_0$ (pole position) are indicated in the table. Theoretical distribution (broken line) for $\mu=\infty$ is as calculated by Würschmidt.

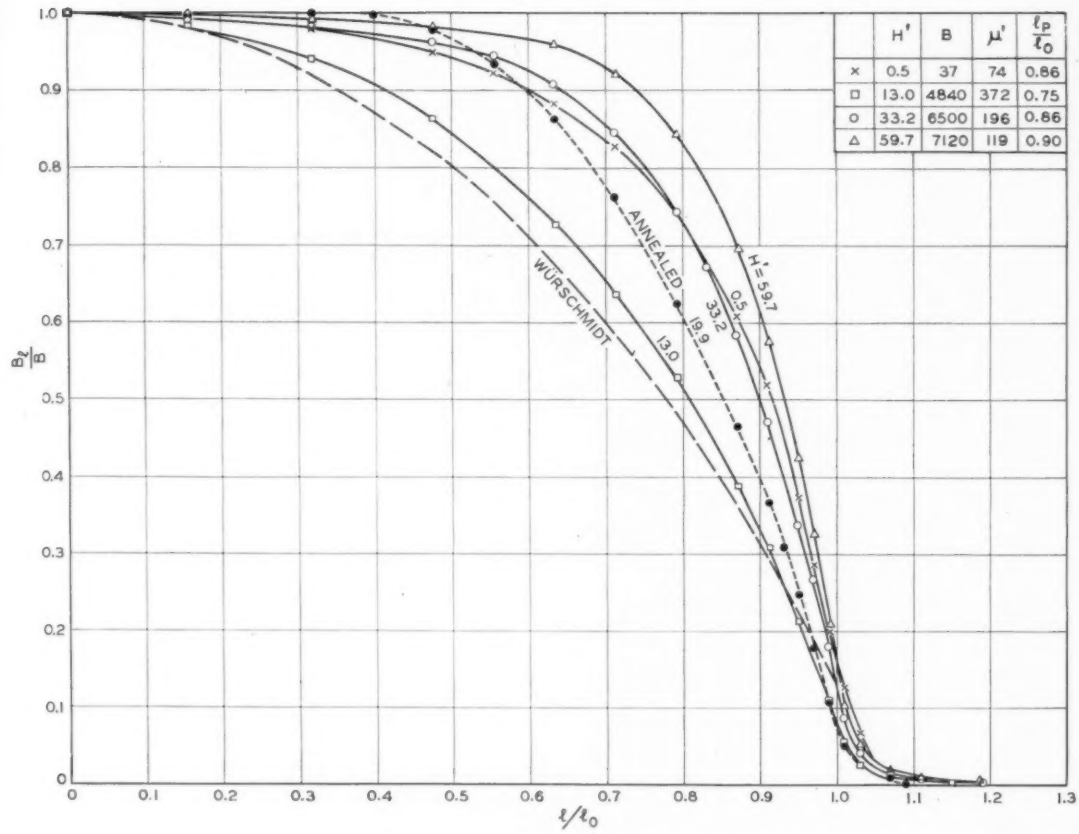


FIG. 4. Distribution of flux in rod of unannealed permalloy ($m=52.4$). $B$, $H'$, $\mu'$ and $l_p/l_0$ are as indicated. Würschmidt's curve (broken line) and an experimental curve for the annealed rod ($H=20$) are shown for comparison.

lations of Würschmidt establish the fact that a high demagnetizing factor and a small interpolar distance are associated with high permeability. Thus, theory and experiment justify the following description of the movements of the effective poles as the applied field is increased from zero. The poles appear first at some position, between $l_p/l_0=0.7$ and $l_p/l_0=1$, determined by the true initial permeability $\mu_0$ of the rod. As $H'$ increases $\mu$ also increases in all ferromagnetic materials and the poles, therefore, move toward the middle of the bar, approaching the limiting position $l/l_0\doteq 0.7$ the more nearly the higher the maximum permeability, $\mu_m$. As $H'$ increases further and $\mu$ declines from $\mu_m$ to 1, the poles move toward the ends of the rod and approach these ends as limits. The positions of the poles are given in the table inserted in Figs. 3 and 4.

When the permeability is well below the highest value the distribution is far from parabolic, as is evident from the curves. In the lowest fields the permeability of the unannealed rod is low and uniform, and it is possible to calculate the flux distribution and compare with experiment. Such calculations could be made as described by Stäblein and Schlechtweg[1] but they are laborious and have not been carried out for this report. When the applied field-strength is increased the permeability at the middle is greater than that at the ends; the poles are then nearer the middle than they would be if the permeability of the whole bar were that of the middle, for the low permeability at the ends effectively shortens the rod. That this is so is indicated by the data for the annealed rod for $H'=0.5$; in this case the poles were already near their closest-in positions because of the high permeability, and the increase in $\mu$ at the middle causes the poles to move in still farther to $l_p/l_0=0.72$, a minimum value for this rod and a value less than that corresponding to Würschmidt's calculated distribution for $\mu=\infty$.

When either rod is subjected to an intense field, the distribution near the middle is naturally quite uniform because the field over a considerable portion of the rod is sufficient to cause saturation. The distribution curve for $H'=20$ for the annealed rod may be contrasted with that for $H'=0.5$ for the unannealed rod. The former curve shows only a very slight dropping of the flux in going from the center to $l/l_0=0.4$, and this is due to the fact that this rod is practically saturated while the unannealed rod has an almost uniform permeability over its entire length.

Attention may be called to the very slight differences in distribution in the unannealed rod when $H'=0.50$ and 33.2. This may be attributed to the relatively slight change in permeability in different parts of the rod, as compared to the large range in permeabilities in the annealed rod.

It seemed desirable to establish for rods of all dimensional ratios the apparent fact that the effective pole has a minimum interpolar distance given by $l_p/l_0 \doteq 0.7$. To this end a wire of 70 permalloy was heat treated in a magnetic field[5] to develop high permeability and its effective pole positions were measured. The wire was 30.4 cm long, 1.01 mm in diameter ($m=300$), its effective permeability $\mu'=18{,}250$,* and the pole positions were found to be $l_p/l_0=0.70$. Thus, the minimum pole separation corresponding to $l_p/l_0 \doteq 0.7$ may be assumed to apply to all cylinders with very high permeability. A rod may be considered to have "very high permeability" for this purpose, if its $\mu$ is so high that increasing it does not increase the $\mu'$ of the rod by more than 10 or 20 percent as indicated by the curves of Fig. 1.

[5] J. F. Dillinger and R. M. Bozorth, Physics **6**, 279–84 (1935).

* Using Neumann and Warmuth's Eq. (12) of reference 1, $N/4\pi=0.00005021$ for $\mu=\infty$ and $m=300$. Combining this with our $\mu'=18{,}250$ gives $\mu=218{,}000$, a value consistent with previous results for this material, reference 5.

## LENGTH OF SEARCH COIL

The distribution curves can now be used to calculate the way in which the flux threading the search coil varies with the coil's length. In practical measurement this amounts to being able to determine $B$ at the middle of the bar from the galvanometer deflection made with a search coil of any length. The calculation is simply the averaging of $B_l$ over the length of the search coil, and results are shown in Fig. 5

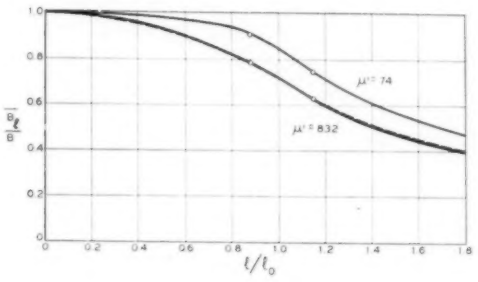


FIG. 5. Effect of length of search coil on measurement of $B$. Search coil (of length $2l$) and rod (of length $2l_0$) are concentric. $B$ is flux density at middle, $\bar{B}_l$ is the average flux density in that part of the rod that is "covered" by the search coil. The dashed line is calculated for the parabolic distribution of Fig. 3.

for the two molybdenum permalloy rods in fields of $H'=0.5$. Search coils of two lengths, one 88 percent of the length of the rod and one considerably longer than the rod, were constructed and points on the curves were checked as indicated in the figure. The dotted line is calculated for the parabolic distribution curve shown in Fig. 3. It is evident that for a rod of dimensional ratio near $m=50$, an effective permeability of $\mu'=700$ ($\mu \doteq 3000$) is sufficiently low to cause an appreciable departure from the curve for the nearly parabolic distribution associated with infinite permeability. For the upper curve of Fig. 5, $\mu'=74$ and $l_p/l_0=0.86$.

# The Electrical Oscillations of a Perfectly Conducting Prolate Spheroid*

ROBERT M. RYDER†
*Sloane Physics Laboratory, Yale University, New Haven, Connecticut*
(Received January 20, 1942)

The forced oscillations of a perfectly-conducting prolate spheroid of eccentricity nearly unity are shown to be decomposable into "harmonics" corresponding to different modes of vibration, each harmonic being quantitatively connected with a certain portion of the impressed electric field which drives the antenna. The harmonics contribute additively to the current and field of the spheroid; each offers a characteristic impedance to the driving field, and the properties of the antenna are a composite depending upon the proportions of the various harmonics present. The behavior of the harmonics with frequency is discussed qualitatively; analytical expressions obtained are useful chiefly at the resonant frequencies of the antenna, where the most important harmonic becomes sinusoidal in character.

THE partial differential equation of the electromagnetic field, as is well known, can be separated in the coordinates of various simple geometrical surfaces. In this way have been studied the fields of a prolate spheroid by Abraham,[1] of a paraboloid by the same author,[2] of an infinite cylinder by Sommerfeld,[3] of two parallel infinite cylinders by Mie,[4] of the sphere by Mie[5] and Debye.[6] Necessarily limited to rather simple surfaces (of which the prolate spheroid seems best to approximate a finite straight wire), the method has compensating advantages: perhaps the most important is the physical insight obtained into the problem.

The diameter of a prolate spheroid falls to half its maximum value at a distance $0.866a$ from the center, where $a$ is the semi-major axis; hence the "equivalent spheroid" is slightly thicker at the center and somewhat longer than the cylinder it represents.[7,8] From this rough idea of equivalence one might expect that measurements on conductors of uniform cross section would give resonant wave-lengths somewhat longer than those calculated by Abraham for the spheroid. "Exact" calculations for the free oscillations of a cylinder have been made by Oseen[9] and extended by Hallén,[10] whose results hold also for curved or even closed coil antennas. Like all the above-mentioned authors Hallén's paper discussed only natural frequencies and logarithmic decrements of free oscillations, leaving the steady state alone; still, the experiments of Englund[11] furnish encouraging confirmation. Two years later the question was reopened by Lindman[12] who in some new measurements obtained the very curious result that the formulas of Abraham derived for the prolate spheroid gave better correspondence than those of Hallén, presumably derived for the cylinders which he was using. Subsequent discussion[13,14] leaves the impression that the mathematical approximations of the various methods may introduce as much error as the physical approximation involved in changing the shape. Accordingly the forced oscillations of a prolate spheroid would appear to be of some practical interest.

In the extensive literature of the antenna there has more often been used the method of calculating the field from some assumed current distribution in the antenna. Many shapes of antenna can be treated; perhaps typical is G. W. Pierce's work on the L-shaped antenna[15]

* Condensed from a dissertation presented to the Faculty of the Graduate School of Yale University in candidacy for the degree of Doctor of Philosophy, 1940.

† Now at Bell Telephone Laboratories, New York, New York.

[1] M. Abraham, Ann. d. Physik **66**, 435 (1898).
[2] M. Abraham, Ann. d. Physik **2**, 32 (1900).
[3] A. Sommerfeld, in Franck and von Mises *Die Differential- und Integralgleichungen* . . . (1925), Volume 2, p. 526.
[4] G. Mie, Ann. d. Physik **2**, 201 (1900).
[5] G. Mie, Ann. d. Physik **25**, 377 (1908).
[6] P. Debye, Ann. d. Physik **30**, 56 (1909).
[7] Lord Rayleigh, Phil. Mag. **8**, 105 (1904).
[8] L. Page and N. I. Adams, Phys. Rev. **53**, 819 (1938).
[9] C. W. Oseen, Archiv. f. Matem. Astr. och Fysik **9**, Nr. 12 (1913); Nr. 13 (1914).
[10] E. Hallén, Uppsala Univ. Arsskr., Matem. o. Naturv. Nr. 1 (1930).
[11] C. R. Englund, Bell Sys. Tech. J. **7**, 404 (1928).
[12] K. F. Lindman, Ann. d. Physik **13**, 358 (1932).
[13] E. Hallén, Ann. d. Physik **14**, 586 (1932).
[14] K. F. Lindman, Ann. d. Physik **15**, 127 (1932).
[15] G. W. Pierce, *Electric Oscillations and Electric Waves* (1910).

which also illustrates the great mathematical complexities involved. A discussion of the validity of these methods is given by Grosskopf.[16] From the point of view of the present paper they are open to the criticism that usually the boundary conditions involved are only approximately satisfied, that no quantitative connection is obtained between antenna current and driving field, and that no explanation appears of why sinusoidal current should be a good assumption in some cases but not in others.

Recently L. V. King[17] has developed another method with the unfortunate property that the fundamental integral equation requires re-solution for each new way of driving the antenna. More recently still Page and Adams[8] have studied oscillations forced in a perfectly conducting prolate spheroid by a uniform electric field parallel to its axis and varying sinusoidally with the time—the problem of the receiving antenna. The present paper may be regarded as a continuation of the study of oscillations forced by a general electric field of that kind. The same problem has been studied by Stratton and Chu,[18] who used rather different methods in their analytical attack on the differential equation.

## I. THE DIFFERENTIAL EQUATION

After the notation of Page and Adams,[8] if $xyz$ are a right-handed set of rectangular coordinates with the $x$ axis along the long axis of the prolate spheroid, and if $\rho^2=y^2+z^2$, then may be introduced the prolate spheroidal coordinates $\xi$, $\eta$, $\phi$, forming a right-handed set in the order named, and given by the relations

$$x=f\xi\eta, \tag{1}$$

$$\rho=f\{(1-\xi^2)(\eta^2-1)\}^{\frac{1}{2}}, \tag{2}$$

$$\phi=\tan^{-1}(z/y), \tag{3}$$

where $-1\leqslant\xi\leqslant 1$, $1\leqslant\eta<\infty$, $0\leqslant\phi<2\pi$. The constant $f$ is the semi-interfocal distance of the common foci of all the prolate spheroids $\eta=\text{constant}=\eta_0$. To the remarks given by Page and Adams on the properties of these coordinates we need add only that for very thin spheroids ($\eta_0-1\ll 1$), $\xi$ represents distance measured along the spheroid from its center in units such that the total length is 2. Also, readers are warned that the definitions of $\xi$ and $\eta$ are interchanged from those used by Stratton and Chu.

We are interested in fields whose time dependence is specified by the factor $\exp(-i\omega t)$, and in axially symmetric waves, so that the only non-vanishing field components are

$$E_\xi=i\left(\frac{\mu}{\kappa}\right)^{\frac{1}{2}}\frac{1}{\epsilon f}\frac{1}{\{(1-\xi^2)(\eta^2-\xi^2)\}^{\frac{1}{2}}}\frac{\partial A}{\partial\eta}, \tag{4}$$

$$E_\eta=-i\left(\frac{\mu}{\kappa}\right)^{\frac{1}{2}}\frac{1}{\epsilon f}\frac{1}{\{(\eta^2-\xi^2)(\eta^2-1)\}^{\frac{1}{2}}}\frac{\partial A}{\partial\xi}, \tag{5}$$

$$H_\varphi=\frac{1}{f}\frac{1}{\{(\eta^2-1)(1-\xi^2)\}^{\frac{1}{2}}}A, \tag{6}$$

where $A\equiv\rho H_\varphi$ satisfies the differential equation

$$(1-\xi^2)\frac{\partial^2 A}{\partial\xi^2}+(\eta^2-1)\frac{\partial^2 A}{\partial\eta^2}+\epsilon^2(\eta^2-\xi^2)A=0 \tag{7}$$

as was shown by Abraham.[1] Heaviside-Lorentz symmetrical units are used throughout. Here $\kappa$ and $\mu$ are, respectively, the permittivity and permeability of the medium surrounding the spheroid, while

$$\epsilon\equiv(\omega/v)f=2\pi(f/\lambda), \tag{8}$$

where $v=c/(\kappa\mu)^{\frac{1}{2}}$ is the normal wave velocity in the medium, $c$ is the velocity of light in vacuum, and $\lambda$ is the wave-length. Noteworthy is the fact that $\epsilon$ is proportional to the frequency $\nu$ of oscillation of the field. Separation of the variables in (7) is effected by putting $A(\xi,\eta)=X(\xi)Y(\eta)$.

$$(1-\xi^2)d^2X/d\xi^2+(\alpha-\epsilon^2\xi^2)X=0, \tag{9}$$

$$(\eta^2-1)d^2Y/d\eta^2+(-\alpha+\epsilon^2\eta^2)Y=0. \tag{10}$$

The constant of separation $\alpha$ may have only certain eigenvalues such that the electric field is continuous on the $x$ axis. Equivalent are the two eigenvalue conditions

$$E_\xi=0 \quad \text{when} \quad \xi=\pm 1, \tag{11}$$

$$X(1)=X(-1)=0. \tag{11a}$$

[16] J. Grosskopf, Hoch. u. Elek: akus. **49**, 205 (1937).
[17] L. V. King, Phil. Trans. Roy. Soc. **A236**, 381 (1937).
[18] L. J. Chu and J. A. Stratton, J. App. Phys. **12**, 241 (1941).

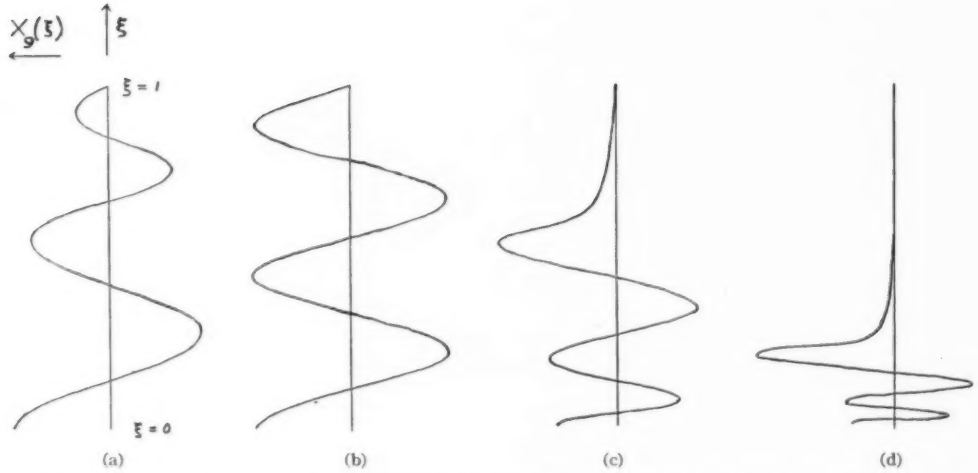


FIG. 1. Qualitative distribution of current in the ninth harmonic: (a) low frequency; (b) resonant frequency; (c) and (d) above resonance.

Since by hypothesis the spheroid is a perfect conductor, at its surface holds the boundary condition

$$E_\xi + E = 0, \quad \eta = \eta_0, \tag{12}$$

in which $E$ is an external exciting or driving field.

There is also a condition on Eq. (10), in that at large distances, in order to represent a divergent wave,

$$Y(\eta) \to e^{i\epsilon\eta} \quad \text{as} \quad \eta \to \infty. \tag{13}$$

## II. QUALITATIVE FEATURES OF THE SOLUTIONS

Both Eqs. (9) and (10) are of the same form:

$$u''(x) + f(x)u(x) = 0. \tag{14}$$

From well-known theorems about the qualitative behavior of continuous solutions of such an equation[19] it is possible to discover some properties not readily obvious from their series developments. For example, take $X_p(\xi)$, the $p$th eigensolution of (9): it is shown below that $X_p(\xi)$ gives the current distribution in the antenna for the $p$th mode of vibration. $X_p(\xi)$ is an oscillatory function with $p+1$ nodes, counting the two at the ends of the antenna; the other $p-1$ nodes are all confined to the interval $-(\alpha^{\frac{1}{2}}/\epsilon) < \xi < +(\alpha^{\frac{1}{2}}/\epsilon)$. At zero frequency ($\epsilon = 0$) $X_p(\xi)(1-\xi^2)^{-\frac{1}{2}}$ is proportional to the associated Legendre polynomial $P_{p1}(\xi)$, and $\alpha_p = p(p+1)$. As the frequency parameter $\epsilon$ increases, so does $\alpha$, but more slowly, so that when $\epsilon = p\pi/2$, $\alpha_p = \epsilon^2$. Meanwhile the current loops at the ends of the antenna have increased until they equal all the other loops in size, and at the "resonance point" $\epsilon = p\pi/2$, $X_p(\xi)$ is a sinusoid.

At frequencies higher than resonance the character of $X_p$ becomes radically different: $\alpha$ becomes and remains less than $\epsilon^2$; the curvature of the graph of $X_p(\xi)$ against $\xi$ is away from the $\xi$ axis for $|\xi| > \alpha^{\frac{1}{2}}/\epsilon$, and the loops and nodes move in toward the center of the antenna. It is evident that it may be difficult to represent $X_p$ by a simple approximation valid over any large frequency range, but near resonance a sinusoid may be useful. Qualitative sketches of $X_9(\xi)$ (showing only half the spheroid) appear in Fig. 1.

From the $Y$ equation in the form

$$Y_p'' + \left(\epsilon^2 - \frac{\gamma_p}{\eta^2 - 1}\right) Y_p = 0, \quad \gamma_p \equiv \alpha_p - \epsilon^2, \tag{10a}$$

it is clear that for large $\eta$, regardless of $p$, any solution approaches the value $Ae^{i\epsilon\eta} + Be^{-i\epsilon\eta}$, where $A$ and $B$ are constants. The notation $Y$ is reserved for that solution which is asymptotically

$$Y_p = U_p + iV_p \to \cos\epsilon\eta + i\sin\epsilon\eta \quad \text{as} \quad \eta \to \infty. \tag{15}$$

Since the coefficients in the equation are real, both $U(\eta)$ and $V(\eta)$ satisfy (10a) separately;

[19] See for example Franck and v. Mises, *Die Differential- und Integralgleichungen* . . . For an acquaintance with these theorems the author is indebted to Professor Einar Hille of Yale University.

clearly also they are independent solutions. For $p$ odd, $U_p$ is proportional to $X_p(\eta)$ and is therefore zero at $\eta=1$; hence $Y_p(1)=iV_p(1)$ is pure imaginary, and $V_p(1)$ has always the same sign as $i^{p-1}$. For $\epsilon \ll p\pi/2$, $|V_p(1)| \gg 1$; for $\epsilon = p\pi/2$, $|V_p(1)|=1$; while for $\epsilon > p\pi/2$, $|V_p(1)|<1$.

## III. ANALYTIC SOLUTIONS OF THE EQUATIONS

### 1. Solutions in Integral Form

The following methods are due to Abraham.[1,2] Let either (9) or (10) be written in the form

$$\varphi(v, y) \equiv (1-y^2)v''(y)+(\alpha-\epsilon^2y^2)v(y)=0. \tag{16}$$

Here $v$ will denote the solution which in the interval $-1 \leqslant y \leqslant 1$ is holomorphic, and vanishes to the first order at the ends of the interval. Now is introduced the transform

$$\frac{w(x)}{1-x^2}=\int_{y_1}^{y_2} \exp(i\epsilon xy)v(y)dy. \tag{17}$$

Substitution of (17) into (16) and proper determination of the integration limits of the former show the following two special forms of $w$ are solutions of (16):

$$w_1(y)=(1-y^2)\int_{-1}^{1} \exp(i\epsilon yt)v(t)dt, \tag{18}$$

$$w_2(y)=(1-y^2)\int_{1}^{1+i\infty} \exp(i\epsilon yt)v(t)dt, \quad y>1. \tag{19}$$

$w_1(y)$ vanishes for $y=\pm 1$; hence except for a multiplicative constant it must be equal to $v(y)$. If we restore the $(X, \xi)$ notation,

$$e_pX_p(\xi)=(1-\xi^2)\int_{-1}^{1} \exp(i\epsilon\xi t)X_p(t)dt, \tag{18a}$$

where $e_p$ is a function both of the eigenvalue index $p$ and of the frequency parameter $\epsilon$.

(19) holds only for $y>1$; we suspect that it may have something to do with $Y(\eta)$. This is indeed the case: integration by parts, followed by a few transformations, shows that

$$\frac{\epsilon^2}{X_p'(1)}w_2(\eta)=e^{i\epsilon\eta}+\frac{(-1)^{p+1}\gamma_p}{i\epsilon e_pX_p'(1)}\int_{-1}^{1}\frac{\exp[i\epsilon(\eta-s)]}{\eta-s}X_p(s)ds, \tag{20}$$

from which is concluded, after Abraham, that

$$\frac{\epsilon^2}{X_p'(1)}w_2(\eta)\equiv Y_p(\eta), \quad \eta>1 \tag{19a}$$

is asymptotic to $e^{i\epsilon\eta}$ for large $\eta$; hence it is the solution sought, representing a divergent wave. Further reduction gives forms suitable for computation:

$$Y_p(\eta)=e^{i\epsilon\eta}+\frac{(-1)^{p+1}\gamma_p}{i\epsilon e_p}\left[\frac{X_p(\eta)}{X_p'(1)}\log\frac{\eta+1}{\eta-1}-G_p(\eta)\right], \tag{21}$$

$$Y_p'(\eta)=i\epsilon e^{i\epsilon\eta}+\frac{(-1)^{p+1}\gamma_p}{i\epsilon e_p}\left[\frac{X_p'(\eta)}{X_p'(1)}\log\frac{\eta+1}{\eta-1}-\frac{2}{\eta^2-1}\frac{X_p(\eta)}{X_p'(1)}-G_p'(\eta)\right], \tag{22}$$

where

$$G_p(\eta) \equiv \frac{e^{i\epsilon\eta}}{X_p'(1)} \int_{-1}^{1} \frac{X_p(\eta) \exp(-i\epsilon\eta) - X_p(s) \exp(-i\epsilon s)}{\eta - s} ds. \tag{23}$$

The point of the manipulations is now clear: Abraham has neatly separated out the parts of the expression which give trouble by becoming large when $\eta \to 1$. The logarithmic term in $Y_p'$ is the only one not finite at $\eta = 1$. For long, thin spheroids values of $\eta$ near 1 are of chief interest; and to good approximation may be written

$$Y_p(\eta) = e^{i\epsilon} + \frac{(-1)^{p+1}\gamma_p}{i\epsilon e_p}[-G_p(1)] \quad \text{if} \quad \eta - 1 \ll 1, \tag{21a}$$

$$Y_p'(\eta) = i\epsilon e^{i\epsilon} + \frac{(-1)^{p+1}\gamma_p}{i\epsilon e_p}\left[\log \frac{\eta+1}{\eta-1} - 1 - G_p'(1)\right] \quad \text{if} \quad \eta - 1 \ll 1. \tag{22a}$$

Since $G_p$ and $G_p'$ depend only upon $X_p$, it is seen that (21) and (22) give the desired solution of (10) in terms of the desired solution of (9), which is found below by a perturbation method.

## 2. Series Solution of (9)

$$X_p''(\xi) + \left(\epsilon^2 + \frac{\gamma_p}{1-\xi^2}\right) X_p(\xi) = 0. \tag{9a}$$

The value $\gamma_p = 0$ gives the most important solution of (9a), that is, the sine wave which applies at resonance. It seems natural, therefore, to try to solve (9a) as a perturbation of the cosine equation, i.e., to find $X_p(\xi)$ as a trigonometric Fourier series. However, even though $\gamma_p$ is small near resonance, we cannot well regard this equation as a perturbation of $X'' + \epsilon^2 X = 0$, for the solutions of the latter do not satisfy the eigenvalue condition (11a). Instead, we write

$$\left[X_p'' + \left(\frac{p\pi}{2}\right)^2 X_p\right] + \left[\theta_p + \frac{\gamma_p}{1-\xi^2}\right] X_p = 0, \tag{24}$$

wherein $\theta_p \equiv \epsilon^2 - \frac{1}{4}p^2\pi^2$ (25) and the second bracket is to be regarded as in the nature of a perturbation. Application of the usual methods develops the following expansions:

$$\gamma_p = \gamma_{p1}\theta_p + \gamma_{p2}\theta_p^2 + \gamma_{p3}\theta_p^3 + \cdots, \tag{26}$$

$$X_p = X_{p0} + X_{p1}\theta_p + X_{p2}\theta_p^2 + \cdots, \tag{27}$$

$$= \textstyle\sum_k a_{pk} \sin \frac{1}{2}k\pi(1-\xi), \quad p+k \text{ even}, \tag{27a}$$

$$= \textstyle\sum_k \sum_j a_{pjk}\theta_p^j \sin \frac{1}{2}k\pi(1-\xi), \quad p+k \text{ even}. \tag{27b}$$

From use of the above come the following expressions for parameters of the integral formulas (21–23):

$$e_p = -\frac{4}{\pi} \frac{\sum_k (1/k) a_{pk}}{\sum_k (-1)^{(k-1)/2} a_{pk}}, \quad k, p \text{ odd}, \tag{28o}$$

$$e_p = -\frac{8i\epsilon}{\pi^2} \frac{\sum_k (1/k) a_{pk}}{\sum_k (-1)^{k/2} k a_{pk}}, \quad k, p \text{ even}, \tag{28e}$$

$$G_p(1) = -\frac{1}{X_p'(1)} \sum_k a_{pk} L_k(\epsilon), \tag{29}$$

$$G_p'(1) = -1 + \frac{1}{X_p'(1)} \sum_k a_{pk} M_k(\epsilon). \tag{30}$$

In (29) and (30) the new symbols $L$ and $M$ are functions of $\epsilon$ only, defined as follows:

$$L_k(\epsilon)\equiv\int_0^2\frac{\exp(i\epsilon t)\sin\frac{1}{2}k\pi t}{t}dt, \tag{31}$$

$$M_k(\epsilon)\equiv\frac{k\pi}{2}\int_0^2\frac{1-\exp(i\epsilon t)\cos\frac{1}{2}k\pi t}{t}dt. \tag{32}$$

Values for the first few coefficients for (26) and (27) are obtained without too much difficulty from the subjoined formulas:

$$\gamma_{p1}=-2/F(2p), \tag{26-1}$$

$$\gamma_{p2}=\frac{8}{\pi^2}\frac{1}{[F(2p)]^3}\sum_k{}'\frac{\{F(p+k)-F(p-k)\}^2}{p^2-k^2},\quad \begin{matrix}p+k\text{ even},\\ p\neq k\end{matrix} \tag{26-2}$$

$$\gamma_{p3}=\frac{2}{[F(2p)]^2}\sum_k{}'a_{p2k}[F(p+k)-F(p-k)]-\tfrac{1}{2}F(2p)\gamma_{p2}{}^2 \tag{26-3}$$

$$a_{p0k}=\begin{cases}1 & \text{if}\quad p=k\\ 0 & \text{if}\quad p\neq k,\end{cases} \tag{27-0}$$

$$a_{p1k}=\begin{cases}\dfrac{4}{\pi^2}\dfrac{1}{F(2p)}\dfrac{F(p+k)-F(p-k)}{p^2-k^2}, & \text{if}\quad p+k\text{ even},\\ 0, & \text{if}\quad p+k\text{ odd or }p=k,\end{cases} \tag{27-1}$$

$$a_{p2k}=\frac{4}{\pi^2}\frac{1}{(p^2-k^2)}\left\{-a_{p1k}+\frac{1}{F(2p)}\sum_m{}'a_{p1m}\{F(m+k)-F(m-k)\}-\tfrac{1}{2}\gamma_{p2}\{F(p+k)-F(p-k)\}\right. \tag{27-2}$$

In looking over these formulas, one observes that $a_{pjk}$ is zero unless the indices $p$ and $k$ are both even or both odd: this condition is required by the symmetry properties of the function $X_p(\xi)$, discussed above. Secondly, unfortunately already in the first order all the sines of the same symmetry as $X_{p0}$ have been introduced. For $|p-k|$ large, however, their coefficients are small. The summations indicated in the formulas for the coefficients are infinite series whose general terms are not known, though in some cases estimates may be found. In practice the finding of higher order terms than those given above involves prohibitive difficulty, so that the analytic solutions found are useful only in the region where the power series for the various functions of $\theta_p$ are satisfactorily approximated by their first three terms. Near resonance it may be expected that the resonant harmonic will be accurately determined: to the other modes we shall have somewhat rough approximations, but ordinarily the other modes are merely small correction terms.

## IV. PROPERTIES OF THE FORCED OSCILLATIONS

Let the spheroid be acted upon by an exciting field

$$\mathbf{E}=\mathbf{i}\mathcal{E}(\xi)e^{-i\omega t} \tag{33}$$

parallel to its axis. The boundary condition (12) at the surface of the perfect conductor becomes

$$(\partial A/\partial\eta)_{\eta=\eta_0}=i(\kappa/\mu)^{\frac{1}{2}}\epsilon f\eta_0(1-\xi^2)\mathcal{E}(\xi). \tag{34}$$

Now any wave which is axially symmetrical can be expanded in a uniformly convergent series of the

eigenfunctions of (7); this particular exciting field is defined by

$$A=\sum_p c_p X_p(\xi)\,Y_p(\eta), \tag{35}$$

$$(\partial A/\partial\eta)_0=\sum_p c_p X_p(\xi)\,Y_p'(\eta_0), \tag{36}$$

wherein the $c$'s may be formally evaluated by substitution of (36) into (34), multiplication by $(1-\xi^2)^{-1}X_m(\xi)$, and use of the fact readily seen from (9a) that the $X_p$'s form an orthogonal set over the interval $-1\leqslant\xi\leqslant 1$ with the weight-factor $(1-\xi^2)^{-1}$. If $N(p)$ symbolizes the normalizing factor of the orthogonal set, then the result is

$$c_p=\frac{i\left(\frac{\kappa}{\mu}\right)^{\frac{1}{2}}\epsilon a\int_{-1}^{1}\mathcal{E}(\xi)X_p(\xi)d\xi}{N(p)\,Y_p'(\eta_0)}, \tag{37}$$

where

$$\int_{-1}^{1}\frac{X_n(\xi)X_p(\xi)}{1-\xi^2}d\xi=\begin{cases}0, & n\neq p\\ N(p), & n=p.\end{cases} \tag{38}$$

The current in the antenna is given by

$$\begin{aligned}I(\xi)&=2\pi c(A)_{\eta=\eta_0}=2\pi c\sum_p c_p X_p(\xi)\,Y_p(\eta_0)\\ &=ig\epsilon\sum_p\frac{\int_{-1}^{1}\mathcal{E}(t)X_p(t)dt}{N(p)\,Y_p'(\eta_0)}X_p(\xi)\,Y_p(\eta_0),\end{aligned} \tag{39}$$

where $g$ stands for the constant

$$g=2\pi c(\kappa/\mu)^{\frac{1}{2}}a \tag{40}$$

and $a=f\eta_0$ is the semi-major axis of the spheroid.

Under the assumption that the set of functions $\{(1-\xi^2)^{-1}X_n(\xi)\}$ is complete, we may write

$$\mathcal{E}(\xi)=\sum_p h_p\frac{X_p(\xi)}{1-\xi^2}=\sum_p\frac{\int_{-1}^{1}\mathcal{E}(t)X_p(t)dt}{N(p)}\frac{X_p(\xi)}{1-\xi^2}. \tag{41}$$

The meaning of Eqs. (33), (39), and (41), which formally solve the antenna problem, may be clarified by considering the situation which would exist if there were acting alone the "unit" driving field

$$\mathcal{E}_p(\xi)=X_p(\xi)/(1-\xi^2). \tag{41a}$$

The current in the antenna would then be

$$I_p(\xi)=ig\epsilon X_p(\xi)\,Y_p(\eta_0)/Y_p'(\eta_0). \tag{39a}$$

Just the $p$th mode of oscillation would be present—none of the others, whose coefficients all vanish by the orthogonality property (38). This result holds regardless of frequency, whether that be right for resonance of the $p$th harmonic or not; but of course the required method of excitation (41a) varies with the frequency. By (41), then, the driving field is broken up into "segments" each of which excites only a single mode in the current. Since the behavior of the spheroid is different for each harmonic, properties of the antenna will depend upon the method of excitation: not ordinarily very critically for resonant antennas, however, for as shown below the resonant mode usually accounts for the major part of the phenomena.

Having thus separated the reaction of the antenna into parts, we may proceed to study the behavior of the single mode given by (41a) and (39a).

### 1. Properties of the $p$th Mode

One of the first things now to be done is to justify the use frequently made in the foregoing of the term "resonance." The resonant behavior near $\epsilon=\frac{1}{2}p\pi$ is due to the factor $Y_p'(\eta_0)$ in the denominator of the expression for the current (39a). By (22a) it is seen that $Y_p'(\eta_0)$ is of the form

$$Y_p'(\eta_0)=b\log\frac{\eta_0+1}{\eta_0-1}+c, \tag{22b}$$

where $b$ and $c$ are not very different in magnitude, though one is real and the other imaginary. Since the spheroid is of great eccentricity, the factor $\log(\eta_0+1)/(\eta_0-1)$ is quite large; and $b$ is a function of frequency which goes through zero at $\epsilon=\frac{1}{2}p\pi$. (22b), then, is a typical "resonance denominator" consisting of two terms, the larger of which vanishes at the point of resonance, leaving the other as a small residual so that the fraction is not infinite. Accordingly the current in the $p$th mode (39a) is much greater when $\epsilon=\frac{1}{2}p\pi$ than for neighboring values.

The sharpness of this resonance is greater for thinner spheroids, whose eccentricity $1/\eta_0$ is nearer unity. A first approximation to the band-width of the antenna is readily computed, and is tabulated below.

The phase angle $\phi$ by which the current leads the driving field can be found in the following manner: in the fraction

$$\frac{I_p(\xi)}{\mathcal{E}_p(\xi)}=ig\epsilon(1-\xi^2)\frac{Y_p(\eta_0)}{Y_p'(\eta_0)}$$

$$=ig\epsilon(1-\xi^2)\frac{e^{i\epsilon}+\dfrac{(-1)^{p+1}\gamma_p}{i\epsilon e_p}[-G_p(1)]}{i\epsilon e^{i\epsilon}+\dfrac{(-1)^{p+1}\gamma_p}{i\epsilon e_p}\left[\log\dfrac{\eta_0+1}{\eta_0-1}-1-G_p'(1)\right]}, \tag{42}$$

it is known from (41) that $\mathcal{E}_p$ is in phase with the driving field if that is all of one phase throughout the length of the spheroid. Thus the phase of the current is the same as that of the fraction (42). From the qualitative discussion it is known that $Y_p(\eta_0)$, which is $Y_p(1)$ in the approximation used here, has always the same phase angle as $\exp(ip\pi/2)$; hence changes in the phase angle of the current depend only on the ratio of the real and imaginary parts of $Y_p'(\eta_0)$. Writing

$$Y_p'(\eta_0)=i^{p+1}(A+iB). \tag{43}$$

Then

$$\tan\phi=B/A. \tag{44}$$

Some more properties of $\phi$ follow from the qualitative discussion: to begin with, $A$ has always the same sign, for, considered as a function of $\eta$, it is the analytic extension of $X_p'(\eta)$, with a constant of proportionality which is real and, although a function of frequency, cannot change sign since it is never zero or infinite for finite $\epsilon$. (Continuity is of course assumed.) Thus $A$ is proportional to $X_p'(1)$; since the latter is always negative, $A$ cannot change sign.

A direct consequence is that $A$ is always positive, for at resonance

$$A\big]_{\epsilon=p\pi/2}=i^{-p-1}\cdot i\epsilon e^{i\epsilon}\big]_{\epsilon=p\pi/2}=p\pi/2>0. \tag{45}$$

Explicitly, the expression for the phase angle is

$$\varphi=\tan^{-1}\left\{\frac{\dfrac{\gamma_p}{\epsilon|e_p|}\left[\log\frac{\eta_0+1}{\eta_0-1}-1-\Re e\{G_p'(1)\}\right]+\Im m[i^{-p}e^{i\epsilon}]}{\Re e[i^{-p}\epsilon e^{i\epsilon}]+\dfrac{\gamma_p}{\epsilon|e_p|}\Im m[G_p'(1)]}\right\}. \tag{44a}$$

For thin spheroids the logarithmic term dominates all the rest, at any rate for the lower harmonics; and the fraction has the same sign as $\gamma_p$. At the resonant frequency, $\gamma_p=0$ and the antenna, in this approximation, presents a pure resistance load to the driving field. Below the resonant frequency the mode is of capacitative character, while above resonance the reactance is inductive. The sharper the spheroid, the larger $\log(\eta_0+1)/(\eta_0-1)$, the faster $\phi$ changes with frequency, and the sharper the resonance.

The radiation field due to the $p$th harmonic is given by (4), (5), and (6). At large distances $E_\eta$ is negligible compared to $E_\xi$ and $H_\phi$; the two latter constitute the radiation field:

$$E_\xi=-\frac{\epsilon\eta_0}{|Y_p'(\eta_0)|}\frac{1}{\{(1-\xi^2)(\eta^2-\xi^2)\}^{\frac{1}{2}}}X_p(\xi)\exp[i(\epsilon\eta-\omega t-\tfrac{1}{2}p\pi-\varphi)],\quad \eta\text{ large}, \tag{46}$$

$$H_\varphi=\left(\frac{\kappa}{\mu}\right)^{\frac{1}{2}}\frac{\epsilon\eta_0}{|Y_p'(\eta_0)|}\frac{1}{\{(1-\xi^2)(\eta^2-1)\}^{\frac{1}{2}}}X_p(\xi)\exp[i(\epsilon\eta-\omega t-\tfrac{1}{2}p\pi-\varphi)],\quad \eta\text{ large}. \tag{47}$$

In these two equations the asymptotic values $Y_p(\eta)\sim e^{i\epsilon\eta}$ and $Y_p'(\eta)\sim i\epsilon e^{i\epsilon\eta}$ have been used, as well as (43) and (44) for $Y_p'(\eta_0)$.

The Poynting flux $-cE_\xi H_\varphi$ in the direction of increasing $\eta$ is then at large distances

$$-cE_\xi H_\varphi=\frac{c\epsilon^2\eta_0^2(\kappa/\mu)^{\frac{1}{2}}}{|Y_p'(\eta_0)|^2}\frac{X_p^2(\xi)}{1-\xi^2}\frac{\cos^2(\epsilon\eta-\omega t-\frac{1}{2}p\pi-\varphi)}{\{(\eta^2-\xi^2)(\eta^2-1)\}^{\frac{1}{2}}},\quad \eta\text{ large}, \tag{48}$$

while the element of area of the large spheroid is

$$dS=2\pi f^2\{(\eta^2-\xi^2)(\eta^2-1)\}^{\frac{1}{2}}d\xi, \tag{49}$$

whence comes the mean rate of radiation of power

$$\begin{aligned}-\tfrac{1}{2}c\int_S E_\xi H_\varphi dS&=\pi cf^2\frac{\epsilon^2\eta_0^2}{|Y_p'(\eta_0)|^2}\left(\frac{\kappa}{\mu}\right)^{\frac{1}{2}}\int_{-1}^{1}\frac{X_p^2(\xi)d\xi}{1-\xi^2}\\&=\left[\frac{dU}{dt}\right]_{\text{av}}=\pi c\left(\frac{\kappa}{\mu}\right)^{\frac{1}{2}}\frac{\epsilon^2a^2}{|Y_p'(\eta_0)|^2}N(p).\end{aligned} \tag{50}$$

The radiation resistance is defined as the pure resistance which would consume the same amount of power as the spheroid when carrying the same current. Since the current varies from point to point, the radiation resistance will depend upon the point chosen for reference—usually a current loop. Except at resonance, the loops vary in size and the choice most convenient may vary with the method of driving the antenna; accordingly the radiation resistance at a point $\xi$ is defined as a function of that point:

$$R_{\text{rad}}=\frac{[dU/dt]_{\text{av}}}{\frac{1}{2}|I|^2}=\left(\frac{\mu}{\kappa}\right)^{\frac{1}{2}}\frac{N(p)}{2\pi cX_p^2(\xi)|Y_p(\eta_0)|^2}. \tag{51}$$

Combination of (51) and (44a) gives the reactance due to radiation:

$$X_{\text{rad}} = -R_{\text{rad}} \tan \phi. \tag{52}$$

It is more usual to give the field strength as a function of antenna current rather than in the form (46). Combining with (39a),

$$E_\xi = -\frac{\eta_0}{g\,|\,Y_p(\eta_0)\,|}\,\frac{1}{(\eta^2-\xi^2)^{\frac{1}{2}}}\,\frac{I_p(\xi)}{(1-\xi^2)^{\frac{1}{2}}}\,e^{i(\epsilon\eta-\omega t-\frac{1}{2}p\pi)} \tag{46a}$$

or, in practical units at large distances,

$$E_\xi = -\left(\frac{\mu}{\kappa}\right)^{\frac{1}{2}}\frac{1}{|\,Y_p(\eta_0)\,|}\,\frac{59.96}{r}\,\frac{I_p(\xi)}{(1-\xi^2)^{\frac{1}{2}}}\,e^{i(\epsilon\eta-\omega t-\frac{1}{2}p\pi)}\ \text{volts/cm}. \tag{46b}$$

This last equation gives a relation between the current distribution in the antenna and the directional characteristics of the field. In polar coordinates, if the field is entirely due to the $p$th harmonic,

$$\left|\frac{E_\theta(\theta)}{E_\theta(0)}\right| = \frac{1}{\sin\theta}\left|\frac{I_p(\xi)}{I_p(0)}\right|. \tag{53}$$

Unfortunately, if other harmonics are present in appreciable amounts, the simple relation (53) does not hold for the total current on account of the weighting factor $1/|\,Y_p(\eta_0)\,|$ in (46b).

### 2. Properties of the $p$th Harmonic near Resonance

Formally the solution of the antenna problem is now complete, but the results will be of quantitative value only if the functions $X$ and $Y$ in (26) and (21) can be computed sufficiently accurately. The complexity of some of the preceding expressions is due to the fact that they hold for all frequencies, and as the qualitative argument shows the functions change very considerably in character over the infinite frequency range. Since in practice the harmonics are important near resonance, the simple approximate formulas due to the leading (sinusoidal) term only may be used. First, at resonance:

$$\epsilon = \tfrac{1}{2}p\pi;\quad \gamma_p = 0;\quad X_p = \sin\tfrac{1}{2}p\pi(1-\xi);\quad Y_p = \exp\,(i\tfrac{1}{2}p\pi\eta); \tag{54}$$

$$c_p A_p = i\left(\frac{\kappa}{\mu}\right)^{\frac{1}{2}}\epsilon a\,\frac{1}{Y_p'(\eta_0)}X_p(\xi)\,Y_p(\eta).$$

Length

$$2a = 2f\eta_0 = p\frac{\lambda}{2}\,\frac{1}{(\kappa\mu)^{\frac{1}{2}}}\,\frac{1}{\{1-(b/a)^2\}^{\frac{1}{2}}}.$$

The current in the antenna due to the $p$th harmonic is

$$I_p(\xi) = ig\epsilon X_p(\xi)\frac{Y_p(\eta_0)}{Y_p'(\eta_0)} = g\sin\frac{p\pi}{2}(1-\xi) \tag{55}$$

in phase with $\mathcal{E}_p$, and is sinusoidal. In practical units—$\mathcal{E}$ measured in volts per centimeter and the current in amperes,

$$I_p(\xi) = 0.01668(\kappa/\mu)^{\frac{1}{2}}a\sin\tfrac{1}{2}p\pi(1-\xi). \tag{55a}$$

At resonance, the field at all distances is given by the sinusoidal functions. In Heaviside-Lorentz

units,

$$E_\xi = -\eta_0 \frac{\sin \frac{1}{2}p\pi(1-\xi)}{\{(1-\xi^2)(\eta^2-\xi^2)\}^{\frac{1}{2}}} e^{i(\frac{1}{2}p\pi\eta-\omega t-\frac{1}{2}p\pi)}, \tag{56}$$

$$E_\eta = -\eta_0 \frac{\cos \frac{1}{2}p\pi(1-\xi)}{\{(\eta^2-1)(\eta^2-\xi^2)\}^{\frac{1}{2}}} e^{i(\frac{1}{2}p\pi\eta-\omega t-\frac{1}{2}p+1\pi)}, \tag{57}$$

$$H_\varphi = \eta_0 \left(\frac{\kappa}{\mu}\right)^{\frac{1}{2}} \frac{\sin \frac{1}{2}p\pi(1-\xi)}{\{(1-\xi^2)(\eta^2-1)\}^{\frac{1}{2}}} e^{i(\frac{1}{2}p\pi\eta-\omega t-\frac{1}{2}p\pi)} \tag{58}$$

or in volts per centimeter

$$E_\xi = -\eta_0 \frac{\sin \frac{1}{2}p\pi(1-\xi)}{\{(1-\xi^2)(\eta^2-\xi^2)\}^{\frac{1}{2}}} e^{i(\frac{1}{2}p\pi\eta-\omega t-\frac{1}{2}p\pi)}, \tag{56a}$$

$$E_\eta = -\eta_0 \frac{\cos \frac{1}{2}p\pi(1-\xi)}{\{(\eta^2-1)(\eta^2-\xi^2)\}^{\frac{1}{2}}} e^{i(\frac{1}{2}p\pi\eta-\omega t-\frac{1}{2}(p+1)\pi)}. \tag{57a}$$

It seems worth noting that for large distances (56a) becomes the approximate formula in standard use for radiation from a free wire in space.[20,21] If we change to spherical coordinates, $f\eta = r$ and $\xi = \cos\theta$:

$$E_\theta = -\frac{a}{r} \frac{\sin [\frac{1}{2}p\pi(1-\cos\theta)]}{\sin\theta} \exp\left[i\left(\frac{p\pi}{2}\frac{r}{f} - \omega t - \frac{p\pi}{2}\right)\right]. \tag{56b}$$

The formulation of the present paper has the advantage that a quantitative connection with the driving field (41) as well as with the current (39a) is found.

The radiation resistance for the resonant harmonic is

$$R_{\text{rad}} = \left(\frac{\mu}{\kappa}\right)^{\frac{1}{2}} \frac{N(p)}{2\pi c \sin^2 \frac{1}{2}p\pi(1-\xi)}. \tag{59}$$

If the radiation resistance at resonance is referred to a current loop, then $X_p^2(\xi) = 1$, and the radiation resistance in ohms is then

$$R_p = (\mu/\kappa)^{\frac{1}{2}} 29.98 F(2p) \text{ ohms}, \tag{59p}$$

wherein

$$F(2p) \equiv \int_0^{2p\pi} \frac{1-\cos x}{x} dx.$$

Since at resonance the current is in phase with the driving field, the phase angle and reactance both vanish.

If the $p$th harmonic is not precisely at resonance, a complete and exact discussion would require the use of all the machinery developed previously, the perturbation expressions (26), (27), (21a), etc. It is, however, possible near resonance to get a reasonable approximation without much labor, simply by the use of only the first few terms.

Near resonance, the frequency parameter becomes

$$\frac{2\pi\nu f(\kappa\mu)^{\frac{1}{2}}}{c} \equiv \epsilon = \left[\left(\frac{p\pi}{2}\right)^2 + \theta_p\right]^{\frac{1}{2}} = \frac{p\pi}{2} + \frac{\theta_p}{p\pi} + \cdots. \tag{60}$$

We still take

$$X_p(\xi) = \sin \tfrac{1}{2}p\pi(1-\xi), \tag{61}$$

[20] Carter, Hansell, and Lindenblad, Proc. I. R. E. **19**, 1773 (1931).
[21] F. E. Terman, *Radio Engineering*, second edition (1937), p. 686.

thus assuming sinusoidal current distribution; but the parameter $\gamma_p$ is no longer 0; it is

$$\gamma_p \doteq \gamma_{p1}\theta_p = -\frac{2}{F(2p)}\theta_p. \tag{62}$$

When we continue the approximation that all the $a$'s are zero except $a_{pp}=1$, there result:

$$Y_p(\eta_0) \doteq Y_p(1) = i^p\left\{1-\frac{Si(2p\pi)}{F(2p)}\frac{\theta_p}{p\pi}\right\}, \tag{63}$$

$$Y_p'(\eta_0) = i^{p+1}\left\{\frac{p\pi}{2}+\frac{\theta_p}{p\pi}-\frac{\theta_p}{2}\frac{Si(2p\pi)}{F(2p)}-i\frac{\theta_p}{F(2p)}\log\frac{\eta_0+1}{\eta_0-1}\right\}. \tag{64}$$

Immediately from (44) and (64) comes the phase angle by which the current leads the driving field:

$$\tan\phi = -\frac{\theta_p}{F(2p)}\log\frac{\eta_0+1}{\eta_0-1}\Big/\left[\frac{p\pi}{2}+\theta_p\left(\frac{1}{p\pi}-\frac{1}{2}\frac{Si(2p\pi)}{F(2p)}\right)\right]. \tag{65}$$

The radiation resistance (51) is

$$R_{\text{rad}} = \left(\frac{\mu}{\kappa}\right)^{\frac{1}{2}}\frac{F(2p)}{4\pi c\,|\,Y_p(\eta_0)\,|^2} \tag{66}$$

or in ohms

$$R_p \doteq \left(\frac{\mu}{\kappa}\right)^{\frac{1}{2}}\frac{29.98F(2p)}{1-2\dfrac{Si(2p\pi)}{F(2p)}\dfrac{\theta_p}{p\pi}}, \tag{67}$$

when referred to a current maximum. The field follows the current both in magnitude and phase (46a). The current (39a) in amperes is

$$I_p(\xi) = 0.01668(\kappa/\mu)^{\frac{1}{2}}a\epsilon\sin\tfrac{1}{2}p\pi(1-\xi)\cdot\frac{1-\dfrac{Si(2p\pi)}{F(2p)}\dfrac{\theta_p}{p\pi}}{\dfrac{p\pi}{2}+\theta_p\left[\dfrac{1}{p\pi}-\dfrac{1}{2}\dfrac{Si(2p\pi)}{F(2p)}\right]-i\dfrac{\theta_p}{F(2p)}\log\dfrac{\eta_0+1}{\eta_0-1}}. \tag{68}$$

Since the logarithmic term in the denominator of (68) is large if the frequency is not too close to resonance, with increasing slenderness of the antenna $\eta_0-1$ becomes smaller and the resonance sharper.

Since this current has been evoked by the "unit" driving field (41a), the power consumed takes the form

$$\mathcal{P} = \Re\int_{-1}^{1}\mathcal{E}_p(\xi)I_p(\xi)\cdot f\eta_0 d\xi$$

$$= 0.01668\left(\frac{\kappa}{\mu}\right)^{\frac{1}{2}}a^2N(p)\Re\left\{\frac{1-\dfrac{Si(2p\pi)}{p\pi F(2p)}\theta_p}{1-\dfrac{Si(2p\pi)}{2\epsilon F(2p)}\theta_p-i\dfrac{\theta_p}{\epsilon F(2p)}\log\dfrac{\eta_0+1}{\eta_0-1}}\right\}. \tag{69}$$

The frequency-dependent portion is confined to the expression whose real part is to be taken. If now in the small correction term involving $\theta_p$ in the numerator we replace $p\pi$ by $2\epsilon$, considerable

simplification results:

$$\mathcal{P}=I_0\mathfrak{a}N(p)\Re\left\{\frac{1}{\theta_p\log\dfrac{\eta_0+1}{\eta_0-1}\Big/\left(1-i\dfrac{}{\epsilon F(2p)-\frac{1}{2}\theta_p Si(2p\pi)}\right)}\right\}, \tag{70}$$

wherein $I_0$ is the current at a current loop at the resonant frequency.

It will be noted that even in this first approximation, on account of the correction term in $Si(2p\pi)$ the pass band of the antenna is not quite exactly symmetrical about the resonant frequency. Numerically, Table I shows the asymmetry to be quite small in the case of the first mode. The edges of the

TABLE I. Properties of the first harmonic near resonance.

| | | | $\log\frac{\eta_0+1}{\eta_0-1}=10$ | | | $\log\frac{\eta_0+1}{\eta_0-1}=15$ | | | $\log\frac{\eta_0+1}{\eta_0-1}=20$ | | | $\log\frac{\eta_0+1}{\eta_0-1}=40$ | | |
|---|---|---|---|---|---|---|---|---|---|---|---|---|---|---|
| $\theta_1$ | $\nu/\nu_r$ | $R_p$ ohms | $\varphi$ degrees | $X$ ohms | $I_0/I_{0r}$ | $\varphi$ degrees | $X$ ohms | $I_0/I_{0r}$ | $\varphi$ degrees | $X$ ohms | $I_0/I_{0r}$ | $\varphi$ degrees | $X$ ohms | $I_0/I_{0r}$ |
| −1.2 | 0.75 | 51 | 72.6 | −160 | 0.28 | | | | | | | | | |
| −1.0 | 0.80 | 53 | 69.4 | −140 | 0.34 | | | | | | | | | |
| −0.8 | 0.84 | 56 | 64.7 | −119 | 0.42 | 72.5 | −180 | 0.29 | | | | | | |
| −0.6 | 0.88 | 60 | 57.7 | −95 | 0.53 | 67.2 | −142 | 0.38 | 72.5 | −190 | 0.30 | | | |
| −0.4 | 0.919 | 63.7 | 46.4 | −67.0 | 0.684 | 57.6 | −101 | 0.532 | 64.6 | −134 | 0.426 | 76.6 | −268 | 0.230 |
| −0.2 | 0.959 | 68.04 | 27.7 | −35.66 | 0.884 | 38.2 | −53.5 | 0.784 | 46.4 | −71.3 | 0.688 | 64.5 | −142.7 | 0.429 |
| −0.1 | 0.980 | 70.47 | 14.7 | −18.44 | 0.966 | 21.4 | −27.65 | 0.930 | 27.6 | −36.87 | 0.885 | 46.3 | −73.74 | 0.690 |
| −0.05 | 0.990 | 71.75 | | | | 11.1 | −14.07 | 0.981 | 14.6 | −18.76 | 0.967 | 27.6 | −37.51 | 0.885 |
| −0.025 | 0.995 | 72.41 | | | | | | | | | | 14.6 | −18.92 | 0.967 |
| 0 | 1 | 73.08 | 0 | 0 | 1.000 | 0 | 0 | 1.000 | 0 | 0 | 1.000 | 0 | 0 | 1.000 |
| 0.025 | 1.005 | 73.76 | | | | | | | | | | −14.6 | 19.26 | 0.968 |
| 0.05 | 1.010 | 74.46 | | | | −11.1 | 14.57 | 0.980 | −14.6 | 19.43 | 0.967 | −27.6 | 38.86 | 0.885 |
| 0.1 | 1.020 | 75.89 | −14.7 | 19.79 | 0.967 | −21.4 | 29.68 | 0.930 | −27.5 | 39.57 | 0.885 | −46.2 | 79.14 | 0.690 |
| 0.2 | 1.041 | 78.93 | −27.5 | 41.08 | 0.885 | −38.0 | 61.61 | 0.787 | −46.2 | 82.16 | 0.692 | −64.4 | 164.3 | 0.432 |
| 0.4 | 1.081 | 85.8 | −46.0 | 88.9 | 0.689 | −57.3 | 133 | 0.538 | −64.3 | 178 | 0.432 | −76.4 | 356 | 0.233 |
| 0.6 | 1.12 | 94 | −57.2 | 146 | 0.53 | −66.7 | 219 | 0.39 | −72.1 | 292 | 0.30 | | | |
| 0.8 | 1.16 | 104 | −64.1 | 210 | 0.43 | −72.1 | 320 | 0.30 | | | | | | |
| 1.0 | 1.20 | 116 | −68.7 | 300 | 0.35 | | | | | | | | | |
| 1.2 | 1.25 | 130 | −72.0 | 400 | 0.29 | | | | | | | | | |

pass band, taken arbitrarily at the half-power points, give a band width in terms of $\theta_p$

$$\Delta\theta_p=2\epsilon F(2p)\Big/\left[\log\frac{\eta_0+1}{\eta_0-1}-\frac{Si(2p\pi)}{4\log\dfrac{\eta_0+1}{\eta_0-1}}\right]. \tag{71}$$

In terms of frequency, setting $\nu_r$ equal to the resonant frequency gives the simple approximate band width

$$\frac{\Delta\nu}{\nu_r}=F(2p)\Big/\left[\frac{p\pi}{2}\log\frac{\eta_0+1}{\eta_0-1}\right], \tag{72}$$

in which the correction term in $Si(2p\pi)$ has been omitted. The presence of higher harmonics will slightly widen the band.

## V. COMPOSITE OSCILLATIONS

Up to this point has been discussed only the behavior of the $p$th harmonic (or mode of vibration) alone; but if any field other than a multiple of the special one $\mathcal{E}_p(\xi)=(1-\xi^2)^{-1}X_p(\xi)$ be acting, then harmonics other than the $p$th will also be excited, by (39). As an example consider a vertical quarter-wave antenna excited at the base. If the ground be regarded as perfectly conducting, the image antenna will be similarly excited, and the two together may be regarded approximately as a single centrally-driven prolate spheroid. If we assume the original driving e.m.f. to have been $Ve^{-i\omega t}$ volts,

(41) may be applied:

$$\mathcal{E}(\xi)=2V/f\eta_0\Delta\xi, \quad -\Delta\xi/2<\xi<\Delta\xi/2;$$
$$\mathcal{E}(\xi)=0 \text{ elsewhere}, \quad (73)$$

$$h_p=\frac{1}{N(p)}\int_{-1}^{1}\mathcal{E}(t)X_p(t)dt=\frac{1}{N(p)}\frac{2V}{a}X_p(0). \quad (74)$$

When this equation is specialized to the fundamental frequency, we find $\epsilon=\frac{1}{2}\pi$, $X_1=\sin\frac{1}{2}\pi\times(1-\xi)$, and $X_1(0)=1$. Thus

$$h_1=1.6409V/a. \quad (75)$$

Rather involved calculations give for the third mode

$$h_3=-1.075V/a. \quad (76)$$

Higher modes are neglected in this example; the same method is applicable, but they are small. The current at the center of the spheroid is

$$\left(\frac{\mu}{\kappa}\right)^{\frac{1}{2}}I(0)=0.02738V$$
$$-0.00545V\frac{i}{\log(\eta_0+1)/(\eta_0-1)}. \quad (77)$$

As expected, the current due to the first mode is much the major part of the total; and the contribution of the third harmonic is practically 90° out of phase with the driving field.

It is apparent that the phase angle of the total current is not zero when the first harmonic alone is in resonance. If the usual engineering criterion of zero phase angle be taken as the criterion for "resonance," since the third harmonic is capacitative in character, the frequency must be slightly increased so that an inductive component of the first mode will appear to cancel this capacitative current. (It should be noted that this cancellation will not hold throughout the spheroid, because the current distributions of the two modes differ; accordingly, the "resonant" frequency depends slightly on the driving point chosen.) For the center-driven antenna, approximate calculations based on (65) and

$$I_1(0)=0.01668(\kappa/\mu)^{\frac{1}{2}}a\cos\varphi e^{-i\varphi}$$
$$=I_{10}\cos\varphi e^{-i\varphi}, \quad (68a)$$

which holds for frequencies near the resonant point, show that this cancellation takes place when

$$\tan\varphi=\frac{-0.2}{\log(\eta_0+1)/(\eta_0-1)};$$
$$\frac{\epsilon}{\frac{1}{2}\pi}=1+\frac{0.16}{[\log(\eta_0+1)/(\eta_0-1)]^2}. \quad (78)$$

For even the fattest of the antennas considered in Table I, this frequency shift is only 0.16 percent.

Another meaning of "resonance" differs from both the foregoing: it is maximum total antenna current. If we continue to neglect the small variation of the non-resonant third harmonic with frequency, it is clear that maximum total current will occur quite near the resonance of its principal component at $\epsilon=\frac{1}{2}p\pi$; in fact, the frequency for current resonance will be just slightly lower than this. The frequency shift for this case is $-0.15$ percent for the fattest antenna of Table I. Here again the "resonant" frequency depends upon the point chosen. Page and Adams[8] have computed this type of resonance for various antennas excited by a field whose complex magnitude is constant along their length.

In practice, optimum antenna performance would seem to demand not zero phase angle, nor yet maximum current; but instead the criterion might well be maximum rate of power radiation. In the general case, if the amounts of harmonics present are given by the numbers

$$h_p=\frac{1}{N(p)}\int_{-1}^{1}\mathcal{E}(t)X_p(t)dt$$

[see (41)], then the mean rate of radiation of power is

$$\left[\frac{dU}{dt}\right]_{\text{av}}=\pi c\left(\frac{\kappa}{\mu}\right)^{\frac{1}{2}}a^2\epsilon^2\sum_p\frac{h_p^2N(p)}{|Y_p'(\eta_0)|^2} \text{ in h.l.u.} \quad (79)$$

obtained by summing (50); cross terms between harmonics drop out by orthogonality (38). If as heretofore the frequency dependence of the non-resonant harmonics is neglected, then maximum rate of radiation of power comes at $\epsilon=\frac{1}{2}p\pi$, so that the sense in which we have been

using the term "resonance" for each mode applies also to the antenna as a whole.

To return to the centrally excited half-wave antenna, its radiation resistance $R_{eff}$ is found:

$$R_1 I_1^2 + R_3 |I_3|^2 = R_{eff} |I|^2, \tag{80}$$

$$R_{eff} = 73.08 \left[ 1 - \frac{0.04}{[\log (\eta_0+1)/(\eta_0-1)]^2} \right] \times \left(\frac{\mu}{\kappa}\right)^{\frac{1}{2}} \text{ ohms.} \tag{81}$$

Thus the radiation resistance of the antenna is only slightly lowered by the presence of the higher mode, despite the smallness of the radiation resistance of the latter, which is on the order of 0.3 ohm.

The radiation field at large distances is practically the same as it would be if the third harmonic were absent. This at first sight amazing result holds in spite of the fact shown by (77) that the amplitude of the third mode may be several percent of the first. Mathematical explanation is given by Eq. (46b), wherein the proportionality factor $|Y_3(\eta_0)|$ is some 17 times larger than the corresponding $|Y_1(\eta_0)| = 1$ at this frequency. Although the third harmonic current may be, say, 5 percent of the first, its radiation field is a mere 0.3 percent. No violation of physical principle is involved, as can be seen qualitatively from the character of the current distribution: the two current loops of third mode at the ends of the antenna are out of phase with the larger central loop, and cancel the field at a distance by interference. Alternatively, one may say that the explanation is the smallness of the third mode's radiation resistance.

The foregoing furnishes an explanation of the rather surprising success attained in predicting the field of an antenna by the oft-used means of assuming sinusoidal current distribution. For example, Pedersen[22] has shown that this assumption gives quite good results for the Copenhagen aerial he studied, in spite of the fact that the current has been measured and found not to be sinusoidally distributed. Physically it is, of course, evident that the current in the antenna must be the cause of the field; yet the contention is sometimes advanced that there are "wattless" components in the current, in phase quadrature with the driving electromotive force, which do not contribute to the field. Such a situation is exhibited here: the third harmonic leads the impressed field by nearly 90°, and also contributes practically nothing to the radiation field at large distances. It is therefore evident that an attempt to predict the radiation field from the measured root-mean-square current distribution of an antenna may encounter serious difficulty —may easily, in fact, go farther astray than a bald assumption of sinusoidal current.

### 1. Composite Oscillations in General

In principle, oscillations induced in a thin spheroid by a field harmonic in time but of arbitrary frequency and spatial distribution may be treated by this method. All that is necessary is to compute the values of $X_p(\xi)$, $Y_p(1)$, $Y_p'(\eta_0)$ for the relevant harmonics; by (41) break up the driving field into corresponding segments; whence the resulting numbers $h_p$ give the amounts of the various harmonics present, in terms of the standard "unit" driving field $\mathcal{E}_p$ (47a). In practice, the method is particularly suited to resonant antennas where $X_p$, essentially the current distribution, may, for the most important harmonic, be approximated by the first term of its Fourier series. The analysis of paragraph 5.2 can be extended to include the second power of $\theta$, but progress beyond that point runs into considerable computational difficulty which impedes application to non-resonant structures. Some entirely different approach such as that of S. A. Schelkunoff[23] would be more suitable for these last. The present theory may be regarded as a justification and expansion of the sinusoidal current assumption for resonant antennas; particularly for the radiation field this assumption is better than might, at first, be expected. Our principal extension is to relate the amplitude and phase of the current to the driving field (39), (44), (68a).

In concluding, a few interesting minor points might be mentioned. The first is pertinent to a discussion of the higher resonances of the

[22] P. O. Pedersen, Ingen. Vidensk. Skr. A. No. 38 (1935).

[23] S. A. Schelkunoff, Proc. I. R. E. **29**, 493 (1941).

antenna: the current nodes predicted by the simple sinusoidal theory are not found experimentally but instead are found nearby minima in the measured (root-mean-square) current. Often the fact that these minima are not zero is attributed to losses of a true ohmic resistive character, but even for a perfectly conducting spheroid the minima do not vanish in general, as the small contribution of the non-resonant modes remains as a residual.

Another point is the following. If a vertical antenna is three-quarters of a wave-length long, it is at the proper length to resonate the third harmonic. In practice, such resonance is quite easy to establish by the action of a lumped electromotive force; but under the influence of an incident plane wave acting along the whole length of the (receiving) antenna, the resulting current distribution is not markedly sinusoidal, but seems fairly smoothly distributed with no great tendency to show nodes.

Qualitatively the result may be explained by considering the coefficients $h_p$ involved in the second case.

$$h_1=\frac{1}{N(1)}\int_{-1}^{1}\mathcal{E}\cdot X_1(\xi)d\xi\sim\frac{8\mathcal{E}}{\pi}\frac{1}{2.4},$$

$$h_3=\frac{2}{F(6)}\int_{-1}^{1}\mathcal{E}\sin\frac{3\pi}{2}(1-\xi)d\xi=\frac{8\mathcal{E}}{\pi}\frac{1}{10.5}.$$

The evaluation of $h_1$ is rough, but indicates that the field has something like five times as great a tendency to excite the first harmonic as the third. The presence of a large amount of first harmonic current in phase quadrature could account for the concealment of the nodes of the third. For the lumped field, the $h_p$ are more nearly equal, and the resonant behavior shows up.

To Professor Leigh Page and Professor Norman I. Adams the author wishes to offer his thanks for illuminating discussions.

## APPENDIX I. $F(2p)$ AND $Si(2p\pi)$

These functions, used frequently in the work, seem not to be available readily without interpolation. The following values were interpolated from the British Association Mathematical Tables.

$$F(2p)\equiv\int_0^{2p\pi}\frac{1-\cos t}{t}dt$$
$$=\log 2p\pi-Ci(2p\pi)+0.57722, \quad \text{(A1-1)}$$

$$Si(2p\pi)\equiv\int_0^{2p\pi}\frac{\sin t}{t}dt. \quad \text{(A1-2)}$$

| $p$ | $F(2p)$ | $Si(2p\pi)$ | $p$ | $F(2p)$ | $Si(2p\pi)$ |
|---|---|---|---|---|---|
| 1 | 2.43766 | 1.41815 | 6 | 4.20756 | 1.54428 |
| 2 | 3.11435 | 1.49216 | 7 | 4.36153 | 1.54807 |
| 3 | 3.51648 | 1.51803 | 8 | 4.49493 | 1.55091 |
| 4 | 3.80296 | 1.53113 | 9 | 4.61264 | 1.55312 |
| 5 | 4.02553 | 1.53903 | 10 | 4.71794 | 1.55488 |

Higher arguments are found to this accuracy from the asymptotic series

$$F(2p)=\log(2p\pi)+0.57722+\frac{1}{p^2\pi^2}-\cdots, \quad \text{(A1-1a)}$$

$$Si(2p\pi)=\frac{\pi}{2}-\frac{1}{p\pi}+\frac{2!}{p^3\pi^3}-\cdots. \quad \text{(A1-2a)}$$

## APPENDIX II

Radiation resistance at resonance for the $p$th mode is given by

$$R_{\text{rad}}=(\mu/\kappa)^{\frac{1}{2}}29.98F(2p)\text{ ohms}. \quad \text{(A2-1)}$$

| $p$ | $R_p(p)$ (ohms) | $p$ | $R_p(p)$ (ohms) |
|---|---|---|---|
| 1 | 73.08 | 6 | 126.1 |
| 2 | 93.37 | 7 | 130.8 |
| 3 | 105.4 | 8 | 134.8 |
| 4 | 114.0 | 9 | 138.3 |
| 5 | 120.7 | 10 | 141.4 |

It should be emphasized that the tabulated values above are not the radiation resistance of the antenna at the corresponding frequencies; though for thin spheroids, where the resonant harmonic dominates, this is a good first approximation. The exact radiation resistance of the antenna of course depends on the proportions of harmonics present.

Again, an ingratiatingly smooth curve can be drawn through these points, but between the points the curve does not correspond to any harmonic, and only by chance would it correspond to some particular method of driving the antenna. The radiation resistance of each harmonic varies with frequency, but along curves quite different from this; see, for example, Table I.

## APPENDIX III

Properties of the first harmonic near resonance. The values of Table I were calculated for four different eccentricities:

(1) $\log(\eta_0+1)/(\eta_0-1)=10$; $b/a=1.35\ (10)^{-2}$
Band width $\Delta\nu/\nu_r=0.155$ from (78)

(2) $\log(\eta_0+1)/(\eta_0-1)=15$; $b/a=1.11\ (10)^{-3}$
Band width $\Delta\nu/\nu_r=0.103$

(3) $\log(\eta_0+1)/(\eta_0-1)=20$; $b/a=9.08\ (10)^{-5}$
Band width $\Delta\nu/\nu_r=0.078$

(4) $\log(\eta_0+1)/(\eta_0-1)=40$; $b/a=4.12\ (10)^{-9}$
Band width $\Delta\nu/\nu_r=0.039$.

Here $\nu_r$ is the resonant frequency, $R_p$ radiation resistance, $\varphi$ the phase angle by which current leads the applied field, $X$ the driving point reactance, referred (like $R_p$) to a current loop; and $I_0$ is the current in the center of the antenna, having the value $I_{0r}$ at resonance. It is assumed that a "unit" amount (47a) of first mode appears.

The data of Table I are calculated from (65), (67), (68),

and (72), which become for this case

$$\tan\phi=\frac{-0.261\theta_1\log\dfrac{\eta_0+1}{\eta_0-1}}{1+0.017\theta_1}, \tag{65-1}$$

$$R_p=\frac{73.08}{1-0.370\theta_1}, \tag{67-1}$$

$$I(\xi)=\frac{0.01668\left(\dfrac{\kappa}{\mu}\right)^{\frac{1}{4}}a\cos\dfrac{\pi}{2}\xi}{1-i\dfrac{0.261\theta_1}{1+0.017\theta_1}\log\dfrac{\eta_0+1}{\eta_0-1}}, \tag{68-1}$$

$$(I_0/I_{0r})=\left|1-i\frac{0.261\theta_1}{1+0.017\theta_1}\log\frac{\eta_0+1}{\eta_0-1}\right|^{-1}, \tag{68-1a}$$

$$\frac{\Delta\nu}{\nu_r}=\frac{1.55}{\log\dfrac{\eta_0+1}{\eta_0-1}}. \tag{72-1}$$

The sign of $i$ is reversed from the usual convention.

## APPENDIX IV

Numerical constants for the first three odd harmonics.

TABLE II

| $k$ | $(\pi^2/4)$ $a_{31k}$ | $(\pi^4/16)$ $a_{32k}$ | $(\pi^6/64)$ $a_{33k}$ |
|---|---|---|---|
| 1 | 0.024055 | −0.00119 7 | 0.00014 33 |
| 3 | | | |
| 5 | −0.02426 6 | 0.00018 53 | |
| 7 | −0.00647 81 | 0.00031 97 | |
| 9 | −0.00272 95 | 0.00016 88 | |
| 11 | −0.00141 82 | 0.00009 543 | |
| 13 | −0.00083 427 | 0.00005 817 | |

| $k$ | $(\pi^2/4)$ $a_{51k}$ | $(\pi^4/16)$ $a_{52k}$ |
|---|---|---|
| 1 | 0.00416 22 | 0.00001 7063 |
| 3 | 0.02119 8 | −0.00041 624 |
| 7 | −0.01831 9 | −0.00001 2531 |
| 9 | −0.00553 24 | 0.00014 396 |
| 11 | −0.00253 19 | 0.00008 7392 |
| 13 | −0.00139 68 | 0.00005 3792 |
| 15 | −0.00086 000 | 0.00003 5051 |
| 17 | −0.00056 989 | 0.00002 4025 |
| 19 | −0.00039 824 | 0.00001 7158 |
| 21 | −0.00028 977 | 0.00001 2657 |

| $k$ | $a_{11k}$ | $a_{12k}$ |
|---|---|---|
| 3 | −0.01406 3 | 0.00039 50 |
| 5 | −0.00278 57 | 0.00017 80 |
| 7 | −0.00099 229 | 0.00007 3 |
| 9 | −0.00046 255 | |

| $k$ | $\gamma_{1k}$ | $\gamma_{2k}$ | $\gamma_{3k}$ |
|---|---|---|---|
| 1 | −0.82046 | −0.56875 | −0.49683 |
| 2 | −0.00186 92 | −0.004281 $\left(\frac{\pi^2}{4}\right)$ | −0.00173 04 $\left(\frac{\pi^2}{4}\right)$ |
| 3 | −0.00003 | −0.000037 $\left(\frac{\pi^4}{16}\right)$ | −0.00001 898 $\left(\frac{\pi^4}{16}\right)$ |

In computing the properties of the third mode which were given in paragraph 6 above, use was made of a numerical check. Since the solutions at zero frequency are known,[8] the series for the $a$'s can be checked against the exact values for $\epsilon=0$. They were found to correspond within a few percent. Data in Table III were then computed for the third mode at $\epsilon=\pi/2$, the resonant point of the first mode.

## APPENDIX V. DRIVING POINT IMPEDANCE

By the method of paragraph V can be found a formula for driving-point impedance to replace (52) and generalize (51):

TABLE III. Properties of the third mode at the resonant point of the first.

| | |
|---|---|
| $a_{31}$ | $=-0.33247$ |
| $a_{33}$ | $=1$ |
| $a_{35}$ | $=0.20609$ |
| $a_{37}$ | $=0.07458$ |
| $a_{39}$ | $=0.03473$ |
| $a_{3,11}$ | $=0.01898$ |
| $a_{3,13}$ | $=0.01148$ |
| $\gamma_3$ | $=10.70$ |
| $\epsilon_3X_3'(1)$ | $=0.6649$ |
| $X_3(0)$ | $=-1.179$ |
| $N(3)$ | 2.195 |
| $\dfrac{2\gamma_3}{i\pi\epsilon_3}$ | $=104.3i$ |
| $Y_3(1)$ | $=-17.12i$ |
| $Y_3'(\eta_0)$ | $=104.3i\log\dfrac{\eta_0+1}{\eta_0-1}+0.0918$ |
| $I_3(0)$ | $=\dfrac{0.00507i\left(\dfrac{\kappa}{\mu}\right)^{\frac{1}{4}}a}{\log\dfrac{\eta_0+1}{\eta_0-1}}$ for the "unit" driving field. |

For the centrally-driven antenna of paragraph 6,

| | |
|---|---|
| $h_3$ | $=-1.075V/a$ |
| $I_3(0)$ | $=-0.00545i\dfrac{\left(\dfrac{\kappa}{\mu}\right)^{\frac{1}{4}}V}{\log\dfrac{\eta_0+1}{\eta_0-1}}$ |
| $R_{\text{rad}}$ | $=0.323\left(\dfrac{\mu}{\kappa}\right)^{\frac{1}{4}}$ ohms. |
| $X_{\text{rad}}$ | $=-336.9i\left(\dfrac{\mu}{\kappa}\right)^{\frac{1}{4}}\log\dfrac{\eta_0+1}{\eta_0-1}$ ohms. |
| $\tan\varphi$ | $=1140\log\dfrac{\eta_0+1}{\eta_0-1}$ |

$$Z_{\text{rad}}=R_{\text{rad}}-iX_{\text{rad}}=\left(\frac{\mu}{\kappa}\right)^{\frac{1}{4}}\frac{59.96N(p)}{X_p^2(\xi)}\frac{Y_p'(\eta_0)}{i\epsilon Y_p(\eta_0)}\text{ ohms.} \tag{51G}$$

Here as throughout the sign of the imaginary unit $i=(-1)^{\frac{1}{2}}$ is opposite to the usual convention; $R$ and $X$ are the ordinary reactance and resistance which the driving point e.m.f. sees. Using the approximations (63) and (64), the impedance presented by the near-resonant harmonic driven at a current loop is

$$Z_p=R_p-iX_p=\left(\frac{\mu}{\kappa}\right)^{\frac{1}{4}}59.96F(2p)\times\frac{\dfrac{p\pi}{2}+\theta_p\left\{\dfrac{1}{p\pi}-\dfrac{1}{2}\dfrac{Si(2p\pi)}{F(2p)}-i\dfrac{\theta_p}{F(2p)}\log\dfrac{\eta_0+1}{\eta_0-1}\right\}}{\epsilon\left\{1-\dfrac{Si(2p\pi)}{F(2p)}\dfrac{\theta_p}{p\pi}\right\}}\text{ ohms.} \tag{67G}$$

# Letter to the Editor

## Effect of Machining and Aging on the Damping Capacity of Steel

LESTER TARNOPOL, *Raytheon Production Corporation, Newton, Massachusetts*

AND

JAMES R. MORGAN, *Alabama Dry Dock & Shipbuilding Company, Mobile, Alabama*

February 20, 1942

SEVERAL years ago, Sonnemann[1] found in one instance that two bars from the same consignment of standard mild steel exhibited widely different damping capacities. The damping capacity of one bar was found to possess from

8 to 10 times that of the other bar at high values of strain. The specific damping capacity is the percent of the total energy absorbed per cycle during free vibration in these measurements.

In order to investigate this phenomenon, we machined four torsional damping capacity specimens from commercial cold rolled S.A.E. 1020 steel. These specimens, in the form of solid cylinders with square center and ends, were tested in a Cambridge Torsional Damping Recorder. Considerable spread in the specific damping capacities at high values of maximum fiber stress was found. Whereas, at 6000 lb. per sq. in. (maximum fiber stress) all specimens had a specific damping capacity of 2 percent; at 24,000 lb. per sq. in. the specific damping capacities were 7.6, 9, 14.5, and 27 percent, respectively.

Since these four specimens varied in diameter from 0.3109" to 0.3124", the need for greater precision was felt. In order to eliminate any effect due to differences in the dimensions of the specimens, three precision specimens were machined from a single bar of cold rolled S.A.E. 1020 stock steel as shown in Table I.

TABLE I.

| Specimen No. | Average diameter inches |
|---|---|
| 5 | 0.3041 |
| 6 | 0.3041 |
| 7 | 0.3041 |

TABLE II.

| Specimen No. | Original Rockwell hardness | Rockwell hardness after 4 hr. at 400°F furnace cooled |
|---|---|---|
| 1 | B93 | B93.5 |
| 2 | B93 | B95 |
| 3 | B93 | B94 |
| 4 | B94 | B96 |
| 5 | B101.5 | B102.5 |
| 6 | B101 | B102 |
| 7 | B103 | B103.5 |

The three precision machined specimens likewise had specific damping capacities of 2 percent at 6000 lb. per sq. in., whereas at 24,000 lb. per sq. in. the specific damping capacities were 4.8, 8.1 and 18 percent, respectively. However, after aging at room temperature for several weeks the damping capacities of these specimens were found to have decreased considerably, bringing them all very close together. At 6000 lb. per sq. in. the specific damping capacities became 1 percent while at 24,000 lb. per sq. in. the percentages had dropped to 3, 3, and 4.

All seven specimens were subsequently given a stress relieving anneal for four hours at 400°F and furnace cooled. After this low temperature anneal, the damping capacities of all seven S.A.E. 1020 specimens were very nearly the same; i.e., 1 percent at 6000 lb. per sq. in. and 3 to 4 percent at 24,000 lb. per sq. in. After annealing, Rockwell hardness tests were made which showed very little change from the original values (Table II).

A similar phenomenon was observed with S.A.E. 2320 steels containing 3.3 percent nickel, the main difference being that the nickel steels did not reveal such large differences in damping capacity among themselves.

Since the fiber stress increases linearly from zero at the cylinder axis of the specimen to a maximum at the outside fiber, the damping likewise to a first approximation may be considered to increase linearly from zero at the center to a maximum at the outside fiber. Therefore the condition of the outer volume of fibers would have the most effect upon the damping capacity. Since one of the precision specimens showed a very high damping capacity immediately after machining and subsequently lost its high value after aging, it would appear that the high damping capacity may have been due to machining which leaves stresses in the outside fibers. The original variations in the damping capacities of specimens No. 1, No. 2, No. 3, and No. 4 might also be partially explained by machining. At any rate, the high values of damping capacity were very probably due to cold work, since the low temperature stress relieving anneal reduced the damping and brought all specimens nearly into coincidence.

The damping resulting from cold work might be partially explained by encouraged plastic flow resulting in stress-strain hysteresis losses. Damping also results from heat flow energy losses caused by temperature gradients produced during deformation, and by eddy current losses due to magnetic effects.[2,3]

Machining could encourage plastic flow by producing lattice warping in the outer fibers, wherein voids of atomic dimensions might exist along with stressed material. These stresses plus temperature energy could greatly increase the energy of certain atoms. Thus a further stress well below the elastic limit of the material would be sufficient to plastically move one of these atoms into a neighboring void. This might start a process whereby a whole series of atoms would flow plastically, following each other in a row, resulting in potential energy losses or damping.

After aging at room temperature plus the effect of vibration when testing specimens, or during a low temperature anneal, the effects of machining gradually disappear. This results in a considerable decrease in damping capacity but effects no change in Rockwell hardness. The relief of stresses at 400°F takes place in a few hours and is easily understood, since strained atoms can readily migrate to positions of lower potential energy at this temperature.

The migration necessary to accomplish relief of strains which occurs at room temperature is more difficult to explain theoretically. Nevertheless, we have abundant evidence from other sources that atoms in metals may diffuse considerably at room temperature.[4] The Boltzmann temperature distribution permits an atom to have sufficient temperature energy, at some time, to hurdle its potential barrier and move to a neighboring position provided the atom is already in a state of strain and is adjacent to a "lattice void." The continuance of this process would ultimately produce the aging results indicated by our experiments.

[1] Sonnemann, Mitt. d. Woehler Inst. Braunschweig, No. 28 (1936)
[2] E. R. Parker, Trans. Am. Soc. Metals **28** (1940).
[3] C. Zener, Phys. Rev. **52**, 230 (1937).
[4] R. Hultgren and L. Tarnopol, Metals Technology (Jan. 1939).